Integrated infection and crowd behavior model for infection risk assessment onboard large passenger vessels

Investigating the effect of ship layout design, operational and behavioral measures on contagious disease spread

Naomi de Haan

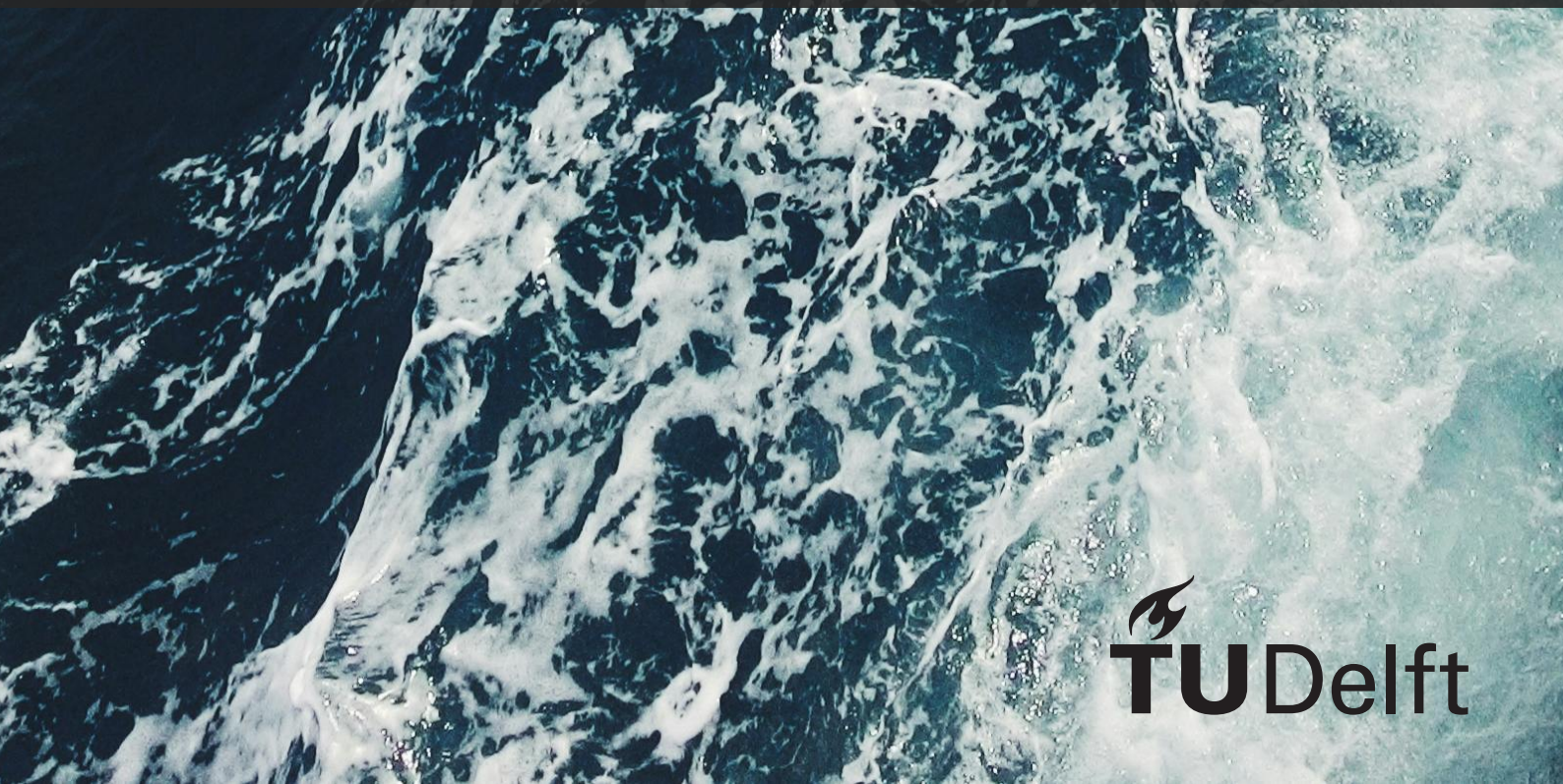

TU Delft

Integrated infection and crowd behavior model for infection risk assessment onboard large passenger vessels

Investigating the effect of ship layout design, operational and behavioral measures on contagious disease spread

by

Naomi de Haan

Thesis for the degree of MSc in Marine Technology in the specialization of Ship Design
to be defended publicly on Tuesday March 26, 2024 at 12:00

Report number:	MT.23/24.024.M.
Student number:	4690257
Project duration:	April, 2023 - March, 2024
Faculty:	Faculty of Mechanical Engineering, Delft
Thesis committee:	Dr. A. A. Kana - TU Delft, Chair
	Dr. B. Atasoy - TU Delft
	Z.P. Oikonomou - TU Delft

An electronic version of this thesis is available at http://repository.tudelft.nl

TU Delft

Preface

This report marks the end of my master Marine Technology at the TU Delft. The graduation research has been interesting, challenging and most of all, a learning experience. There were rough patches when the progress was slow and the motivation hard to find. However, having arrived at the end, these challenges seem less important than the final accomplishment which cannot be presented without acknowledging some important people.

First and foremost, I would like to thank my supervisors Dr. A. A. Kana and Dr. B. Atasoy. Austin, I stepped into your office over a year ago after spending eight months onboard the Global Mercy. From the start, you were enthusiastic and open-minded which resulted in a graduation topic connected to my experiences onboard the Global Mercy during COVID-19. I appreciated the clear structure and diligent feedback on every draft I submitted. I would like to thank Bilge for the second perspective. You have brought up critical and observant questions whenever we were discussing conclusions or results. It has been a pleasure working with you both.

I would also like to acknowledge the individual master research by Daan van Gisbergen. Your work has been a major help during my research, as was your advice whenever I got stuck in programming.

Lastly, I would like to thank my family and friends who supported me through this graduation. Mum and Dad, sometimes talking just made things make more sense. Thank you for being good listeners with the full confidence that I would get this done. Lisanne, I think it is impossible to separate my time studying in Delft from the friendship with you. Let's just leave it at that. Deborah, you are an amazing friend and I am grateful that we experienced the graduation process together. Hanna and Roos, the weekly study sessions got me through the final parts of my report. And Daan, good food makes all the difference. Thank you for all the conversations discussing my graduation progress, struggles and topics far beyond that. I will close with you, sis. Thank you for your never-ending love and support, the postcards and the messages. I could not have done this without you.

To the reader, thank you for taking the time to read my thesis and I hope it is of interest to you.

Naomi de Haan
Delft, March 2024

Summary

From 2020, the global COVID-19 pandemic has had a significant impact on the world and specifically the maritime industry. Striking examples were COVID-19 outbreaks onboard the U.S.S. Theodore Roosevelt aircraft carrier and the Diamond Princess cruise vessel. These outbreaks happened at the start of the pandemic and point to the complexity of contagious disease management onboard large passenger vessels. This complexity is amplified by the international character of the industry, shared facilities and confined environment. The COVID-19 pandemic showed the need to prepare for new or reemerging infections onboard ships and support 'disease readiness' tailored to the needs of the shipping industry. This report therefore aims to: *investigate the effect of ship layout design and behavioral measures on contagious disease spread onboard large passenger vessels*. The novelty of this research lies in the developed integrated infection and crowd behavior model which provides an agent-specific infection risk assessment, incorporating guest and crew circulation through a passenger vessel layout.

Firstly, the state-of-the-art concerning contagious disease spread, disease prevention and control in confined spaces was investigated. This state-of-the-art presents four disease transmission modes and it introduces operational measures, behavioral measures and ship layout design adaptions that might support disease prevention and control. Building on this background information, a research gap was identified. This research gap covers initial stage retrofit design for large passenger vessels. The preferred result is a limitation of contagious disease spread through the implementation of adapted ship layout design, operational and behavioral measures. A key detail in the research gap is the incorporation of guest and crew circulation through a ship layout. The research gap was then expanded into a set of model requirements. Various infection and crowd behavior model combinations were explored and the compatible combinations were tested against the requirements.

From the investigated model combinations, an integrated mesoscopic route choice model (RCM) and modified Wells-Riley infection model was selected. This combination calculates agent-specific infection risk and it is layout dependent without being overly complex. The guest and crew movement in the RCM is modeled based on a detailed activity schedule where agents move between nodes (destinations) via links (connections). The infection risk calculation is controlled by the RCM output, medical parameters, ventilation assumptions and spatial parameters. The ship layout used in this research is a cruise ship layout provided by the SAFEGUARD project. The sample case features an average infection risk of 0.807% with a variation between 0% and 2.5% over the day. The guest average infection risk is 0.730% compared to a crew average risk of 1.04%. Additionally, peaks were identified for the number of agents with a risk above 50% around 11:30, 16:00 and 21:00 with respectively 18, 7 and 14 agents. The sample case has been validated against similar cases presented in literature. These cases covered attack rates onboard the Diamond Princess and infection risk for office spaces, an out-patient hospital building and a reception scenario. The sample case proved to be sufficiently validated as a baseline for disease prevention and control scenario evaluation.

Finally, the integrated model was used to evaluate small-scale layout adjustments, capacity reductions and mask wearing scenarios. The node locations showed significantly higher infection risk than the links, which can be explained by the extended exposure time and increased occupancies. Local risk improvements, although too small to be detectable in full-ship average infection risks, were achieved for small-scale layout adjustments. Implementing capacity reductions above 50% resulted in average risk improvements but might also introduce economic and operational feasibility issues. More significant risk improvements were achieved for mask wearing, with average risk reductions over 40% with respect to the sample cases. The largest improvements were found for combined capacity reduction and mask wearing scenarios with average risk reductions over 55% compared to the sample cases. Additionally, for mask wearing and the combined scenarios, the amount of agents with a risk above 50% decreases significantly. Given these infection risk results, the developed integrated model has proven to be a valuable tool for investigating infection risk onboard a large passenger vessel.

Contents

Nomenclature

Abbreviations

Abbreviation	Definition
ATR	Adjusted time range
CFD	Computational fluid dynamics
CR	Capacity reduction
COVID-19	Coronavirus disease 2019
HVAC	Heating, ventilation and air conditioning
ICU	Intensive care unit
IR	Infection risk
LOA	Length over all
PAC	Portable air cleaner
PPE	Personal protective equipment
PS	Portside
PtD	Prevention through design
RCM	Route choice model
SB	Starboard
SC1	Sample case 1
SC2	Sample case 2
SD	Social distance
SEIR	Susceptible-Exposed-Infected-Recovered
SIR	Susceptible-Infected-Recovered
WHO	World Health Organization

Symbols

Symbol	Definition	Unit
A	Ventilation rate	$[AC/h]$
ACH	Ventilation rate	$[AC/h]$
C	New infected cases	[-]
C^+	Normalized droplet nucleus concentration	[-]
d	Social distance	$[m]$
E_z	Ventilation index	[-]
H_c	Average ceiling height	[-]
I	Infected individuals	[-]
N	Total population	[-]
p	Pulmonary ventilation rate	$[m^3/s]$
$p_{adjusted}$	Pulmonary ventilation rate with surgical mask	$[m^3/s]$
P	Infection probability	[-]
P_d	Social distance index	[-]
P_I	Infection probability	[-]
q	Quanta production rate	$[quanta/s]$
$q_{adjusted}$	Quanta production rate with surgical mask	$[quanta/s]$
Q	Room ventilation rate	$[m^3/s]$
R	Recovered individuals	[-]
S	Susceptible individuals	[-]

Symbol	Definition	Unit
t	Exposure time	[s]
V	Space volume	[m^3]
$[E]$	Risk	[-]
$[FN]$	From-node	[-]
$[LD]$	Link ID	[-]
$[LL]$	Link length	[m]
$[LO]$	Link occupancy	[-]
$[NA]$	Node area	[m^2]
$[S]$	State	[-]
$[TN]$	To-node	[-]
β	Contact rate susceptible to infected	[-]
γ	Recovery/removal rate	[-]
η_E	Exhalation filtration efficiency	[-]
η_R	Respiratory filtration efficiency	[-]
σ	Standard deviation	[-]

1

Introduction

The development of the global COVID-19 pandemic from 2020 onward has had a significant impact on the world and specifically the maritime industry. The shipping industry had to deal with restricted travel, changing trade volumes, increased waiting times and stricter security measures in ports [98]. As seafarers kept working through the COVID-19 pandemic; quarantines, travel restrictions and country entering measures became standard practice and seafarers faced challenges renewing their maritime certification [40].

The cruise shipping sector was confronted with significant challenges during the pandemic, amplified by the international nature of the industry. Onboard, diverse populations live in close proximity to each other for longer periods of time [98]. There is a potential for international disease spread once guests return to their home countries [95, 98]. The diamond Princess cruise vessel, which can house over 3700 guests and crew, is frequently mentioned in literature concerning COVID-19. At the beginning of February 2020, a COVID-19 outbreak occurred onboard the Diamond Princess, resulting in over 700 positive cases [89]. Early after the discovery of the outbreak, a rigorous 14-day quarantine was instituted for all guests and crew still onboard [75]. Using SEIR (Susceptible-Exposed-Infected-Recovered) compartment models, it was estimated that an additional 2000 cases might have been prevented by the implementation of quarantine and disembarkation measures [75].

Another outbreak example can be found onboard the nuclear aircraft carrier U.S.S. Theodore Roosevelt at the start of the pandemic. Throughout the COVID-19 outbreak, approximately 27% of the 2779 complement tested positive for COVID-19 and nearly half of the positively-tested crew never developed symptoms [39]. Research showed that confined work spaces, packed bunks and crowded general spaces might have facilitated the transmission of COVID-19 [39]. Methods to deal with COVID-19 proved difficult to match with life onboard navy vessels which are often more cramped than regular cargo or passenger vessels [75]. Different from a cruise ship, disease outbreaks onboard a navy vessel can impact readiness in terms of the ability of the ship to carry out its mission [55].

The COVID-19 pandemic showed the necessity to prepare for new or reemerging infections, even though some infections have been controlled or eradicated in the past [61]. This ‘disease readiness’ should be tailored to the specific needs of the shipping industry because a large passenger vessel or aircraft carrier is different from a building. These vessels are by definition a confined space which crew and guests are often not able to leave. Within the ship as a confined space, geometry, facility and population based characteristics are important to discuss. Firstly, the geometry of a large commercial passenger vessel is based on the requirement to efficiently transport a large number of guests at reasonable speed [89]. The ship therefore has limited space and will feature shared living, dining and sanitation areas. For naval ships, the space limitations can be even more extreme in order to satisfy survivability and redundancy requirements [89].

The second category of characteristics is related to the facilities onboard. For cruise ships, the spaces allocated for activities, accommodation and restaurant facilities are spread throughout the vessel. This leads to frequent and complex movement patterns for both guests and crew [99]. Also, the medical

facilities onboard large passenger vessels might differ significantly for various vessels and there is limited capacity in treating for example COVID-19 patients that require intense care (ICU) [58]. For cargo vessels, the medical facilities are even more limited as there are no physicians onboard and the shipmaster or second mate is designated to perform medical care [63].

Thirdly, populations onboard large passenger vessels have specific characteristics. Taking another look at cruise ships, the guest population is frequently changing and there is ample opportunity to bring diseases onboard [94]. Within the guest population there are differences in age, health condition and nationality [57]. The population onboard a naval vessel features different characteristics as the crew needs to adhere to military health requirements [44]. The COVID-19 outbreak onboard the U.S.S. Theodore Roosevelt showed that a healthy young crew might lead to milder symptoms and a higher proportion of asymptomatic cases. This made early disease detection and intervention more difficult [44].

The specific characteristics of large passenger vessels, together with the Diamond Princess and U.S.S. Theodore Roosevelt COVID-19 examples show the need to investigate ways to limit and control the spread of contagious disease onboard large passenger vessels. Operational measures, behavioral measures and possible ship layout design adaptions onboard large passenger vessels might be options to decrease disease spread and therefore increase resilience in case of a disease outbreak.

1.1. Research Goal

The main objective of this research project will be to: investigate the effect of ship layout design, operational and behavioral measures on contagious disease spread onboard a large passenger vessel. To achieve this, an integrated model is developed combining two existing models: a crowd behavior model which simulates guest and crew movement, and a disease infection model.

1.1.1. Scope

The scope of this research is defined by the details as described in the primary research objective. The scope of the measures and interventions tested is limited to: operational measures, behavioral measures and ship layout design. The effect of these measures will be investigated through model simulations. The study of ventilation and ventilation system design onboard large passenger vessels in relation to contagious disease spread falls outside the scope of this research.

1.1.2. Primary research objective

The primary research objective will be to:

Investigate the effect of ship layout design, operational and behavioral measures on contagious disease spread onboard large passenger vessels, by combining an infection model with a crowd behavior model.

In this report, the following research questions will be answered:

1. What is the state-of-the-art of contagious disease spread, contagious disease prevention and contagious disease control in confined spaces such as a large passenger vessel?
2. What are the requirements for an integrated infection and crowd behavior model, if this model is used to investigate the effect of ship layout design, operational and behavioral measures on contagious disease spread?
3. Which infection model and which crowd behavior model can be combined to fulfill the requirements of research question 2?
4. What is the architecture of the integrated infection and crowd behavior model?
5. What are the infection risk results of a sample case scenario when the integrated infection and crowd behavior model is applied?
6. How can the infection risk results from the integrated model be validated?
7. What are the infection risk results of selected prevention and/or control actions onboard a large passenger vessel when the integrated infection and crowd behavior model is applied?

2

State-of-the-Art

This chapter aims to answer the first research question:

1. *What is the state-of-the-art of contagious disease spread, contagious disease prevention and contagious disease control in confined spaces such as a large passenger vessel?*

The first section provides information regarding diseases onboard large vessels and the different disease transmission mechanisms. Section 2.2 continues to describe the state-of-the-art in disease prevention and control. The chapter will close with the gap in research for prevention and control measures to limit contagious disease spread onboard large passenger vessels. A literature search was performed using different search terms for the WorldCat, Google Scholar and Semantic Scholar databases. The search terms for the disease angle were: *disease, contagious disease, communicable disease, airborne infections, epidemic, spread, transmission, COVID-19, respiratory disease* and *Norovirus*. The environment angle was covered by the following search terms: *confined space, enclosed space, ship, ship layout, cruise ship, built environment, navy ship* and *public transportation*.

2.1. Disease transmission

Diseases have been a part of daily human life throughout history, and some diseases will be remembered because of their deadliness and scope. The black death, for example, resulted in an estimated 25 to 40 million deaths and the 1918 Influenza pandemic led to approximately 50 million deaths. Specifically looking at disease onboard ships, one should mention diseases like smallpox, plague, and scurvy (vitamin C deficiency) which were historically relevant [58]. Diseases that are currently linked to life at sea are: tuberculosis, Noroviruses, influenza and coronaviruses [54, 38]. The diseases are often categorized in terms of gastrointestinal infections, respiratory infections, and diseases related to food and water sources [62].

2.1.1. Transmission modes

Next to the different diseases that can occur on ships, it is relevant to discuss the way these diseases spread. The way by which a disease spreads is also called a mode of disease transmission [54]. Mangili and Gendreau describe four general modes of disease transmission related to infectious disease transmission during commercial air travel [54]. The four modes are:

- *Contact transmission*
  Contact transmission includes person-to-person contact, contact with a contaminated intermediate host and large droplet transmission; when someone for example inhales large droplets generated when an infector sneezes or coughs [54]. The contaminated intermediate host might be a surface, elevator button or door handle.

- *Airborne transmission*
  Airborne transmission covers very small droplet residua (nuclei) that travel over long distances. These aerosolized infectious agents might move around because of circulation inside a space, mechanical ventilation or they end up in filtration systems [54, 85].

- *Common vehicle transmission*
  Common vehicle transmission is associated with food and water sources [54].

- *Vector-borne transmission*
  Vector-borne transmission relies on insects or rodents to spread a disease [54].

The exact transmission routes and dominant transmission routes for specific diseases remain a point of discussion and motive for research. There are many factors, like human behavior and environmental conditions, that play a role when studying disease transmission [25]. Also, the scale of the research covering transmission routes varies significantly: from modeling individual micrometer infectious droplets up to simulating disease spread in an entire population. The scale of the study is often related to the scale of the transmission mechanism studied which might lead other transmission mechanisms to be underexposed.

For this research project, the ultimate interest lies with ship layout adaptions and operational and behavioral measures decreasing contagious disease spread onboard ships. Therefore, the least complex medical disease transmission model will be used that fits the requirements instead of investigating more complex medical research areas like disease-specific modes of transmission onboard ships. In order to move towards a fitting medical model, it is relevant to apply the general transmission modes to a confined space like a passenger vessel.

2.1.2. Transmission modes onboard large passenger vessel

As mentioned before, a large passenger vessel can be considered a confined space characterized by shared facilities, crowded spaces, and a diverse population of guests and crew from different countries. Guests and crew onboard a large passenger vessel will have close and frequent contact because of the common areas and densely populated environment [7]. This is related to the following transmission modes: person-to-person contact and contact with a contaminated intermediate host. Additionally, the air in enclosed spaces is shared by the people inside the space and the ventilation is often restricted [60]. The chance for large droplet transmission therefore increases in crowded confined spaces where individuals are relatively close together [60]. The small particle airborne transmission is the most debated transmission mode and its importance is related to the disease in question. It should be noted that large passenger vessels often have interconnected HVAC systems which theoretically means that aerosolized infectious particles can move through the entire ship. As mentioned before, the topic of ventilation will be kept outside the scope of this research project and this transmission mode will therefore be difficult to take into account. The common vehicle transmission mode is easier to apply to passenger vessels because of the shared food and water sources. The vector-borne transmission can be applicable to large passenger ships although the geographical setting might determine the insects and/or rodents that come into play. The various transmission modes and their occurrence onboard a large passenger ship have been visualized in Figure 2.1.

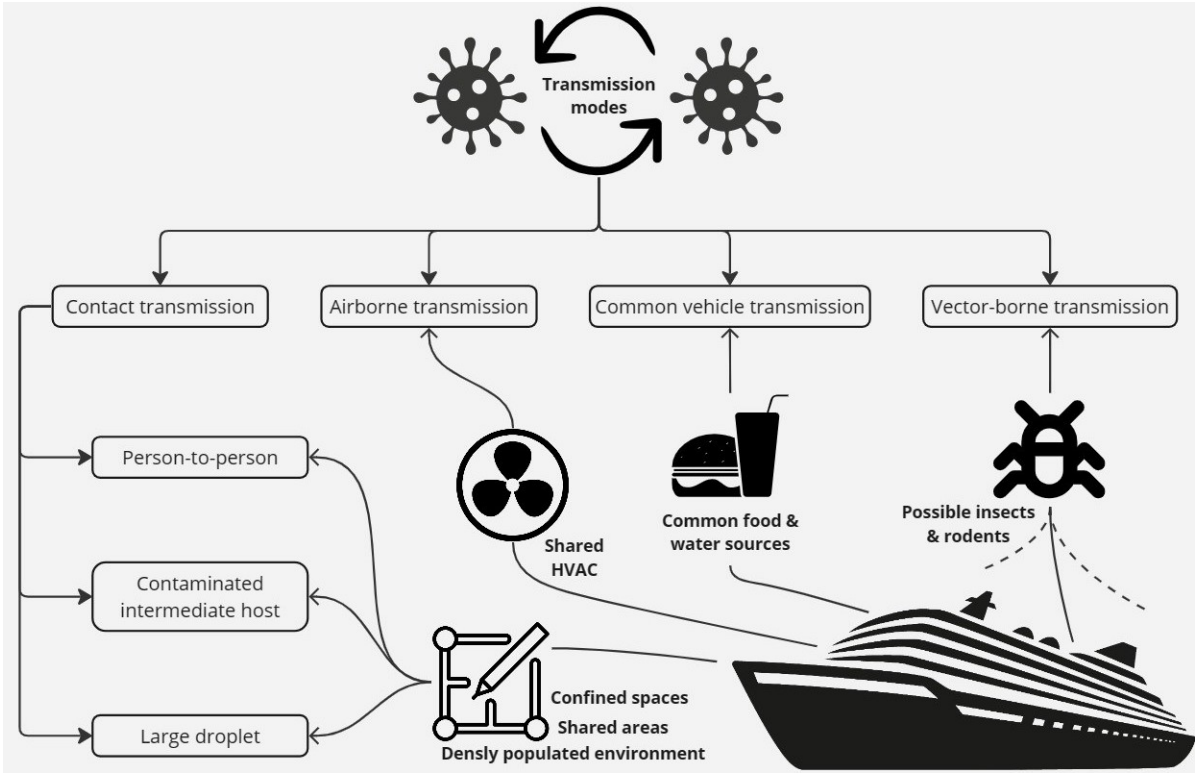

Figure 2.1: Transmission modes onboard a large passenger vessel

2.1.3. Examples: Norovirus & SARS-CoV-2

Two disease examples will be discussed in more detail: Norovirus and SARS-CoV-2. These diseases are frequently mentioned in literature concerning diseases onboard large passenger vessels. Norovirus is a gastrointestinal infection and SARS-CoV-2, also called COVID-19, is a respiratory infectious disease. Norovirus is a very contagious virus that can cause vomiting and diarrhea because of acute gastroenteritis [34]. Norovirus can be characterized by a 1-2 day incubation period and individuals are infectious for approximately 2 days [70]. Common settings where Norovirus outbreaks occur are: healthcare facilities, schools, restaurants and cruise ships [34]. The virus is transmitted faecal-orally, often starting at a common food or water source after which the virus spreads through person-to-person contact and contaminated surfaces [45]. The transmission of Norovirus already shows the complexity of disease spread as the total transmission is a combination of different transmission modes.

Since the COVID-19 pandemic, a lot of research has been done into the transmission mechanisms of this contagious coronavirus. COVID-19 has strong transmission characteristics compared to other contagious coronaviruses like SARS and MERS [101]. The Diamond Princess COVID-19 outbreak suggests an incubation period of 5 days and a 10-day infectious period for COVID-19 cases onboard a cruise ship [75]. One should note that a significant amount of COVID-19 infected individuals do not experience symptoms or they are not aware of the symptoms. For this group, the infection proceeds (initially) asymptotically which makes detection and the timely implementation of control measures more challenging [52]. The transmission mechanisms of COVID-19 are: contact transmission, droplet transmission and small particle airborne transmission [101]. Contact transmission and respiratory droplet transmission are considered primary transmission routes [10]. Transmission via fomites, previously referred to as the intermediate host transmission, is also a generally accepted transmission route for COVID-19 [82]. Virus aerosolization or the airborne transmission route for COVID-19 is, however, very much debated [10]. For the Diamond Princess outbreak, one source claims that ventilation and therefore long-range airborne transmission did not play a role in the outbreak at all [97]. Another source claims the exact opposite, namely, that airborne transmission is likely the dominant contributor in the outbreak [5]. In general, researchers seem to agree that airborne transmission could be possible and should therefore not be ignored, especially for poorly ventilated indoor and confined spaces [82, 71].

Airborne transmission is also proposed as an explanation for super spreader events which can happen in “closed environments, environments with poor ventilation, crowded places, and long duration of potential exposure” [3].

2.2. Disease prevention and control

This subsection will focus on the state-of-the-art in methods to prevent or control disease transmission onboard large passenger vessels. The subsection covers three types of interventions. The first type of interventions are related to *ship layout design* which could help limit the spread of disease and/or promote disease prevention. The second type of interventions covers *operational measures*. These measures are overarching policies implemented by for example a ship operator, a captain, a specific port or a country. These measures might include preventive screening, capacity reductions or even a complete lockdown of the vessel. The last category covers *behavioral interventions* like keeping a social distance or wearing a mask.

2.2.1. Ship layout design

The concept of using design as a way to prevent disease spread can be linked to the concept of prevention through design (PtD). This is “The concept of anticipating workplace hazards and configuring the work environment (e.g. a cruise ship) to ‘design out’ the hazards” [7]. In this situation, the hazard can be defined as a severe uncontrollable disease outbreak onboard a large passenger vessel. The design should therefore aim to prevent an outbreak from starting and facilitate outbreak control in case prevention fails. Figure 2.2 provides a summary of possible ship layout interventions. Additional background information for the specific ship layout measures can be found in Appendix A.

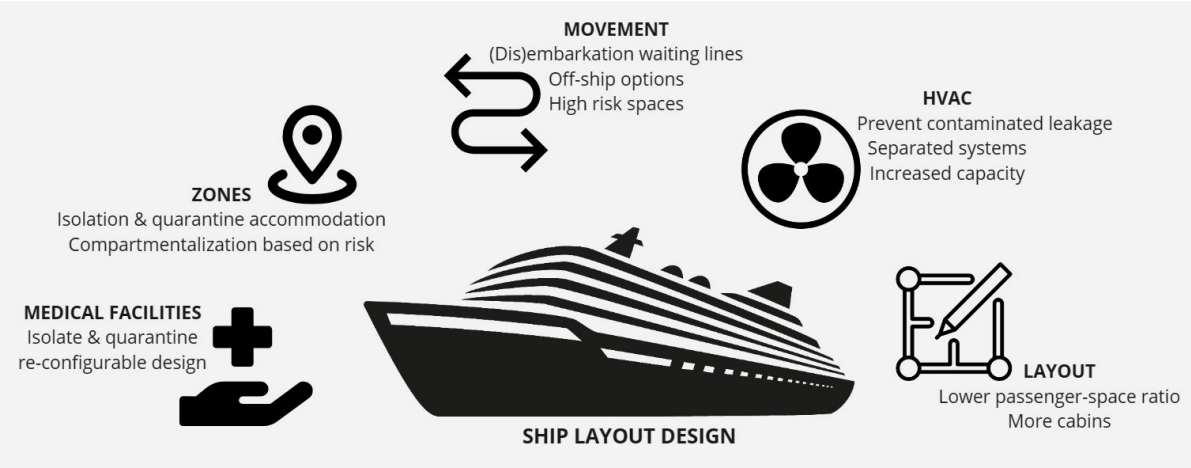

Figure 2.2: Ship layout design interventions

Current research

A literature search using the medical search terms mentioned at the start of this chapter combined with *ship design* and *ship layout* search terms, revealed one paper focused on ship layout design connected to contagious disease. This paper discusses the refit of an Italian ferry as a fast medical support vessel [80]. The paper was written as a consequence of the COVID-19 pandemic which showed the need for “a quick help, the transport of materials for med aids, the transport of mechanized tools for police missions and/or support to populations” [80]. The authors propose significant modifications to the general arrangement of a MDV 3000m fast ferry vessel built by Fincantieri [80]. For example, a helipad and morgue are installed and the entire upper deck can function as a hospital with separated HVAC, black and grey water systems[80]. The main deck is adapted to accommodate a seating area, emergency accommodation and food distribution facilities [80]. Also, the production and safe distribution of high-quality medical Oxygen is discussed as high-flow Oxygen forms an integral part of COVID-19 therapy [80]. An impression of the modifications can be seen in Figure 2.3, which shows the original general arrangement for the upper decks of the Italian ferry, and Figure 2.4 which illustrates the proposed modifications.

Additionally, one relevant project was found in a general online search using similar search terms. The specific project is the Healthy Sailing project “under the Horizon Europe Framework Programme” which started in September 2022 [32]. The project aims to: “improve the quality of passenger shipping services, facilitate recovery from the COVID-19 pandemic and make passenger shipping safer, more resilient, competitive and efficient” [32]. There are no scientific publications or results available on their website yet.

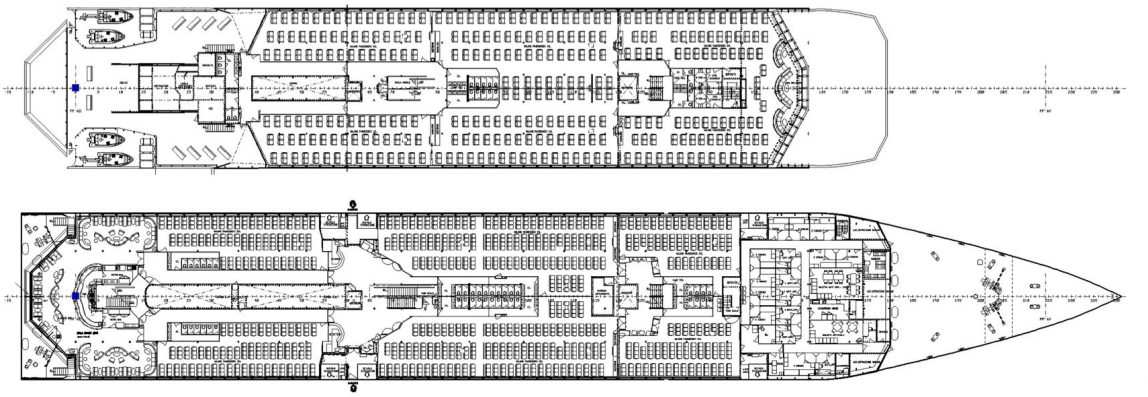

Figure 2.3: MDV 3000m original general arrangement of upper and main deck [80]

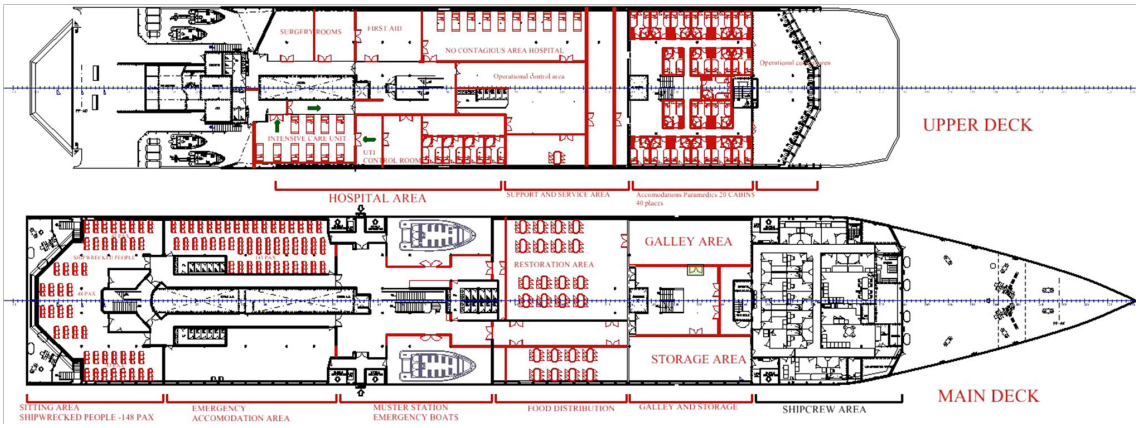

Figure 2.4: MDV 3000m modified general arrangement of upper and main deck [80]

Using ship layout design to prevent or control disease spread will always remain a complex issue. Most of the mentioned design and layout options, seen in Figure 2.2, lead to the need for a higher space versus guest ratio. Creating bigger or more cabins, adding a staircase or implementing multi-functional areas will all require space. As discussed before, space is an in-demand item onboard any ship. Design optimization for large passenger ships tries to fit a high number of guests onboard a vessel of a certain size to ensure economic feasibility. This is in direct contrast with the proposed design measures and might lead ship operators to look into operational and behavioral measures before implementing ship design adaptions.

2.2.2. Operational measures

This group of operational measures covers a selection of overarching measures regarding embarkation requirements, onboard operational routines, surveillance and management, and people movement restrictions. A visual summary of the operational measures is given in Figure 2.5. Some of the measures are related to gastrointestinal diseases (food and water) but most measures are related to respiratory infectious diseases. The different operational measures are discussed in more detail in Appendix A.

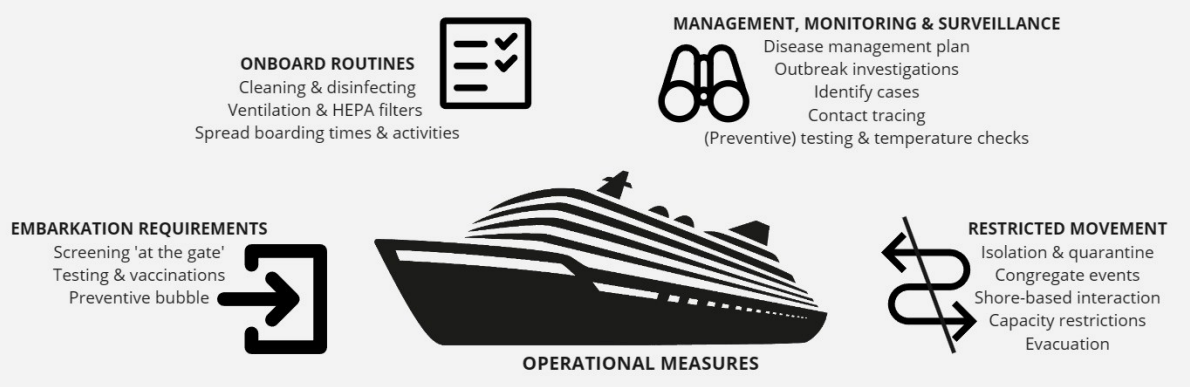

Figure 2.5: Operational measures

2.2.3. Behavioral measures

Behavioral measures are widely known since the COVID-19 pandemic. Four main categories can be recognized in Figure 2.6: PPE, social distancing, personal hygiene and vaccinations. Appendix A presents further details for the individual categories.

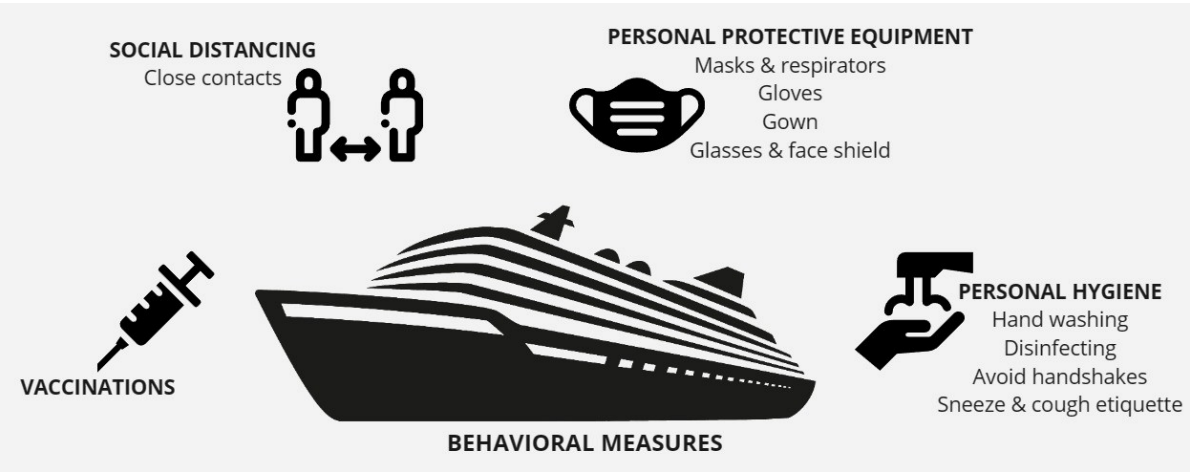

Figure 2.6: Behavioral measures

Summary

In conclusion, the possible ship layout interventions, operational and behavioral measures found in literature are summarized in Figure 2.7. These measures are connected to two real-life COVID-19 outbreak cases onboard the Diamond Princess cruise vessel (February 2020) and the USS Theodore Roosevelt (March 2020). The colors in Figure 2.7 correspond to the applied measures which could be found in literature for these specific cases [100, 97, 72, 59, 53, 75, 39, 42, 87]. Vaccinations are not relevant for these two specific outbreak cases as they occurred at the start of the pandemic and vaccinations were not yet available. For both vessels, no literature was found implementing specific ship layout design interventions. This could be due to the large consequences of these interventions and

the fact that these interventions would take significant time and funds to implement. This is especially complicated at the start of a pandemic when information was still limited and research ongoing.

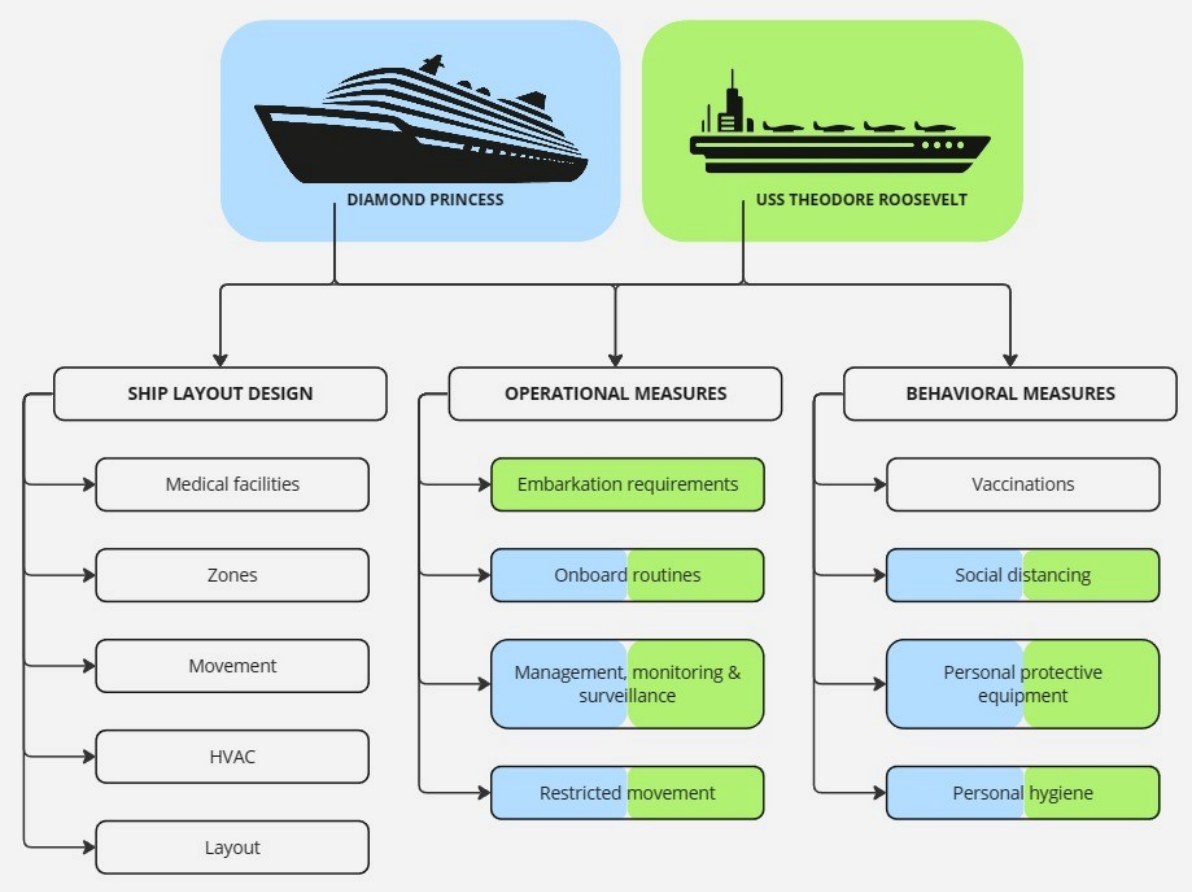

Figure 2.7: Ship layout design, operational and behavioral measures applied to Diamond Princess cruise ship and U.S.S. Theodore Roosevelt aircraft carrier

2.3. Research gap analysis

A research gap was identified during the literature review concerning contagious disease spread onboard ships, and possible interventions to limit this disease spread. The research gap is defined in more detail and given in Table 2.1. The research gap covers the initial retrofit ship design stage. In this stage, the layout is still modified and impactful design decisions might be frequently revised. It is important to take contagious disease spread into account in this design stage because the layout can still be adapted. This layout will for example cover the location, size and number of general areas, cabins and corridors. The research gap focuses on large passenger vessels as section 2.1 showed the challenge of controlling and preventing a contagious disease outbreak, specifically for this ship type.

As section 2.2 showed, there are multiple and diverse measures and interventions in order to limit contagious disease spread. The investigated parameters can be defined within three categories: ship layout design, operational and behavioral measures. The preferred result of these interventions is the limitation of contagious disease spread onboard. There is literature available analyzing past outbreaks and disease interventions on large passenger ships like the Diamond Princess cruise ship during the COVID-19 pandemic. In general, literature is mainly focused on infection rates of real-life cases and verifying infection models against real-life data sets. The research gap lies in modeling the effectiveness of a variety of different interventions, including layout adaptions, before an outbreak has happened in order to achieve a more disease resilient ship design.

Two key details were formulated in the research gap adding to the novelty of this research. The first detail has to do with the normal day movement, also called circulation, of crew and guests. Section 2.1

on disease transmission leads to the conclusion that the movement of people inside a confined space such as a large passenger vessel matters for disease spread. The movement of crew and guests onboard ships has been researched, largely to inform evacuation procedures and show compliance with ship evacuation regulations. This research often models a single movement, for example from 'a start position' to an assembly station or lifeboat. The most important output for these models is the time it takes to complete evacuation. When disease spread is investigated, a research gap can be found because disease spread is not just related to a single movement during a limited time. Instead, disease spread is related to the normal day circulation through a specific layout. This circulation will include multiple destinations in sequence based on the activities guests and crew undertake. The destinations depend on the ship layout which links to the second key detail: incorporation of movement through a layout.

Design stage	The research covers initial retrofit design
Ship type	The research focuses on large passenger vessels
Preferred result	The preferred result of the implemented measures is the limitation of contagious disease spread
Investigated parameters	The research will investigate the impact of ship layout design, operational and behavioral measures on contagious disease spread
Detail 1	The research will incorporate crew and guests circulation onboard the ship
Detail 2	The research will incorporate movement through a specified ship layout

Table 2.1: Research gap summary

3

Integrated Model Analysis

The identified research gap from the previous chapter leads into the second and third research question:

2. *What are the requirements for an integrated infection and crowd behavior model, if this model is used to investigate the effect of ship layout design, operational and behavioral measures on contagious disease spread?*
3. *Which infection model and which crowd behavior model can be combined to fulfill the requirements of research question 2?*

This second research question is answered in section 3.1. Section 3.2 and Appendix B provide an investigation into different types of movement and infection models. In section 3.3, a model analysis matches the requirements from section 3.1 with various combinations of movement and infection behavior models in order to choose the most suitable model combination for further implementation.

3.1. Model requirements

Table 3.1 presents the connections between the formulated requirements and the research gap from section 2.3. R1 and R9 are related to the design stage as converging results are required within a time frame that is acceptable for initial stage design. R2 covers the population size and is therefore connected to the vessel type. The preferred result of the simulations would be the limitation of disease spread and the simulation results should thus indicate disease performance as discussed in R3. R10 and R11 are linked to the preferred result as time spent inside a space and the space occupancy influence disease spread. The effectiveness of certain interventions on the limitation of disease spread could vary with the disease and is thus connected to R12.

R10 and R11 are also related to the investigated parameters: layout design, operational and behavioral measures. R10 and R11 specify requirements to monitor the time spent in certain spaces and space occupancy. This information can inform variations in layout design to avoid crowding. Additionally, 'time spent' information is needed to implement certain operational measures like spreading the activities of the people onboard by changing their activity schedules.

R6, R7 and R8 are requirements regarding the normal day circulation of crew and guests. These requirements cover the need for individual movement, some amount of controlled random movement, and multi-leg movement in order to model circulation realistically. R4 and R5 are the requirements needed to ensure the incorporation of ship layout, space flow and capacity limitations.

Design stage	Initial stage retrofit ship design	R1	R9		
Ship type	Large passenger vessel	R2			
Preferred result	Limiting contagious disease spread	R3	R10	R11	R12
Investigated parameters	Ship layout design, operational and behavioral measures	R10	R11		
Detail 1	Incorporating crew and guests circulation	R6	R7	R8	
Detail 2	Incorporating movement through a ship layout	R4	R5		

Table 3.1: Research gap combined with requirements

Requirement 1 - Convergence

The simulation results converge within an acceptable time frame

The first requirement states that the simulation results converge within an acceptable time frame. As a result, there are limits to the computational complexity of the model and the time it takes to run a scenario as simulation repetitions are required. The model will be used for testing variations on scenarios related to adjusted ship layout, and preventive and control measures for disease spread. Scenario repetitions provide a chance to recognize and investigate outlier results and show that the model results converge. The maximum model run time on a standard computer and the number of repeated simulations will be defined during the model development stage. If the model does become too computationally intensive for a laptop, the use of DelftBlue, the TU Delft supercomputer, should be considered.

Requirement 2 - Population size

3000-4000 Individual agents can be modeled (guests and crew)

The scope of this research focuses on large passenger vessels. The capacity of these large cruise ships can be estimated between 2500 and 3500 guests [81]. The Diamond Princess cruise ship, for example, has a total capacity of around 2700 guests and 1100 crew [73]. The total population size will also be connected to the ship layout available for modeling. Previous research using a route-choice movement model to simulate agent movement onboard a large cruise vessel used the layout data from the SAFEGUARD project [26]. This project did full-scale evacuation experiments onboard a 2500-guest passenger vessel to produce data for validation and calibration of ship evacuation models [24]. This validation data set and the corresponding ship layout might also be applicable for studying disease spread onboard large passenger vessels. Taking these two examples into account, the model should be able to simulate 3000 up to 4000 individual agents, which includes both guests and crew.

Requirement 3 - Disease performance indication

The model results indicate scenario performance for contagious disease spread
The model results indicate where *in the layout agents are most at risk for infection*
The model results enable performance comparison between different scenarios

The integrated model will be used to investigate contagious disease spread onboard a large passenger vessel. The results of the model should, therefore, say something about how well the scenario performs with respect to contagious disease spread and infections onboard. Examples of disease performance indicators are: the number of infections, the number of close contacts and infection risk. The model results also need to provide relevant data to inform the scenario variations to test. For scenarios changing the ship layout, it is relevant to know *where* agents have the highest chance of getting infected. The layout design in these locations with high infection risk could be modified to test if the infection risk can be reduced. Lastly, the results from the model should be useful for comparison between different scenarios. This research project will make certain assumptions, especially concerning medical infection modeling. The simulation results should be viewed in light of these assumptions and might lack accuracy when looking at the values themselves. However, this research specifically compares several scenarios with ship layout adaptions or implemented operational and behavioral disease

measures. The model results should enable the comparison between different scenarios and not just provide one set of results for one scenario.

Requirement 4 - Layout incorporation

The model is layout dependent
The model supports layout dimensions from 5 up to 50 meters per space

The integrated model should be layout dependent. This means that the layout of the space, in this situation a passenger vessel, is taken into consideration when modeling the movement of the agents. This is of particular importance as ship layout variations will be tested to see the performance with respect to disease infection risk. If the layout is not a variable input parameter in the model, it will not be possible to test these ship layout variations. Also, the layout will be detailed because of a high number of spaces. A large passenger vessel is not just one space in which agents move around. The layout features a significant number of small spaces, large spaces, corridors and stairs connecting the decks. The way agents move through this layout and the time they spent in certain spaces might influence the risk for infection. The layout dimensions will be in the range of 5 meters for small spaces, up to 50 meters for larger 'activity' spaces like restaurants.

Requirement 5 - Space capacity and flow

The model takes limited capacity of spaces into account
The model takes limited flow between spaces into account

In line with the requirement regarding layout, the model should also be able to account for limitations regarding the flow and capacity of spaces. The spaces themselves will have a limited capacity. When this capacity is reached, agents should not be able to move into the space until the occupancy is decreased. For disease control measures, this capacity can also be altered so that fewer people are allowed in a space at the same time. Additionally, the flow between the spaces is limited which means that the amount of agents that can change spaces is limited. For example, only one or two agents fit through a door at the same time. These limitations can lead to queuing; large occupancies in corridors and staircases even though these spaces might not be 'destination' spaces.

Requirement 6 - Individual movement

Movement can be modeled for each individual agent
Individual agent movement can be tracked and movement data is stored

To simulate a realistic situation onboard a large passenger vessel, it is important that the individual movement of agents can be modeled. A guest onboard the vessel will have a different 'schedule' than a crew member onboard the same vessel. Within the guest and crew groups, the activities and destinations throughout the day are different. It should therefore be possible to implement varying movement destinations for each individual agent. To speed up entering the input data, some overlap could be applied where for example groups of four agents have the same activity schedule. Looking at the output of the model, the movement of each agent needs to be tracked as agents with similar destinations might take varying routes to reach their destinations. Also, the movement data should be stored as this data says something about how crowded certain spaces in the layout are. This can in turn be used to inform variations on ship layout as space occupancy can influence infection risk.

Requirement 7 - Random movement

There is controlled randomness in the activities that agents undertake
There is controlled randomness in when *agents start different activities*
There is controlled randomness in the routes agents take to their destinations

As mentioned in the previous requirement, in real life, agents with similar destinations might take different routes. This can be modeled by including randomness in the way agents choose the route they take. However, a completely random choice is not realistic as this could lead agents to move from

deck 3 to deck 4 via deck 8. The length of the chosen route and the convenience of the route, like the amount of stairs, matter for the choice an agent will make. The model should thus include some degree of chance in route choice combined with an assessment of how 'good' a route is. When the simulation is run multiple times, as discussed in requirement 1, the output will differ slightly as the route choices of agents can vary. In the end, this randomness in the way agents move will provide more realistic modeling results. Also, a second and third random movement requirement relate to the activities that agents undertake during the simulation. There should be controlled randomness regarding the activities, and thus destinations, that the agents undertake. There should also be controlled randomness in the timing of these activities. These two requirements avoid the situation where all agents will visit the same activities at the same time.

Requirement 8 - Multi-leg movement

Agents can move between multiple destinations in one simulation
The time an agent stays at a single destination can be adjusted

An additional requirement related to the agent movement in the integrated model has to do with the implemented destinations. Well-known in the shipping industry are movement models simulating evacuations onboard ships. These models, however, often only implement single-leg movement with a start location and a single destination. This destination can be an assembly station or a lifeboat. When disease spread onboard a vessel is investigated, a longer time range becomes relevant. This could be a single day or even multiple days during which agents move between multiple spaces. It should therefore be possible to implement multi-leg movement. This means that agents will have multiple destinations over time in one simulation run. These destinations might be activity spaces, outside decks, a swimming pool, a crew mess or a cabin. The time the agents spent at these destinations should also be programmable. This way, an activity schedule can be implemented for both the crew and guests which represents a 'normal' day or week onboard the vessel.

Requirement 9 - Medical complexity

The medical model is as simple as possible while producing relevant results

As discussed in section 2.1, disease infection models can become complicated very quickly. There are complete studies on small particle airborne transmission in a single elevator or the infectiousness between two people talking. This level of detail is not required for this research project as its focus lies on the implications of ship layout design, operational and behavioral measures in dealing with contagious disease onboard large passenger vessels. The medical model, which is combined with the movement model, should be as simple as possible while still producing a relevant indication for disease infection performance.

Requirement 10 - Time spent

The time spent at each location is known for every agent
The time spent at each location is incorporated when calculating infection risk

As the agents move through the layout, they will spend a certain time in specific spaces. This time spent should be known and taken into account by the integrated model as it directly influences the risk for infection. The longer an agent stays in a confined space, the higher the infection risk becomes [84]. The time agents spent at their destination locations can be directly retrieved from the input data. However, it is also relevant to know the time agents spent in corridors, staircases and other spaces as they move between their destinations. These spaces on agents routes might be crowded which could relate to a higher infection risk, especially if an agent is stuck in that space for a longer period.

Requirement 11 - Space occupancy

The space occupancy is known for each time step
The space occupancy changes with the agents entering and exiting spaces
The space occupancy is incorporated when calculating infection risk

Another factor which is relevant to infection risk, is the number of agents that are in the same space at the same time. A higher space occupancy, especially in small confined spaces, can lead to a lower social distance and therefore higher infection risk [84]. Similar to requirement 10, the space occupancy should be known and incorporated when looking at the infectious disease performance. Additionally, the model should take into account that the occupancy of a space changes over time as agents enter and exit spaces on their routes. This requirement 11 is connected to requirement 4 as space occupancy cannot be determined without layout implementation. Space occupancy as value in itself could inform variations in ship layout in order to decrease crowding. This is possible as high space occupancies imply crowding when combined with a limited space volume. It is also possible to use space occupancy data from simulations and decide to limit the capacity of certain spaces as an operational measure against disease spread.

Requirement 12 - Disease specific

The model should (to a degree) take differences between diseases into account

The final requirement relates to the diseases investigated with the integrated model. In section 2.1, two examples of frequently mentioned disease onboard passenger vessels were mentioned. These examples were the Norovirus and SARS-CoV-2, and it was seen that the transmission routes are quite different. One disease might be more contagious as people spread the disease more quickly or when a smaller amount of infectious particles leads to infection. These variables influence the way a disease will spread and the risk of infection for the agents involved. Disease spread of Norovirus and other gastrointestinal diseases are primarily related to the consumption of food and/or water and transmission via the faecal-oral route [54]. These transmission routes are less compatible with the proposed model combining agent movement and disease infection. Respiratory diseases rely more on person-to-person and airborne transmission and are therefore a better match with the proposed model [62]. Coronaviruses, the flu and possibly Tuberculosis might be relevant diseases to model on ships in combination with the movement of guests and crew. For example, there is significant literature available with respect to COVID-19 disease spread onboard large passenger vessels. This literature also includes research into real-life cases which could function as reference data.

Table 3.2 provides a summary of the model requirements, answering research question 2 as formulated in section 1.1.

Requirement		Details
1	Convergence	The simulation results converge within an acceptable time frame
2	Population size	3000-4000 Individual agents can be modeled (guests and crew)
3	Disease performance indication	Model results indicate scenario performance for contagious disease spread
		Model results indicate *where* in the layout agents are most at risk for infection
		Model results enable performance comparison between different scenarios
4	Layout incorporation	Model is layout dependent
		Model support layout dimensions from 5 up to 50 meters per space.
5	Space capacity and flow	Model takes limited capacity of spaces into account
		Model takes limited flow between spaces into account
6	Individual movement	Movement can be modeled for each individual agent
		Individual agent movement can be tracked and movement data is stored
7	Random movement	There is controlled randomness in the activities that agents undertake
		There is controlled randomness in *when* agents start different activities
		There is controlled randomness in the routes agents take to their destinations
8	Multi-leg movement	Agents can move between multiple destinations in one simulation
		The time an agent stays at a single destination can be adjusted
9	Medical complexity	Medical model is as simple as possible while producing relevant results
10	Time spent	Time spent at each location is known for every agent
		Time spent at each location is incorporated when calculating infection risk
11	Space occupancy	Space occupancy is known for each time step
		Space occupancy changes with the agents entering and exiting spaces
		Space occupancy is incorporated when calculating infection risk
12	Disease specific	Model should (to a degree) take differences between diseases into account

Table 3.2: Model requirements summary

3.2. Movement and infection models

In the previous section, a set of requirements for the integrated infection and crowd model was proposed. This section aims to answer the following research question:

3. *Which infection model and which crowd behavior model can be combined to fulfill the requirements of research question 2?*

The first step is the evaluation of different movement and infection models. The movement models chosen frequently appeared in literature investigating the movement of people onboard ships or ship evacuation modeling. Also, the three model groups provide a range for the level of detail, from macroscopic pipe flow models to microscopic agent-based models. Next, three medical infection model categories were researched. These models were potential candidates for integration with the discussed crowd behavior movement models. In-depth information for both the movement and infection models is presented in Appendix B. This section only provides background information and characteristics

of the chosen movement and infection model. After researching the different models, the movement models were combined with the medical models and matched with the requirements from section 3.1. The most suitable combination, based on the requirements, was chosen.

3.2.1. Mesoscopic route choice model

Route choice models can be found in work from Narayan et al. and Van Gisbergen [64, 51, 26]. Narayan et al. present a "model combining activity and movement of guests in a cruise ship" and use the SAFEGUARD data set with this model [64]. Figure 3.1 shows a potential scenario where the agent has two activities with a 'leg' between them. This 'leg' or path taken is ship layout dependent. The novelty of this research is the modeling of guest and crew behavior onboard a large cruise ship during normal day operation. In comparison, most research is focused on evacuation scenarios with a short period and single-leg movement [64]. Van Gisbergen works with Narayan's model to further develop a large-scale simulation for a large vessel implementing an activity schedule for all crew and guests [26]. The model itself incorporates layout as a set of nodes and links. The nodes represent one or multiple spaces in the layout and the different nodes are connected via one-directional links [64]. The nodes and links can have a certain capacity and the links additionally feature a flow capacity. This flow capacity is the amount of agents that can enter or exit the link at the same time [26]. The model is agent-based as all agents make their own route choices. However, the model does not provide a Cartesian location for each agent but rather transfers the agents between nodes. Different options for the route choice model are available like: shortest path, least turns, logit or mixed logit [26]. Van Gisbergen chooses the mixed logit route choice model in his work as this model combines "path utility and path choice based on probability" [26].

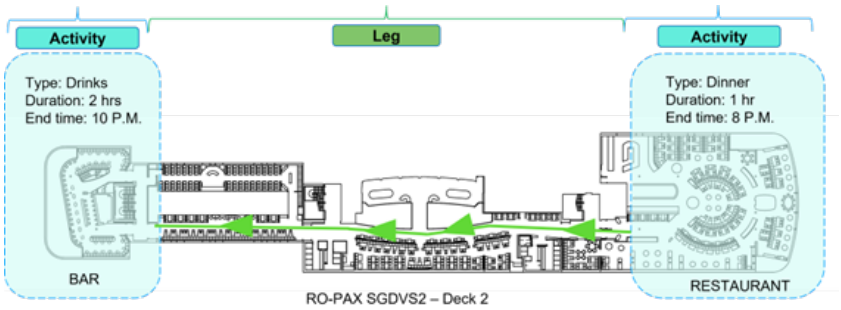

Figure 3.1: Activity-based demand with path in ship layout [64]

3.2.2. Modified Wells-Riley infection model

One of the two risk based models investigated, is the infection model developed by Sun and Zhai [84]. The goal of their research was to provide quantitative answers to the following questions: "what is the safe distance?" and "what is sufficient ventilation?" related to social distance and ventilation control strategies during the COVID-19 pandemic [84]. They directly implement a social distance index and a ventilation index in the Wells-Riley model [84]. The ventilation index will not be discussed in more detail as ventilation is outside the scope of this research project. However, the distance index could be relevant for this research project and will therefore be investigated further. The distance index is a curve fit based on "the relationship between the statistical probability of droplets in different sizes and their transmission distances based on the analysis of distribution and transmission of the experimental exhaled droplets" [84]. The following figures show how this distance index is constructed. Firstly, Figure 3.2 shows the distribution of particles for each diameter [84]. Secondly, Figure 3.3 provides the distribution of transmission distance for each diameter droplet [84]. As expected, the smaller size droplets will move away further and thus have a higher transmission distance.

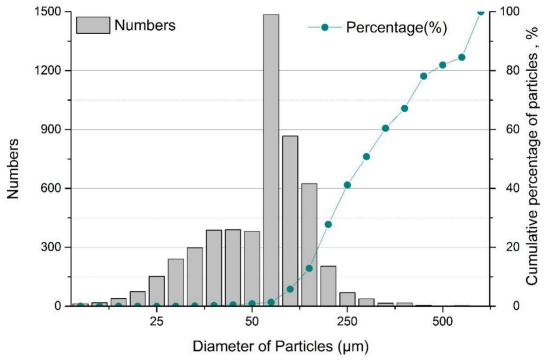

Figure 3.2: Particle size distribution [84]

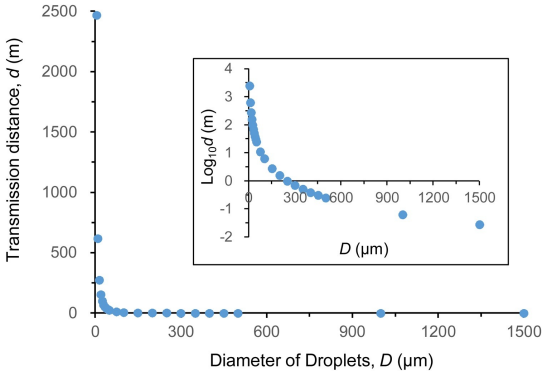

Figure 3.3: Particle transmission distance [84]

When the two distributions are combined, a probability distribution of particles against transmission distance can be constructed. This distribution is shown in Figure 3.4 [84]. The transmission distance is on the horizontal axis and the vertical axis shows the probability of different distance. This probability of different distance essentially provides a representation of exposure probability. Suppose that the transmission distance is almost zero. This means that two agents are extremely close together. In this situation, the probability of different transmission distance will be 100% because all particles will have a transmission distance larger than zero. The exposure probability will also be 100%. If a larger transmission distance is taken, for example 1 meter, the probability of different transmission distance is approximately 40%. This percentage means that 40% of all particles will have a different (larger) transmission distance than 1 meter. Therefore, these particles can cross the distance between two agents and cause infection. The exposure probability at 1 meter is therefore 40%.

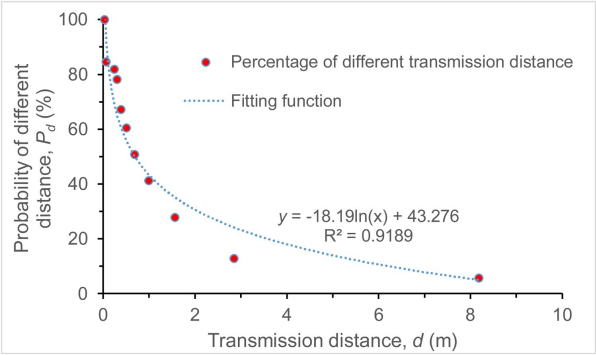

Figure 3.4: Droplet transmission distance versus exposure probability [84]

The distance index P_d is a line fit from the data in Figure 3.4 and given in Equation 3.1 as a function of social distance *d* between agents [84]. Next, the original Wells-Riley equation, shown in Equation 3.2, is combined with the distance index and a ventilation index E_z in Equation 3.3. The parameters are as follows; P_I: probability of infection, *C*: new cases, *S*: susceptible individuals, *I*: number of infectors, *p*: pulmonary ventilation rate of susceptible individuals [m^3/s], *q*: quanta production rate per infected individual [$quanta/s$], *t*: time [s] and *Q*: room ventilation rate [m^3/s].

$$P_d = \frac{-18.19\ ln(d) + 43.276}{100} \tag{3.1}$$

$$P_I = \frac{C}{S} = 1 - exp(-\frac{Iqpt}{Q}) \tag{3.2}$$

$$P_I = \frac{C}{S} = 1 - exp(-P_d\frac{Iqpt}{QE_z}) \tag{3.3}$$

It should be noted that this Wells-Riley infection probability only accounts for airborne disease transmission in a confined space. Especially for long-term exposure, other factors besides airborne transmission might become more important. These factors could be other transmission modes like person-to-person contact and contaminated host contact. The model is therefore better suited for short-term exposure situations. Also, it should be mentioned that determining the quanta production rate, is quite difficult. In literature discussing COVID-19, this value is a debated parameter which could be in a range from 10 qph to more than 2000 qph, dependent on the level of respiratory activity like singing or speaking [82, 16]. Sun and Zhai calculate the quanta production rate to be $q = 0.238\ qps = 856.8\ qph$ based on a real-life case of COVID-19 infections on a bus [84].

3.3. Model analysis

In Appendix B, all investigated crowd behavior movement and medical infection models have been presented. The possible combinations for these models are presented in Table 3.3. This table shows that five combinations are not compatible, three combinations have limited compatibility and four combinations are a potential match. The argumentation behind these different compatibilities is presented below the table. The combinations with limited compatibility and the combinations with a potential match will be reviewed against the requirements from Table 3.2. In the end, the model combination that best fits the model requirements will be chosen for further implementation.

Combination	Crowd behavior movement model	Medical infection model	Compatibility
P1	Pipe flow	Compartment	No match, movement model does not influence infection model results
P2	Pipe flow	Risk based EXPOSED	Limited match, movement model output data might be insufficient
P3	Pipe flow	Risk based modified Wells-Riley	Limited match, movement model output data might be insufficient
P4	Pipe flow	Agent-based	No match, movement model output data insufficient for medical model
R1	Route choice	Compartment	No match, movement model does not influence infection model results
R2	Route choice	Risk based EXPOSED	Limited match, movement model output data might be insufficient
R3	Route choice	Risk based modified Wells-Riley	Potential match
R4	Route choice	Agent-based	No match, movement model output data insufficient for medical model
A1	Agent-based	Compartment	No match, movement model does not influence infection model results
A2	Agent-based	Risk based EXPOSED	Potential match
A3	Agent-based	Risk based modified Wells-Riley	Potential match
A4	Agent-based	Agent-based	Potential match

Table 3.3: Crowd behavior movement and medical infection model combinations

3.3.1. Non-compatible combinations

Firstly, the non-compatible combinations will be discussed. These are the combinations where the movement model and the medical model could not be matched. This is the case for all combinations including a compartment model like SIR or SEIR. The specific combinations are: P1, R1 and A1. The main reason for this non-compatibility is the fact that the movement model is not needed to run the medical model and the movement data does not change anything in the medical model results. The compartment medical models are based on a single space or population which is well-mixed and homo-

geneous. These models assume that every individual has the same chance of contact with any other individual. Therefore, pure compartment models are independent of agent location and layout, and the results of the medical model are independent from how people move.

Two other non-compatible combinations are P4 and R4. These are the pipe flow movement model and the route choice movement model combined with an agent-based infection model. The problem with these combinations is that the agent-based medical model always requires the spatial location of all agents. The pipe flow model and the route choice model do not provide this data. The pipe flow model is not based on individuals moving through the system as the model only looks at flow. The route choice model is agent-based but does not provide the spatial location either. The model moves agents from node to node but does not provide the location or distance between agents who are located on the same node. In the end, the output of these two movement models is insufficient for implementation with an agent-based medical model.

3.3.2. Limited compatible combinations

The limited compatible combinations are P2, P3 and R2. P2 is the combination of a pipe flow model and the EXPOSED risk based model. There is limited compatibility as the pipe flow model does not look at individual agents and it is therefore not possible to count contacts within a certain radius of an agent. The movement model output is insufficient to match directly with the infection model. P3 is the combination of a pipe flow model and the modified Wells-Riley model. A similar challenge arises for this combination as the modified Wells-Riley model requires information on social distance and the time spent in a certain situation. The movement model output is, again, insufficient to match directly with the medical model. For both combinations, there might be options to link ‘pressure’ from the pipe flow model to either chance of infection or expected social distance as the ‘pressure’ says something about crowdedness somewhere in the layout. P2 and P3 are labeled as limited compatible because finding actual relations between these factors could prove challenging.

The last limited compatible combination is R2 which combines the route choice model with the EXPOSED model. The route choice model would provide more detailed data than the pipe flow model for the movement of crew and guests. The EXPOSED model does require the locations of agents in order to determine close contacts. Within the route choice model, the agent space location for a specific time step is known, but the exact Cartesian location is not. Similar to pressure in the pipe flow model, space occupancy might be an indication for a contact probability as input for the EXPOSED model. In conclusion, these three combinations only have limited compatibility as the disease performance indication is based on indirect relations between the movement output data and the medical model input (like social distance and close contacts). The questionable quality of the disease performance indication is also visible in Table 3.4; where the models are compared to the set of requirements.

For the pipe flow combinations P2 and P3, the combinations do not meet the requirements for individual, random and multi-leg movement. This is related to the pipe flow movement model which does not have this level of detail. P2 and P3 also do not meet the requirements related to tracking the time agents spent at locations and the space occupancies. Both risk-based medical models are not overly medically complex and meet the medical complexity requirement. The EXPOSED model is not disease specific; as the authors behind the model ought to create a generic model that could work for multiple diseases [76]. The modified Wells-Riley is disease specific because the quanta values implemented are disease specific.

R2 meets almost all requirements except for being disease specific and the disease performance indication remains questionable. As discussed before, the combination is not diseases specific as the EXPOSED medical model is generic by design. Implementing a route choice model instead of a pipe flow model means that there are more options with respect to the movement of the agents. The individual, random and multi-leg movement requirements are met. Also, the route choice model provides information on the time agents spent in certain spaces and the space occupancy is known.

	Requirement	Combination		
		P2	P3	R2
1	Convergence	✓	✓	✓
2	Population size	✓	✓	✓
3	Disease performance indication	~	~	~
4	Layout incorporation	✓	✓	✓
5	Space capacity and flow	✓	✓	✓
6	Individual movement	✗	✗	✓
7	Random movement	✗	✗	✓
8	Multi-leg movement	✗	✗	✓
9	Medical complexity	✓	✓	✓
10	Time spent	✗	✗	✓
11	Space occupancy	✗	✗	✓
12	Disease specific	✗	✓	✗

Table 3.4: Requirement analysis for limited compatible combinations

3.3.3. Compatible combinations

The last category covers combinations which are expected to be compatible. The combinations are: R3, A2, A3 and A4. R3 is the combination of a route choice and a modified Wells-Riley model. The risk-based modified Wells-Riley model requires a social distance and time spent in a certain situation as input parameters to determine infection risk. The route choice model does not provide spatial locations, which leads to the limited compatible combination R2, but it does provide node locations for each agent over time. This location data could easily be converted to an expected social distance based on the number of agents on a node and the floor area that the node covers.

The three other compatible combinations feature agent-based movement models. These combinations are expected to be compatible as the agent-based movement models are detailed models and provide the spatial location for each agent over time. This information on the location of agents is sufficient input for the EXPOSED model, modified Wells-Riley model and an agent-based infection model. For the EXPOSED model, the spatial location can be used to determine the number of close contacts and determine the agents between these contacts occur. The exposure matrix is then created for each agent. The spatial location from the movement model can also be used to determine average social distance as a value to be used in the Wells-Riley model. The compatibility of the agent-based movement and agent-based medical model speaks for itself. This A4 combination is the only combination where sufficient data is available for an agent-based medical infection model.

	Requirement	Combination			
		R3	A2	A3	A4
1	Convergence	✓	✗	✗	✗
2	Population size	✓	~	~	~
3	Disease performance indication	✓	✓	✓	✓
4	Layout incorporation	✓	✓	✓	✓
5	Space capacity and flow	✓	✓	✓	✓
6	Individual movement	✓	✓	✓	✓
7	Random movement	✓	✓	✓	✓
8	Multi-leg movement	✓	~	~	~
9	Medical complexity	✓	✓	✓	~
10	Time spent	✓	✓	✓	✓
11	Space occupancy	✓	✓	✓	✓
12	Disease specific	✓	✗	✓	✓

Table 3.5: Requirement analysis for compatible combinations

In subsection 3.3.2, it was shown that combination R2 meets almost all requirements except for the disease performance indication requirement and the disease specific requirement. Combination R3 meets all requirements as the modified Wells-Riley model is disease specific. Also, the disease performance indication requirement is met as the connection between the output of the movement model and the input of the medical infection model is direct. For R3, the agent node locations can be converted to space occupancy which can be linked to social distance. This provides a higher quality disease performance indication than the indication for combination R2; where close contacts were related to close contact probability based on space occupancy. Additionally, the social distance for R3 is location specific which is useful when layout changes and operational or behavior measures are to be evaluated.

The combinations A2, A3 and A4 show some similarities when these combinations are compared with the requirements. First of all, there are concerns that these models will not provide results that converge within an acceptable time frame. The level of detail for these models leads to long run times and the need for extensive computational power. It is expected that the convergence requirement, within an acceptable time frame, is therefore not met. This requirement is important as this research aims to test a large number of different scenarios to compare ship layout and the efficiency of various measures. The convergence requirement is also connected to the population size the models can deal with. The population sizes for large passenger vessels might cause long run times to achieve convergence for the results. For combination A4, it would be possible to account for different transmission modes and assign every agent a state (like infected or susceptible). This model can account for individuals transitioning between different disease states and it is possible to 'see' the infection progress over time via specific individuals. This type of modeling requires a longer time frame as it may take multiple days for the disease to spread. A4 is therefore even more complex and possibly time-intensive than combinations A2 and A3. One could argue that the medical complexity of A4 is too large. The considerations regarding convergence, population size and medical complexity can also be seen in Table 3.5.

A2, A3 and A4 show potential for layout incorporation, queuing and disease performance indication. They also meet the individual and random movement requirements. However, the multi-leg movement requirement might require some attention. This has to do with the fact that most agent-based movement models are based on complete random movement of all agents inside a layout or single-leg movement. The multi-leg movement requirement specifies that it should be possible to assign multiple locations and model the agent executing an activity schedule. Some adaptions might be needed to be able to implement this multi-leg movement. Lastly, A2 features the EXPOSED model which is not disease specific and as a result, the last requirement is not met.

3.3.4. Model combination choice

Summarizing, this subsection has covered possible combinations of the movement and medical infection models as described in section 3.2, section B.1 and section B.2. The combinations that demonstrated limited compatibility or compatibility were tested against the set of model requirements from section 3.1. Combination R3 is the only combination that meets all requirements. This combination integrates a route choice movement model with a modified Wells-Riley infection model and calculates infection risk for each individual at different times in the simulation. The combination is not as complex and time-intensive as the agent-based movement models but does provide a strong disease performance indication. Also, the disease performance indication is layout dependent so different layouts can be investigated and compared. In conclusion, combination R3 meets all requirements and this combination is going to be developed further. A research proposal, integrating model combination R3, is described in the next chapter.

4

Integrated Model Architecture

This chapter will provide an overview of the developed model integrating a modified Wells-Riley infection model and a crowd behavior model. The chapter answers the follow research question:

4. *What is the architecture of the integrated infection and crowd behavior model?*

The first section provides background on the chosen movement model: a route choice model (RCM) initially developed by Narayan et al. and adjusted by Van Gisbergen [64, 26]. The second section describes the integrated model which connects the RCM results and modified Wells-Riley infection model. Thereafter, the third section will report on small-scale test cases which were used to verify and test the model.

4.1. Route choice movement model

The high-level structure of the route choice model described by Narayan et al and Van Gisbergen, can be found in Figure 4.1. The model is written in C++ and run in Microsoft Visual Studio 2022 with an academic license. First, the file system is defined and eighteen start parameters are specified. The start parameters are given in Table 4.1. Within the main() function, output folders are created and a clock is defined so that the elapsed time can be given at the end of a run simulation. The simulationruns() function is called within the main() function and three steps can be distinguished within this simulationruns() function. The initialize function makes sure that the flow, capacity and length parameters are set to zero at the start of the simulation. In the second step, output files for flow, link occupancy and output times are created within the output folders created under the main() function. The activity and mobility simulator can be run after these two steps and Figure 4.2 shows the simulator process.

Agents & layout	Time & repetition	Chosen route choice model	Path separation
agent_data	simulation_time	R_C_M	path1
network_data	time_step	turn_penalty	path2
number_of_agents	number_of_runs	angular_penalty	path3
number_of_nodes		double gamma	
number_of_links		draws	
		direction_angular_threshold	

Table 4.1: Start parameters route choice model

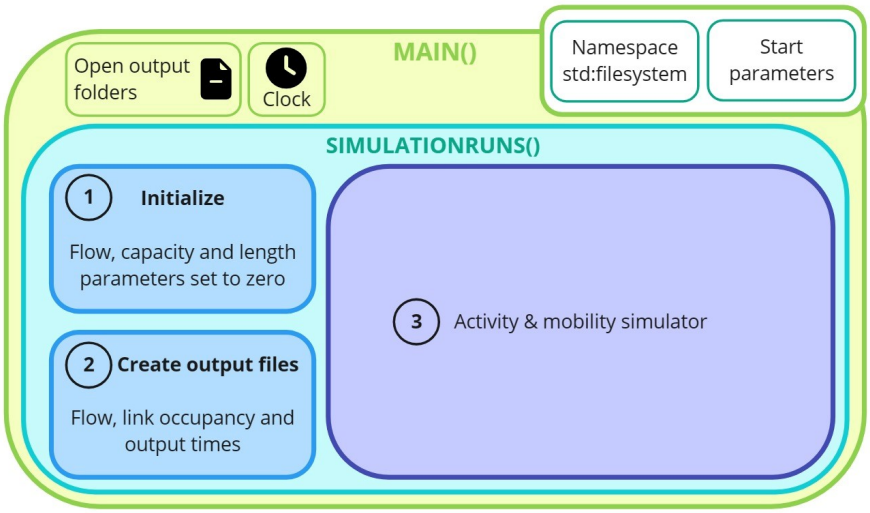

Figure 4.1: Route choice simulation - overview

Figure 4.2 shows the process in the activity/mobility simulator. This process is run for each agent for every timestep. The process features four states that the agent can have: activity, wayfinding, walk and stay. The wayfinding state has been highlighted as it features some complex considerations which will be explained in more detail in Figure 4.3.

- *Activity*
  The simulation is initialized at the activity state to avoid “all agents starting to walk at the same time once the simulation has started” [26].
- *Wayfinding*
  The agent will move to the wayfinding state if the activity time at a certain location has been completed. The activity node location and the duration of the activities are stored in an activity schedule which looks like Table 4.2. The path to the next destination node is determined in the wayfinding state.
- *Stay*
  The agent will be assigned the stay state when the wayfinding state is completed. The agent remains in this state if the capacity of the next link does not allow movement.
- *Walk*
  The agent moves from the stay state to the walk state. The agent keeps walking as long as the link and flow capacities are smaller than the set maximum. When the end of a link has been reached and that link is the last link in the determined path, the agent is transferred to the activity state, provided that the entire schedule is not yet finished. If the link is not the last link in the determined path, the agent iterates over the next link between two nodes. The simulator will end when the activity schedules for all agents have been completed.

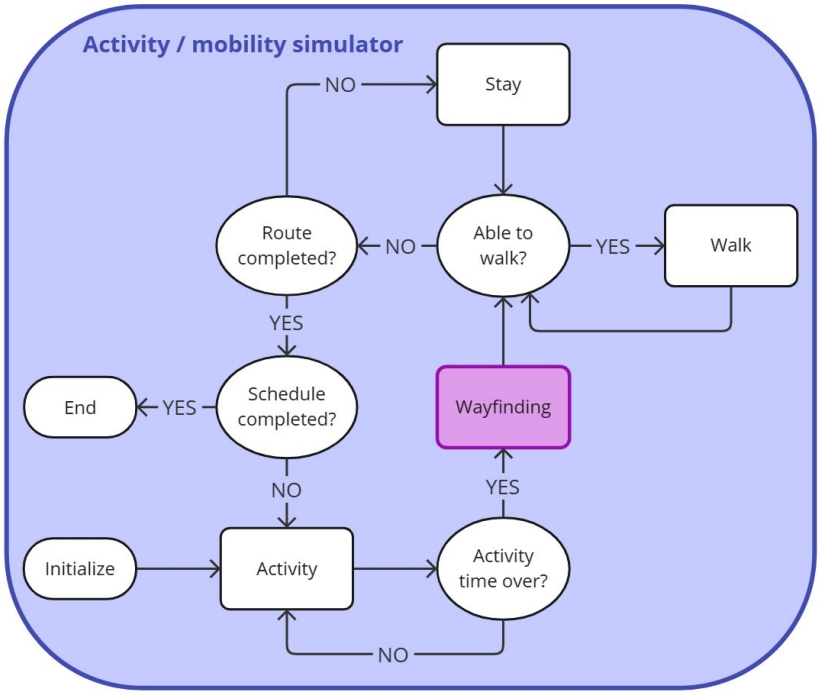

Figure 4.2: Route choice simulation - activity and mobility simulator

agentID	speed	start	activation time	end1	activity1	end2	activity2	end3	...
0	1.2	286	1800	262	7200	372	7200	203	...
1	1.2	55	1800	272	7200	201	7200	3	...
2	1.2	327	1800	367	7200	325	7200	2	...
3	1.2	133	1800	220	7200	142	7200	57	...
...	...	...	...	...	...	...	...	...	...

Table 4.2: Example of activity schedule structure [26]

Van Gisbergen implemented path separation for the wayfinding state in order to decrease the computational time for longer routes [26]. The path separation can be seen in Figure 4.3 and the adjusted path generator 2 is only called when the start and end node are far enough apart. If the path does not qualify, the regular path generator will calculate a single path list. The size of this list can be adjusted in terms of the variation, and the route choice model will choose its final path from this list. For longer paths, the new path generator will create four lists between staircase 1 and staircase 2 as they connect the entire ship [26]. The final path is the combination of two paths which takes the least amount of time to complete.

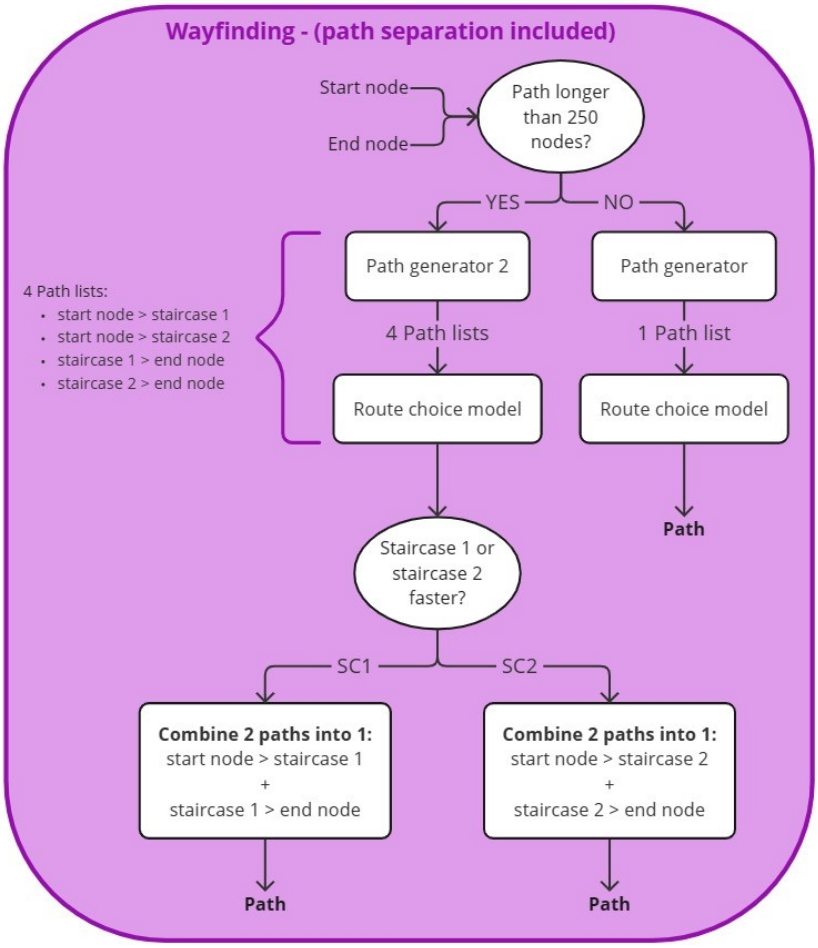

Figure 4.3: Route choice simulation - wayfinding state (path separation included)

4.2. Integrated model architecture

This section provides an in-depth explanation for the developed Python model connecting the movement and infection model. Agent location, state and link occupancy results from the RCM, as described in section 4.1, are used as basis input for the developed model. In subsection 4.2.6, the modified Wells-Riley infection model can be recognized and this subsection also describes how the infection model is implemented. The model output is a matrix providing agent-specific infection risk for every timestep over a day. The model is run in Spyder, a free and open-source IDE for Python. Figure 4.4 shows an overview of the model architecture and the various elements will be discussed in more detail in the subsections below the figure.

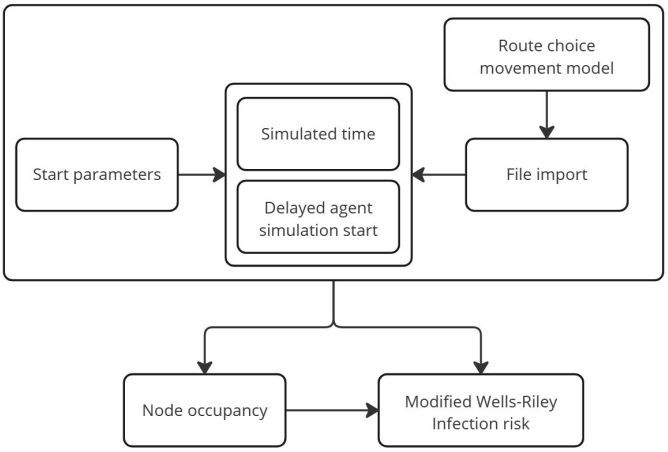

Figure 4.4: Model architecture - overview

4.2.1. Start parameters

At the start of the model, eleven important parameters are defined. The parameters and their assigned values can be seen in Table 4.3. In the model, it is possible to run a limited calculation when only part of the full simulation time (a day) is used. A partial time can be defined using the 'partial time simulation' and 'simulated time' parameters. The model will automatically run a full simulation if the 'partial time simulation' parameter is set to zero. The table also shows medical and ventilation parameters which are integral to the modified Wells-Riley infection risk calculation and are thoroughly investigated in chapter 5.

Parameter	Description	Assigned value	Unit
Number of links	Amount of connections between locations in the layout	968	[-]
Number of nodes	Amount of locations in the ship layout	389	[-]
Number of agents	Amount of agents in the simulation	2848	[-]
Partial time simulation	Decision to run a full or limited calculation	1 (full) or 0 (limited)	[-]
Simulated time	Define time steps for partial simulation	0 - 86400	[s]
I	Number of infectors	Discussed in chapter 5	[-]
p	Pulmonary ventilation rate of susceptible individuals	Discussed in chapter 5	$[m^3/s]$
q	Quanta production rate per infected individual	Discussed in chapter 5	$[quanta/s]$
ACH	Air changes per hour	Discussed in chapter 5	[-]
H_c	Average ceiling height	Discussed in chapter 5	[m]
Q_z	Ventilation index	Discussed in chapter 5	[-]

Table 4.3: Start parameters for integrated model

4.2.2. File import

Besides the start parameters, more information with respect to agent location, agent state, link occupancy and layout dimensions is required in order to calculate infection risk. Agent location, agent state and link occupancy are directly retrieved from a completed route choice movement simulation and this data is therefore scenario-dependent. The route choice model determines the length of each link as

part of the calculation and, therefore, link length can also be directly used from the RCM model. Additionally, node area, link length and link ID are used in the model to determine location specific average social distance.

Agent location
The from-node $[FN]$ and to-node $[TN]$ matrices provide agent location over time. Every row is a time step of 1 second with $t = [t_0, t_1, \cdots, t_q, \cdots, t_f]$. The maximum number of rows is related to the activity schedule and will be less than 1 day or 86400 seconds (rows). Every column represents an $agent_{ID} = [0, \cdots, i, \cdots, n]$. A structural example of the FN and TN location matrices is given in Equation 4.1 and Equation 4.2. The location can be a node (for the activity state) or a link (for other states). The location file is required as the agent location indicates the time spent at a certain location and the location itself will be linked to a social distance indication. These parameters are both needed in the modified Wells-Riley model.

$$FN_t^i = \begin{bmatrix} fn_{t0}^0 & \dots & fn_{t0}^i & \dots & fn_{t0}^n \\ \vdots & \ddots & \vdots & \ddots & \vdots \\ fn_{tq}^0 & \dots & fn_{tq}^i & \dots & fn_{tq}^n \\ \vdots & \ddots & \vdots & \ddots & \vdots \\ fn_{tf}^0 & \dots & fn_{tf}^i & \dots & fn_{tf}^n \end{bmatrix} \quad (4.1) \qquad TN_t^i = \begin{bmatrix} tn_{t0}^0 & \dots & tn_{t0}^i & \dots & tn_{t0}^n \\ \vdots & \ddots & \vdots & \ddots & \vdots \\ tn_{tq}^0 & \dots & tn_{tq}^i & \dots & tn_{tq}^n \\ \vdots & \ddots & \vdots & \ddots & \vdots \\ tn_{tf}^0 & \dots & tn_{tf}^i & \dots & tn_{tf}^n \end{bmatrix} \quad (4.2)$$

Agent state
The state output file is a matrix which specifies the agent state over time. Again, the rows represent time steps and the columns represent agents. An example of this matrix is presented in Equation 4.3. This file is required to get more insight into agent states during the simulation. Especially the activity state is important because the agent is not located inside a link but rather on a specific node. This activity location will have certain dimensions and a specific occupancy which can be translated to average social distances.

$$S_t^i = \begin{bmatrix} s_{t0}^0 & \dots & s_{t0}^i & \dots & s_{t0}^n \\ \vdots & \ddots & \vdots & \ddots & \vdots \\ s_{tq}^0 & \dots & s_{tq}^i & \dots & s_{tq}^n \\ \vdots & \ddots & \vdots & \ddots & \vdots \\ s_{tf}^0 & \dots & s_{tf}^i & \dots & s_{tf}^n \end{bmatrix} \quad (4.3)$$

Link occupancy
The average link and node social distance is determined using the space dimensions combined with node and link occupancy. The node occupancy is not directly available from the route choice model and will be calculated in subsection 4.2.5. However, the link occupancy is directly available and in the structure as shown in Equation 4.4 with $link_{ID} = [1, \cdots, i, \cdots, m]$.

$$LO_t^i = \begin{bmatrix} lo_{t0}^1 & \dots & lo_{t0}^i & \dots & lo_{t0}^m \\ \vdots & \ddots & \vdots & \ddots & \vdots \\ lo_{tq}^1 & \dots & lo_{tq}^i & \dots & lo_{tq}^m \\ \vdots & \ddots & \vdots & \ddots & \vdots \\ lo_{tf}^1 & \dots & lo_{tf}^i & \dots & lo_{tf}^m \end{bmatrix} \quad (4.4)$$

Link length and node area
Both the link length and node area are imported as vectors. The link length is calculated in the RCM model and the vector $[LL]$ thus provides the length in meters for each link with $link_{ID} = [1, \cdots, i, \cdots, m]$. The node area is defined in a similar way where the vector provides the area for each node in meters squared and $node_{ID} = [1, \cdots, i, \cdots, w]$.

$$LL_i = \begin{bmatrix} ll_1 & \dots & ll_i & \dots & ll_m \end{bmatrix} \tag{4.5}$$

$$NA_i = \begin{bmatrix} na_1 & \dots & na_i & \dots & na_w \end{bmatrix} \tag{4.6}$$

Link ID
A final imported file is connected to the links because the link ID number needs to be derived from the agent from- and to-node in the model. Therefore, a file with every link ID and the corresponding nodes is imported as shown in Equation 4.7. The first row defines the from-nodes and the second row defines the to-nodes. The index of this matrix corresponds to the link ID numbers. The nodes are not necessarily presented in an ascending order.

$$LD_i = \begin{bmatrix} ld_1 & \dots & ld_i & \dots & ld_w \\ ld_1 & \dots & ld_i & \dots & ld_w \end{bmatrix} \tag{4.7}$$

4.2.3. Simulation time
The simulation time is determined based on the size of the imported state matrix for a full calculation. This, because the RCM simulation time differs slightly for each run and the output matrices will thus have different sizes each time the RCM is used. The 'simulated time' start parameter will be used as input when a partial calculation is chosen.

4.2.4. Delayed agent simulation start
In the RCM model, the agents will not start the simulation all at the same time. This results in agents whose from-node and to-node are zero as they are not yet participating. However, these agents are onboard the ship at some location. To compensate for this delayed start, the agents are put at their initial location even if they have not yet started the simulation. Listing C.1 shows the Python code used to compensate for this delayed start. The values in the $[No]$ vector are used in situations where agent locations are still zero.

4.2.5. Node occupancy
At this point, the node occupancy can be calculated as the start parameters are defined, the run time is determined and the required files are imported. Listing C.2 provides the Python code used to calculate the node occupancy. The node occupancy is calculated using a nested loop over the run time and the number of agents. The node occupancy is determined at each timestep and the agent-loop is therefore inside the time-loop. An agent is located at a node during an activity or when the activity schedule is completed. For all other states: wayfinding, stay, walk, the agent is located on a link and the corresponding link occupancy has already been determined by the RCM. When the agents' from-node is zero, the first non-zero from-node will be used as described in subsection 4.2.4.

4.2.6. Infection risk
The infection risk calculation can be divided into four parts and these four parts are discussed separately. The first part concerns the nested loop and exposure time reset, and can be found in Listing C.3. The second part of the calculation determines the average node social distance for agents in the activity or end state. After this calculation, the average link social distance for agents in the wayfinding, wait or walk state is calculated. The final step is the risk calculation using the medical start parameters and the average node/link social distance.

Similar to the nested loop in subsection 4.2.5, this nested loop is also defined over time and the number of agents. However, the sequence of the loops is different as the calculations are done for every agent going through all time steps tracking the exposure time. The exposure time is reset for three situations:

- Moving to a new agent
- When an agent changes spaces
- When an agent starts an activity

The second step, given in Listing C.4, features the calculation of the average social distance for agents located at a node. The social distance index is set to zero when the node occupancy is 1, because there can not be an infector present. The average social distance is determined using the appropriate node area and node occupancy. This average social distance is used to calculate the social distance index according to the paper by Sun and Zhai [84].

After some initial testing, it turned out that the social distance index becomes negative for a social distance larger than $d \approx 10.8m$. The agents will not have an 'infectious' effect on each other as they are too far apart, according to the particle model used by Sun and Zhai [84]. The social distance index in the integrated model is therefore set to zero for this specific situation as seen in Listing C.4.

Listing C.5 shows the third step of the infection risk calculation. This step results in the average social distance index for agents located on a link. This is the case for agents in the wayfinding, walking and waiting state. The from-node and to-node are retrieved from the input files. These nodes are agent and timestep specific and are used to find the associated link ID number. After this, the social distance index can be calculated. Similar to the second node calculation step, the social distance is also set to zero when the social distance is too large or when there is no infector present in the space.

The final part of the integrated model is found in Listing C.6. This part features the actual infection risk calculation for every agent at every timestep. The results are stored in an empty matrix. Infection risk is dependent on the ventilation rate, medical parameters, the social distance index, the ventilation index and the exposure time. The location-specific ventilation rate is calculated based on the air changes per hour (ACH) and location area. The choice for a variable ventilation rate, incorporating the ACH parameter, is preferred over an average ventilation rate for all spaces, as a constant ventilation rate would lead to overestimated ventilation for small spaces and underestimated ventilation for large spaces.

4.3. Small-scale test cases

This section describes five small-scale test cases which were used for the initial verification of the integrated model. The RCM model input, like from-nodes or state files, is not used for these test cases. Instead, representative arrays and matrices for location, state and link-occupancy are defined for each test case and directly used within the model. The medical parameters are, for now, chosen based on the work of Sun and Zhai and given in Table 4.4 [84].

Parameter	Description	Assigned value	Unit
I	Number of infectors	1	[-]
p	Pulmonary ventilation rate of susceptible individuals	$8.333 * 10e-5$	$[m^3/s]$
q	Quanta production rate per infected individual	0.238	$[quanta/s]$
ACH	Air changes per hour	15	[-]
H_c	Average ceiling height	2.35	[m]
E_z	Ventilation index	1	[-]

Table 4.4: Medical parameters for integrated model [84]

4.3.1. Test case 1,2 and 3 - stationary agents

The first three test cases relate to stationary agents at three different locations. A vector or matrix for link occupancy has not been defined as agents are not moving and the link occupancy is thus zero for all links over the run time. The locations in the test cases are related to the SAFEGUARD project layout for the Radiance of the Seas cruise ship operated by Royal Caribbean International [23]. Additional ship specific information is given in chapter 5 when the sample case is defined, and the deck plans can be found in Appendix D.

The first test case features one stationary agent located in the aft restaurant at deck 5 (node 104). The restaurant has a capacity of 477 people over 363 square meters. The location, from-node and to-node, does not change and the agent is in an activity state.

The second test case models two stationary agents in three different locations: node 104 (restaurant deck 5), node 15 (corridor deck 2) and node 17 (small corridor deck 2). The floor area of node 15 is approximately 6 m^2 and 2 m^2 for node 17. The third test case models four stationary agents at node 15 and node 17. All three test cases are run for 1 hour.

Test case	**1**	**2A**	**2B**	**2C**	**3A**	**3B**
Number of agents	1	2	2	2	4	4
Run time [s]	3600	3600	3600	3600	3600	3600
From-node	105	105	16	16	16	16
To-node	104	104	15	17	15	17
State	1	1	1	1	1	1

Table 4.5: Test case 1,2 and 3 - characteristics

The results of test cases 1, 2 and 3 are given in Figure 4.5 up to Figure 4.10. Figure 4.5 and Figure 4.6 show a constant infection risk of zero. For test case 1, this can be explained by the fact that there is no infector in the space, just a single agent who can not infect itself. Test case 2A gives a similar result but for a different reason as the space and thus the social distance is too large for two agents to have an impact on each other. This test case also demonstrates an assumption with respect to the average social distance: agents distribute themselves over the available space. In reality, this might not be the situation as agents in a large space group together, resulting in a smaller social distance.

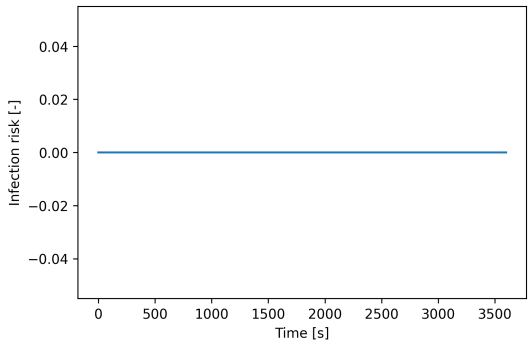

Figure 4.5: Test case 1 - infection risk

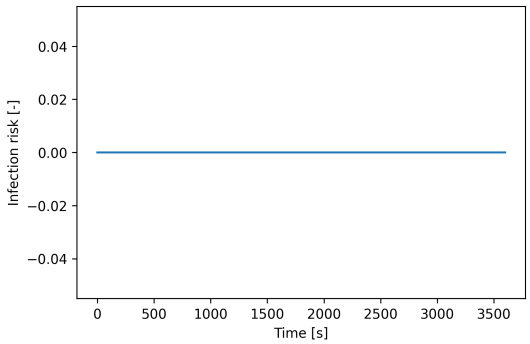

Figure 4.6: Test case 2A - infection risk

Figure 4.7 and Figure 4.8 present the results for two stationary agents at two locations on deck 2. Both figures show that the infection risk increases over time according to an exponential relationship where Figure 4.8 asymptotically approaches a 100% infection risk. This behavior can be explained by the modified Wells-Riley equation used to calculate infection risk, given in Equation 3.3. These two figures also show that the smaller space in test case 2C, results in higher infection risks reached after a shorter amount of time. These test cases thus indicate that a difference in the space area matters for the infection risk results.

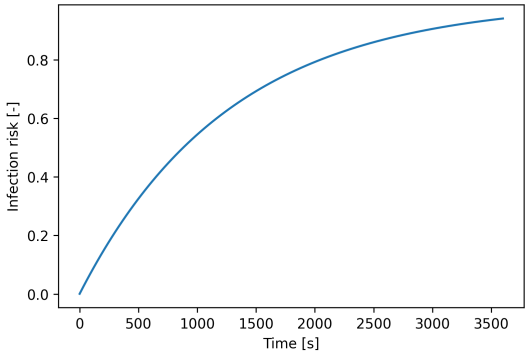

Figure 4.7: Test case 2B - infection risk

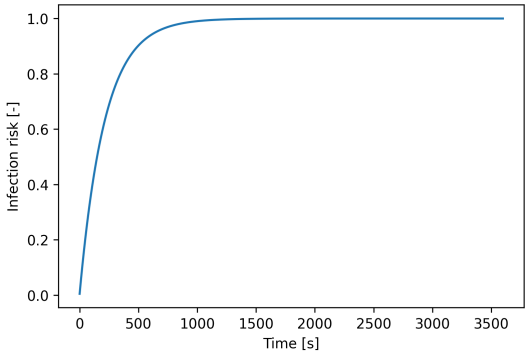

Figure 4.8: Test case 2C - infection risk

The results for test cases 3A and 3B are given in Figure 4.9 and Figure 4.10. The infection risk gives similar outcomes concerning test cases 2B and 2C. This is expected as the test cases only differ in the number of agents involved and the locations stay the same. The agents in test case 3A reach higher infection risks than the agents in test case 2A and they also reach these risks after a shorter time. This can be explained by the smaller average social distance because the space is shared by four agents instead of two. Also, for test case 3B, the infection risk approaches 100% more quickly because of the smaller social distance. Comparing test cases 2B and 2C with 3A and 3B leads to the conclusion that the number of agents in a space has, as expected, an (increasing) effect on infection risk.

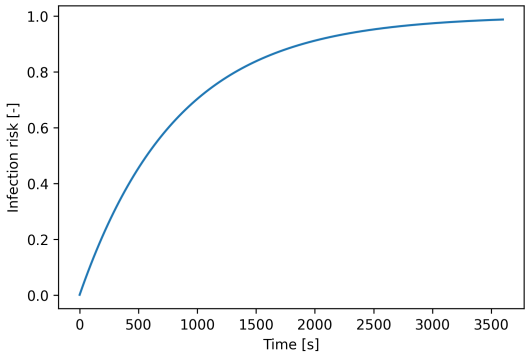

Figure 4.9: Test case 3A - infection risk

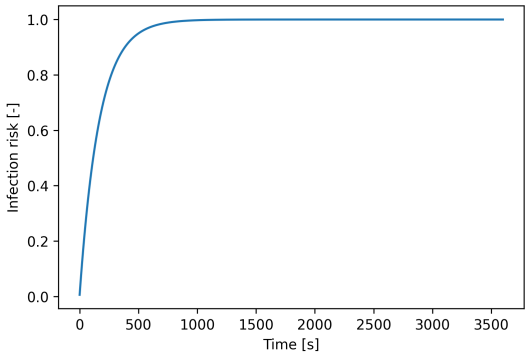

Figure 4.10: Test case 3B - infection risk

4.3.2. Test case 4 - two moving agents

Test case 4 models two agents who move from a 6 m^2 corridor on deck 2 (node 15) to a 2 m^2 corridor on deck 2 (node 17) via node 16 which connects these two locations. The agents move together and the specific data defined for this test case is presented in Table 4.6. The infection risk for the test case is given in Figure 4.12. Three conclusions can be drawn from this figure. Firstly, the infection risk increases over time as long as the agents stay in the same space. Secondly, the infection risk goes to zero when the agents change spaces around timestep 3600 s. The time which is spent walking from node 15 to 16 and from node 16 to 17 is short and does not give high infection risk values. Thirdly, the risk does increase significantly when the agents arrive at the second location, time step 3840 s, which features a smaller space and thus a smaller average social distance than the first location.

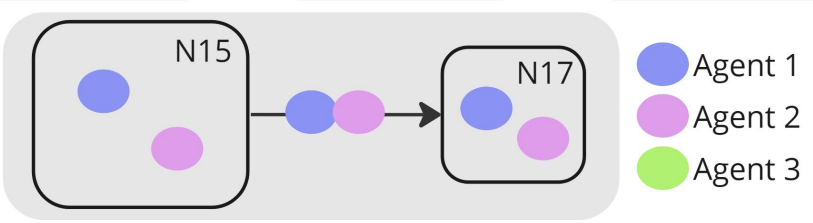

Figure 4.11: Test case 4

Time step [s]	0	3600	3720	3840	7440
From-node	18	15	16	16	16
To-node	15	16	17	17	17
State	1	0	0	1	1
Link occupancy	0	2 (link 11)	2 (link 499)	0	0

Table 4.6: Test case 4 - characteristics

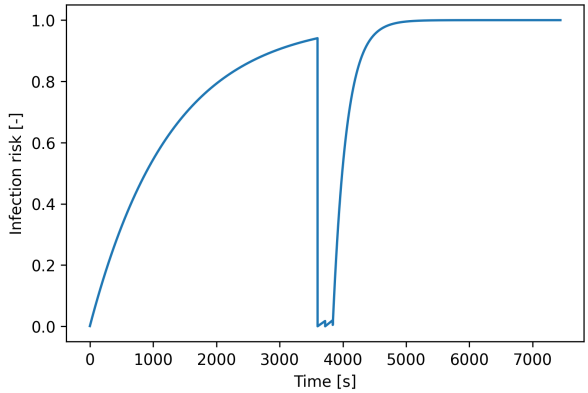

Figure 4.12: Test case 4 - infection risk

4.3.3. Test case 5 - two stationary and one moving agent

The final test case models two stationary and one moving agent. The moving agent is first located close to the FWD stairs deck 6 port side (node 155) and moves to the starboard side close to the same stairs (node 157). Both locations have an equal floor area of approximately 9 m^2. The two stationary agents are located at the SB side of the stairs (node 157). The specifics for the location, state and link occupancy over time are noted in Table 4.7 and Table 4.8. Figure 4.14 shows the infection risk over time for test case 5. For the moving agent, the risk is zero until the agent enters node 157 and the risk increases after time step 3840 s. The risk is zero up to time step 3840 s, because the moving agent is the only occupant in these spaces. The stationary agents experience risk from the start of the simulation as they are both located at node 157. When the moving agent enters node 157, the infection risk of the stationary agents shows an upward jump as the average social distance decreases.

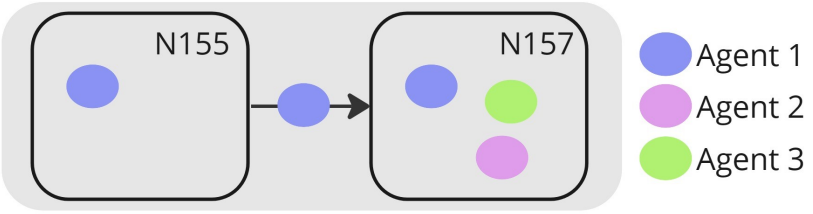

Figure 4.13: Test case 5

Time step [s]	0	3600	3720	3840	7440
From-node	151	155	158	158	158
To-node	155	158	157	157	157
State	1	0	0	1	1
Link occupancy	0	1 (link 181)	2 (link 667)	0	0

Table 4.7: Test case 5 - characteristics moving agent

Time step [s]	0	3600	3720	3840	7440
From-node	158	158	158	158	158
To-node	157	157	157	157	157
State	1	1	1	1	1

Table 4.8: Test case 5 - characteristics stationary agents

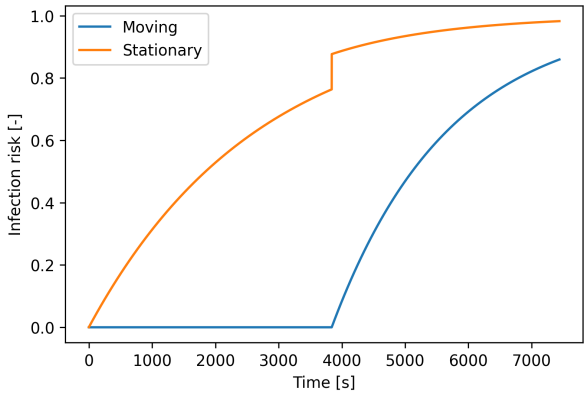

Figure 4.14: Test case 5 - infection risk

After executing the five test cases, it can be concluded that the model provides infection results matching initial expectations:

- Infection risk increases with time for spaces with more than one agent and average social distances smaller than approximately 10.8 m.
- Infection risk shows exponential behavior, which can be related to the modified Wells-Riley Equation 3.3 used to calculate the risk.
- Infection risk increases faster and to higher values for spaces with an increasing number of agents.
- Infection risk increases faster and to higher values for spaces with a smaller size.
- Infection risk goes to zero when agents change spaces.
- Infection risk increases when an agent enters a space.

5

Sample Case

This chapter will build on the integrated model described in chapter 4 and will answer the following research questions:

5. *What are the infection risk results of a sample case scenario when the integrated infection and crowd behavior model is applied?*
6. *How can the infection risk results from the integrated model be validated?*

First, a sample case is defined which is used in a convergence study for the RCM model. The RCM model itself is based on probabilities and will provide different results every time the model is run, even if the input parameters stay the same. Therefore, a convergence study is used to determine the repetitions required to achieve converging input results for the integrated model. Second, a parameter sensitivity study will be completed for the integrated model. This study will determine the effect or 'sensitivity' of medical and ventilation parameter changes, on the final infection risk results. This sensitivity study combined with results from scientific literature will inform the final choice for medical and ventilation parameters used during the layout, operational and behavioral scenario simulations in chapter 6.

5.1. Sample case

The sample case can be described covering two main topics: the ship layout and the activity schedule for the guests and crew. The activity schedule aims to realistically represent the real-life movements onboard a cruise vessel. The sample case ship layout is taken from the second data set from the SAFEGUARD project. Under this EU project, full-scale data sets for passenger evacuation response times onboard a RO-PAX ferry (with and without cabins) and a cruise ship were generated [8]. These data sets are used to validate the results of mandatory evacuation simulations for passenger vessels. The second data set provides the deck plans for a cruise ship operated by Royal Caribbean International [23]. The complete cruise ship layout can be found in Appendix D. This layout corresponds to the Radiance of the Seas cruise vessel and the ship characteristics as provided in Table 5.1 and Figure 5.1.

Figure 5.1: Radiance of the Seas [14]

Ship	Radiance of the Seas
Owner	Royal Caribbean Group
Maiden Voyage	7 April 2001
Tonnage	90,090 GT
Length (LOA)	293.2 m
Beam	32.2 m
Draft	8.63 m
Decks	13 (12 guest accessible)
Speed	25 kn
Capacity	2466
Crew	894

Table 5.1: Radiance of the Seas - main ship characteristics [79]

5.1.1. Guest activity schedule

The activity schedule prescribes the location for individual guests over the course of a day. The schedule is structured as presented in Table 4.2 where location nodes and waiting times alternate. The guests complete seven legs per day: cabin $\rightarrow$ breakfast $\rightarrow$ activity $\rightarrow$ lunch $\rightarrow$ activity $\rightarrow$ dinner $\rightarrow$ activity $\rightarrow$ cabin. All schedules follow the same trend (7 legs) but the differences in activities and meal locations lead to variety in the schedules. The activity and meal locations are chosen arbitrarily and the guest route choice is based on the mixed logit method. Additional characteristics of the sample case guest activity schedule are given in Table 5.2. Looking at extreme cases, two groups can be distinguished. A first group of agents would start their day earliest and have the shortest activity and meal durations. The guests in this group move to breakfast at 08:00, after which the agents have six activities/meals of 130 minutes and complete the schedule around 21:00. A second 'extreme' group will go to breakfast at 09:00 and have 150 minute activity durations. This group then completes its schedule around 24:00.

Characteristic	**Specifics**
Number of agents	2148
Groups	Every 4 agents follow the same schedule
Activity/Meal duration	140 minutes $\pm$ 10 minutes
Moving to breakfast	Uniform distribution 08:00 till 09:00
Final move to cabin	Between 21:00 and 24:00

Table 5.2: Sample case guest activity schedule

5.1.2. Crew activity schedule

The cruise vessel can house over 850 crew from which 700 agents will be modeled. This choice is made because part of the crew has limited contact with the guests. This can, for example, be a crew member working in the engineering or deck department. The crew schedule specify eight legs: cabin $\rightarrow$ shift $\rightarrow$ break $\rightarrow$ shift $\rightarrow$ break $\rightarrow$ shift $\rightarrow$ break $\rightarrow$ shift $\rightarrow$ cabin. The crew works four shifts with three breaks in between. Contrary to the guest schedule, there are two schedules for the crew: an early and a late shift. Two specific assumptions are made with respect to the work location of the crew. Firstly, the activity crew can rotate between the activity locations on the ship. Their shift workplace over the day can change after breaks. However, the restaurant crew will work in the same place for the entire day. The deviation for the crew schedule lies much lower than for the guest schedule because the crew is expected to show up in time for work. Additional crew activity schedule characteristics can be found in Table 5.3.

Characteristic	**Specifics**
Number of agents	700
Shift duration	180 minutes (4x)
Break duration	30 minutes (3x)
Early shift	07:30 $\pm$ 3 minutes till 21:00 $\pm$ 3 minutes
Late shift	10:30 $\pm$ 3 minutes till 00:00 $\pm$ 3 minutes

Table 5.3: Sample case crew activity schedule

5.2. RCM Convergence

In the previous section, the ship layout and activity schedules for the sample case were described. It is important to note that the route choice model will provide different outcomes for every simulation, even if the input parameters are kept the same. This can be explained by the implementation of probabilities and probability distributions influencing the routes that the agents will take. Therefore, five sample case simulations were run and the infection results have been analyzed. After these simulations, it was noted that the model presented unrealistic results at the start and end of the day. The action undertaken to address this issue is explained in subsection 5.2.2. Subsection 5.2.3 describes the results for the adjusted model and compares these results to the sample case simulations from subsection 5.2.1.

5.2.1. Sample case simulations

The assigned input parameters for the sample case simulations can be found in Appendix E, where Table E.1 specifies the RCM input parameters and Table E.2 gives the integrated model parameters.

The infection risk results are given in Table 5.4. During the calculation, risk locations and average infection risks over time were determined. The high-risk locations are locations where the largest group of agents experience their highest infection risk over the day. The average infection risk, over time, was also calculated for the guests (agent 0 up to 2147) and the crew (agent 2148 up to 2848) as specific groups. Additionally, a mean and standard deviation were determined over the five sample case runs. The mean average risk for these five sample runs is 27.5% with a standard deviation of 0.359. The mean average guest risk of 23.3% lies lower than the total value but shows a higher standard deviation over the five runs. The mean average crew infection risk of 40.5% lies higher than the guest and total infection risk. However, the crew standard deviation is smaller which might be explained by the fact that the crew follow similar activity schedules between themselves which results in smaller differences in the routes chosen for the five runs.

The risk locations 1, 4 and 5 are the same for all five sample case runs. Risk location 1 is node 5 which is a move-through area in front of the stairs on deck 2. Interestingly, this node gives high values while it is not expected to be a location where agents spent much time. The high value can be explained by the activity schedule for the crew. Node 5 is, together with node 33, set as the first node in the crew activity schedule because the crew quarters are not modeled. At the start of the simulation, the crew will build up high levels of infection risk as part of the crew is ‘waiting’ on these nodes until their shift

starts. Node 33 can be recognized as risk locations 2 and 3 in the table. Risk locations 2 and 3 are not constant over the five runs as the frequency (amount of agents which has their highest infection risk at that location) lies close together for nodes 33 and 330. Node 330 and node 293 feature restaurant locations on deck 12 aft and deck 11 starboard. Node 388 is the Viking Crown lounge on deck 13. These are spaces where large numbers of agents are expected to spend significant time, which results in high infection risks.

Run	**1**	**2**	**3**	**4**	**5**	**Mean**	σ
Average IR [%]	27.4	27.4	27.4	28.1	27.2	27.5	0.359
Average guest IR [%]	23.2	23.2	23.1	24.0	22.8	23.3	0.438
Average crew IR [%]	40.1	40.4	40.5	40.8	40.6	40.5	0.241
Risk location 1	5	5	5	5	5	-	-
Risk location 2	33	330	33	33	330	-	-
Risk location 3	330	33	330	330	33	-	-
Risk location 4	293	293	293	293	293	-	-
Risk location 5	388	388	388	388	388	-	-

Table 5.4: Results for five sample case runs

Figure 5.2 shows a frequency distribution for the average infection risk over time for the complete group of agents. In the figure, the five different sample case runs are presented and they show a similar trend. The figure shows a frequency peak between 20% and 25% average infection risk which lies close to the average infection risk mean as calculated in Table 5.4. The figure also shows that there are agents with average infection risks above 60%. Also, there are only a few agents with a low average infection risk between 0% and 10%.

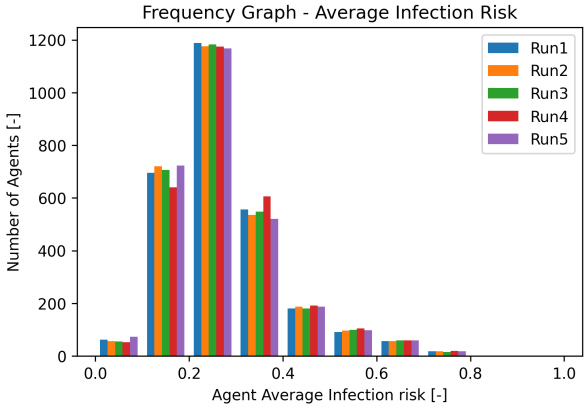

Figure 5.2: Average infection risk - five sample case runs

In Figure 5.3, a different type of frequency distribution is presented. This figure shows the number of agents with an infection risk above 90% over time. Figure 5.3 thus provides information which is more related to the population as a whole and shows the fraction of the population that is at significant risk over time. The developed model does not move past risk, assigning agents to become infected, sick or recover. Therefore, it is only possible to present risk and not the number of infected individuals. The 90% risk condition was chosen because, if infection were modeled, at least these agents are likely to become infected. All five runs show similar results with the slight exception of run 4. At the end of the simulation for run 4, the risk peak seems to be steeper and lie earlier in time.

At the start of the simulation, Figure 5.3 shows a steep peak around timestep 10:15 as more than 800 agents have an infection risk above 90%. This is the moment just before the crew late shift starts. As mentioned before, the crew quarters are not modeled and half of the crew population is waiting on either node 5 or node 33. These agents build up unrealistic infection risks as they are waiting on locations with limited dimensions for a longer period. At this point, all guests will have moved to breakfast. Guests

who started breakfast early are approaching the end of their breakfast and this group has been building up risk over the duration of their breakfast. The combination of the crew and guest situations results in the identified peak.

Near the end of the simulation, the amount of agents with a high risk increases again beyond the values seen during the day. This can be explained by the fact that the early shift crew is now gathering on nodes 5 and 33 as they have completed their schedule. Just like the peak at the start of the simulation, this situation results in high infection risks accumulated at an unrealistic location.

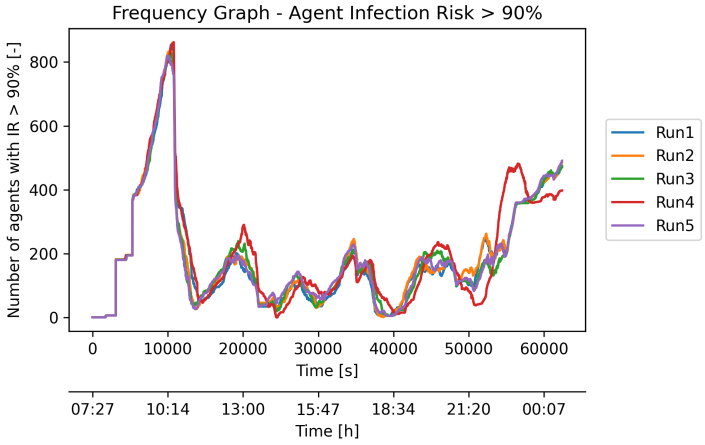

Figure 5.3: Infection risk above 90% - five sample case runs

The infection risk peak around 10:15 and the large number of high-risk agents after 21:30 highlight a shortcoming in the current model for the situation where the agents are not participating in the simulation yet or have finished the activity schedule:

- The late shift crew builds up unrealistic risk before 10:30 at node 5 and node 33 because the crew quarters have not been modeled.
- The early shift crew builds up unrealistic risk after 21:00 at node 5 and node 33 because the crew quarters have not been modeled.
- Congestion at node 5 and node 33 due to waiting crew could lead to high infection risks and waiting times for the guests moving through these locations.
- The infection risk results for guests in their cabins, when they are not participating yet or have finished, are questionable since cabins are not modeled individually. The guest cabin accommodations are currently modeled as if the occupants of a group of cabins are located in one open space.

5.2.2. Adjusted Time Range

Various solutions were considered to deal with the shortcoming identified in section 5.2. The RCM model could be adjusted to include the ship layout for the crew quarters and decrease the group size for guest cabins to produce a more realistic scenario. This would be a time-intensive solution as both the layout and the activity schedule need to be adjusted. Additionally, it is relevant to consider that this research is specifically focused on infection risks incorporating normal-day movement instead of long-term stationary behavior.

Another option would be to look at a time range during the day, disregarding the unrealistic infection risks at the start and end of the simulation. The complication with this solution lies in determining the boundaries of the results taken into consideration. The late shift crew starts to participate in the simulation after 10:30, so the first boundary should lie beyond this point in order to avoid the high infection risks of the late shift crew. However, before this point in time, all guests have started to participate and their movements are relevant for the final results. For example, putting the first boundary at 11:00 excludes a significant part of the behavior of the guests. Using this solution would resolve unrealistic outcomes

by introducing different unrealistic outcomes as certain agent behavior is unrepresented. In the end, the problem can be traced to the spread-out movement of the agents which means that no agent starts or finishes the simulation at the same time. However, this spread-out movement is implemented to represent a real-life scenario where people do not move uniformly.

Finally, a variation on the second solution was implemented. In the integrated model, the infection risk for every individual agent is considered to be zero when the agent is not yet participating or when the agent has finished the activity schedule. The relevant code can be found in Listing C.7 and Listing C.8. In Listing C.7, two relevant indices for each agent are found. These indices correspond to the time when the agent first starts moving (state = 0) and the time when the agent has completed the activity schedule (state = 4). These indices are used in Listing C.8 as boundaries. Before and after these boundaries, the social distance index is set to zero, which leads to an infection risk of 0% at that timestep.

The implementation can be recognized in this chapter under the abbreviation ATR (Adjusted Time Range), as the time range taken into consideration is individually adjusted. All simulations in section 5.3 and chapter 6 were completed under the assumption that the infection risk is zero before and after participating in the simulation, and this assumption will thus not be specifically mentioned after section 5.2.

5.2.3. Sample case simulations - ATR

Table 5.5 presents the results for the sample case simulations both with and without the ATR adjustment. The average infection risks have significantly decreased for the ATR simulations. The mean average infection risk has decreased from 27.5% to 21.7% and both the guest and crew infection risks have decreased. These changes were expected as high infection risks at the start and end of the simulation are not affecting the average value anymore. The average risk decrease for the crew is much larger, from 40.5% to 24.7%, than the decrease for the guests, from 23.3% to 20.7%. This was also expected as the crew is no longer building up high risks at nodes 5 and 33 before and after their shifts.

The standard deviations of the average IR and guest IR have more than doubled while the standard deviation of the crew average infection risk has hardly changed. Additionally, this crew standard deviation is much lower than the guest standard deviation.

Run	**1**	**2**	**3**	**4**	**5**	**Mean**	σ
Average IR [%]	27.4	27.4	27.4	28.1	27.2	27.5	0.359
Average guest IR [%]	23.2	23.2	23.1	24.0	22.8	23.3	0.438
Average crew IR [%]	40.1	40.4	40.5	40.8	40.6	40.5	0.241
Adjusted time range							
Average IR [%]	21.5	21.5	21.4	23.0	21.2	21.7	0.748
Average guest IR [%]	20.5	20.5	20.3	22.4	20.0	20.7	0.953
Average crew IR [%]	24.3	24.6	24.6	24.9	24.8	24.7	0.244

Table 5.5: Results five sample case runs with and without ATR

Figure 5.4 and Figure 5.5 visualize the average infection risk frequency for the ATR adjusted model. The first figure shows the five different runs and it can be seen that run 4 deviates from the other runs. For this run, there is a larger amount of agents with a higher average infection risk than the other runs. Minor differences for run 4 can also be recognized in Figure 5.2 for the unadapted model. The larger differences for run 4 will also contribute to higher standard deviations as seen in Table 5.5 for the adjusted model.

Figure 5.5 compares the sample case for the adjusted and original model. The five runs are averaged and no longer visible in this figure. For the ATR model, there are no agents with an average infection risk above 60%. The frequency distribution has moved left as more agents have an average infection risk below 20%. The frequency peak for the ATR model lies around 20% which matches with the mean value found in Table 5.5.

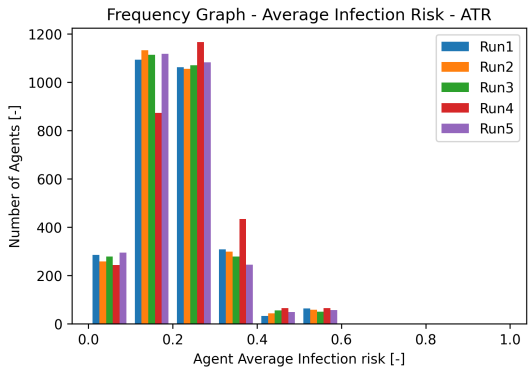

Figure 5.4: Average infection risk - ATR

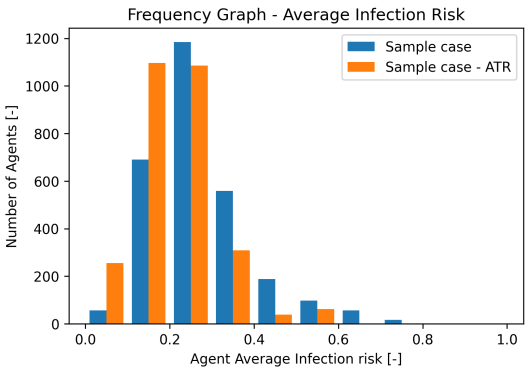

Figure 5.5: Average infection risk - comparison

Next to average infection risk figures, the frequency distributions for agents with more than 90% infection risk were calculated and can be seen in Figure 5.6 and Figure 5.7. Some observations can be made using these figures. Firstly, Figure 5.7 shows the ATR model results against the original sample case. The differences lie solely at the start and end of the simulation where the infection risk is corrected. The ATR adjustment lowers and delays the peak around 10:15 and eliminates the risk build-up at the end of the simulation.

Secondly, the difference for run 4 is more evident than seen in Figure 5.3, especially after 18:30. The last two peaks seem to occur later in time than the other runs. The last peak does have a similar shape to the last peaks of runs 1 and 2 but it occurs later in time. This corresponds to a situation where guests (as the crew has a more rigid schedule) move to their last activity later which then delays the final guests movement to the cabins. The peak lies just before they move to their cabins as they build up risk from being at one activity location with other people for a longer period. This run 4 shows that even with equal input values for the RCM model, there are differences in when agents move and how much time they spend in one location as the model incorporates controlled randomness on purpose. However, there seems to be a general trend for both average infection risk and time-specific risks when five simulations are run.

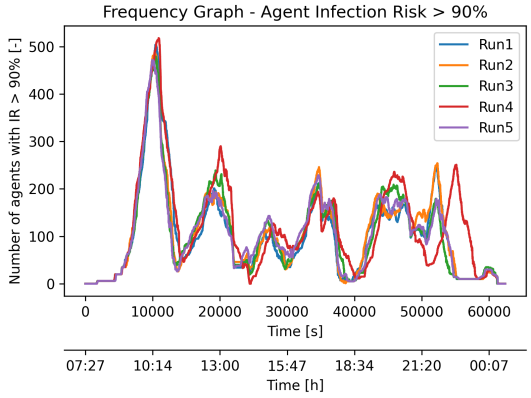

Figure 5.6: Infection risk above 90% - ATR

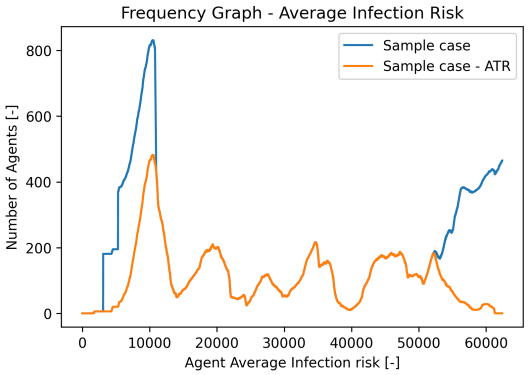

Figure 5.7: Infection risk above 90% - comparison

5.3. Parameter sensitivity study

This section provides an investigation into five parameters used in the integrated model. These parameters are: the number of infectors, air change per hour, social distance, pulmonary ventilation rate and quanta production rate. The last four parameters are varied while documenting the impact on the infection risk results. The parameters which are not investigated are kept constant with assigned values as specified in Table 4.4. The parameter variations are repeated using the five sample case simulation runs from section 5.2 to determine an average result.

5.3.1. Number of infectors

The first important parameter needed in the modified Wells-Riley equation, is the number of infectors in a single space. This parameter is complex as the Wells-Riley infection risk in this research is used for a dynamic situation with multiple spaces while the original modified Wells-Riley equation was only used for one space [84]. This parameter is set to one infected person per space introducing a fundamental assumption for the integrated infection and crowd behavior model; the risk for an agent is determined 'as if there is a single infected agent in every space the agent enters'. Theoretically, there could be multiple infectors or no infectors at all in one space. However, determining the actual amount of infectors would require the model to assign disease states (like infected, recovered etc.) and track the disease progression over time. The model would then become a microscopic agent-based model and as explained in section 3.3, the choice was made to work with a risk-based model instead of an agent-based medical infection model. Therefore, the number of infectors is set to one infected agent per space.

5.3.2. Air change per hour

The second parameter is related to ventilation and describes the rate at which the air is changed. As discussed in subsection 4.2.6 and Listing C.6, a variable ACH-based ventilation rate was implemented, instead of a constant room ventilation rate in m^3/s used in the original work by Sun and Zhai [84]. This adjustment means that the room ventilation rate for a dining room is larger than the ventilation rate for a small corridor, keeping the ACH constant. The ACH parameter is varied over the following range: $ACH = [1, 5, 10, 15, 20, 25, 30]\ h^{-1}$. As the time which agents spent in cabins or rooms is not taken into account, it is important to note that the ACH parameter is related to the general spaces onboard the ship. In literature regarding ventilation and spread of disease, ACH values between 6 and 12 are mentioned [82, 5, 102]. The Royal Caribbean Group mentions on its website in 2021, during the COVID-19 pandemic, that they achieve 15 up to 20 air changes per hour onboard their their ships [1].

Figure 5.8 provides the average infection risk for ACH values from 1 up to 30 air changes per hour. The average infection risk decreases with higher ACH values. The guest and total average infection risk seem to follow a similar trend while the crew average infection risk lies somewhat higher than the total and guest value. At very low ACH values, the infection risk increases most and the guests achieve a higher average infection risk than the crew for $ACH = 1\ h^{-1}$.

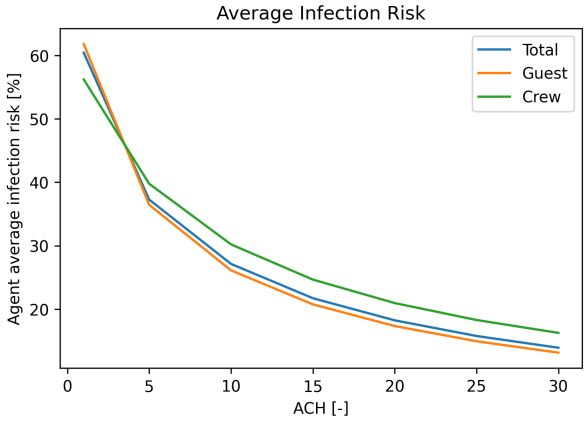

Figure 5.8: Average infection risk - ACH rates

Figure 5.9 and Figure 5.10 show frequency distributions for a range of ACH values. It can be seen that the distribution in Figure 5.9 moves to the right for lower ACH values, especially for $ACH = 1\ h^{-1}$ and $ACH = 5\ h^{-1}$. At these lower air change rates, there are more agents with higher average infection risks. Next to higher average values, the number of agents with high infection risks (above 90%) over time also increases for lower ACH values. This can be seen in Figure 5.10. This figure shows that the number of high-risk agents increases significantly for $ACH = 1\ h^{-1}$ and $ACH = 5\ h^{-1}$. The results for ACH values higher than 15 changes per hour lie closer together and these results present less

variation over time.

In terms of decreasing infection risk, it can be concluded that implementing higher ACH values decreases the risk of infection significantly. However, taking a very ACH value of 25 or even 30 air changes per hour might not be completely realistic compared to the values mentioned in literature [82, 5, 102]. Additionally, in a recent paper studying the virus spreading and ventilation inside the cabin of a passenger ship, it was concluded that a higher ventilation rate might increase virus spread because droplets spread further [74]. This paper suggests operating a 3 ACH rate when guests are in the cabin and "increase to 15 ACH for at least 12 minutes after it has been vacated" [74]. In a report on "Emergency Response to Infectious Disease Outbreak on Cruise ships", it was similarly noted that "the filtration of re-circulating air can reduce spread risk, but it may not counteract the increased transmission risk by high horizontal air-change rates" [13]. The chosen ACH value will therefore be a compromise ensuring a realistic value while recognizing possible negative effects at high ACH values, which are not visible in the current integrated model. The ACH value used for the continuation of this research is 15 air changes per hour.

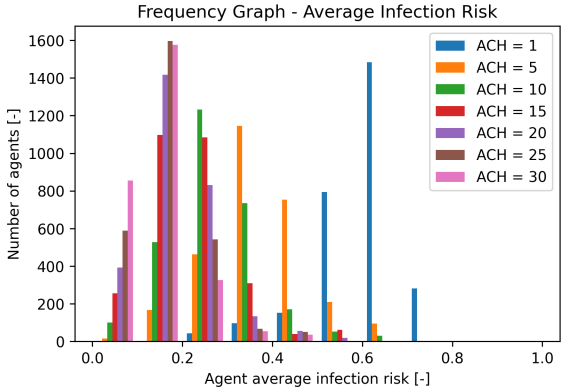

Figure 5.9: Average infection risk distribution - ACH rates

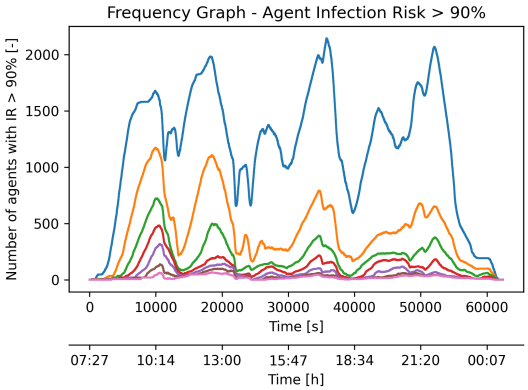

Figure 5.10: Infection risk above 90% - ACH rates

5.3.3. Social distance

This subsection provides more insight into the effect of social distance on the infection risk results. This parameter is slightly different from the other parameters discussed in this section as it is not a direct medical input parameter. Instead, the social distance is calculated by dividing the location area by the variable occupancy over time. This 'simple' calculation assumes all occupants to be uniformly spread over the available area and thus ignores crowd behavior mechanisms inside a space. For example, a small number of agents in a large space might group together and thus have a smaller social distance than currently calculated. Or a family would always stick together when they move through the ship. To investigate the effect of this behavior on the final infection results, the social distance was reduced by a percentage. The tested percentages of the original social distance are: $d = [10, 30, 50, 70, 90, 100]$ %.

Suppose one of the ship restaurants has a floor area of 50 m^2 and an occupancy of 30 agents. The social distance is then calculated to be $d = 50/30 = 1.67\ m$. With the reductions, the social distance would be: $d = [0.17(10\%), 0.5(30\%), 0.83(50\%), 1.17(70\%), 1.5(90\%), 1.67(100\%)]\ m$ for that same space and occupancy.

Figure 5.11 presents the average infection risk over the social distance percentage. As expected, the average infection risk increases when the social distance is reduced and a smaller percentage is used. The crew average risk lies higher than the guest average risk for all social distance values.

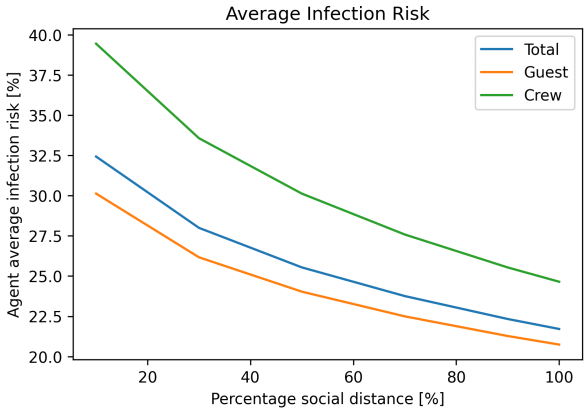

Figure 5.11: Average infection risk - social distance reduction

Figure 5.12 and Figure 5.13 present the frequency distributions for the social distance parameter. For lower social distance values, the distribution moves to the right in Figure 5.12, as was seen for the ventilation in Figure 5.9. However, the effect of a decreasing social distance is much less than the effect of a change in the ventilation rate. This can also be seen in Figure 5.10 and Figure 5.13. Even for a social distance reduction of 90%, the number of agents with a risk above 90% stays below 800 while for 1 air change per hour, this number goes above 2000 agents. In Figure 5.13 it can also be noted that for large social distance reductions, the peaks increases but the peak location and general trend of the results stay the same.

In reality, the social distance is likely to be smaller than the calculated 100%. The degree of reduction is, however, difficult to determine and would require additional research into agent behavior inside a space. Again, this investigation would move into the microscopic agent-modeling domain in order to find an average social distance reduction based on how agents actually move through or stay inside a space. The current model was specifically designed to be mesoscopic in terms of the level of detail for agent movement modeling. This social distance research would lie outside the research boundaries of this project and therefore, the decision was made to not implement any social distance reduction as it would be an arbitrary choice.

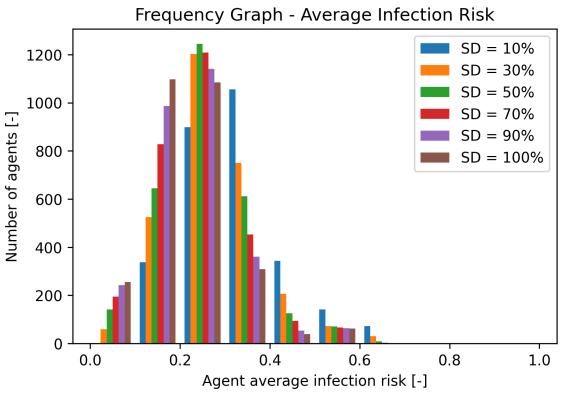

Figure 5.12: Average infection risk distribution - social distance reduction

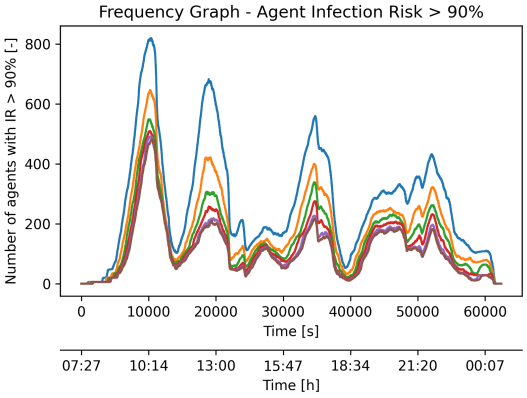

Figure 5.13: Infection risk above 90% - social distance reduction

5.3.4. Pulmonary ventilation rate

The fourth medical parameter is the pulmonary ventilation rate which is related to the rate at which susceptible agents breathe. At a higher pulmonary ventilation rate, agents would be able to absorb more viral particles from their surroundings in the same amount of time. The pulmonary ventilation rates investigated are: $d = [1, 5, 6, 15, 30, 42]\ L/min$. The ventilation rate of 5 L/min is used in the

original research by Sun and Zhai [84] and Table 5.6 shows different activities and their corresponding pulmonary ventilation rates. The pulmonary ventilation rates for running or participating in sports might be as high as $60 - 100\ L/min$ [56]. Figure 5.14 shows the relation between average infection risk and pulmonary ventilation rate. The average infection risk increases for higher ventilation rates and the crew average lies somewhat higher than the guest average value. For very high pulmonary ventilation rates, the guest average lies above the crew average which was also seen for low ACH rates.

Activity	p	
Resting	1-6 L/min [56]	$2 - 10 * 10^{-5}\ m^3/s$
Sitting / light indoor activity	5 L/min [84]	$8.333 * 10^{-5}\ m^3/s$
Walking	15 L/min [56]	$25 * 10^{-5}\ m^3/s$
Fast walking	30 L/min [56]	$50 * 10^{-5}\ m^3/s$
Going up-stairs	30-40 L/min [56]	$50 - 70 * 10^{-5}\ m^3/s$

Table 5.6: Pulmonary ventilation rates

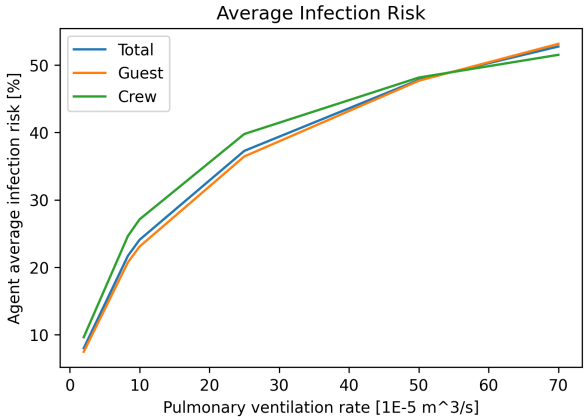

Figure 5.14: Average infection risk - pulmonary ventilation rates

Figure 5.15 presents a frequency figure that differs from the graphs corresponding to ventilation and social distance variations. The smallest pulmonary ventilation rate of 1 L/min gives a very large number of agents, over 2000, with an average infection risk below 10%. The number of agents with a risk above 90% in Figure 5.16 presents as a line close to zero with little variation over time. For larger pulmonary ventilation rates, the average infection risk distribution moves to the right. Different from the figures for ventilation and social distance, the results are more spread out. In Figure 5.9, specifically the distributions and its peak for 1 and 5 air changes per hour moved while the distributions for the other ACH-values stayed closer together. The distributions for the reduction of social distance in Figure 5.12 also stayed closer together than the distribution in figure Figure 5.15. In Figure 5.16, the peaks are more extreme for higher pulmonary ventilation rates. Also, for 5 or 6 L/min, the highest number of high-risk agents lies at the start of the day around 10:15 while for higher pulmonary ventilation rates, the maximum peak lies around 13:00. Looking at the general trend of the figure, the four peak locations recognized in Figure 5.16 at approximately 10:15, 13:00, 17:30 and 21:30 can also be seen in Figure 5.12 although the height of the peaks differ.

In general, a lower pulmonary ventilation rate decreases the infection risk. During the COVID-19 pandemic activities with high pulmonary ventilation rates like indoor sports were not allowed as these situations would put individuals at a higher risk of getting infected, which is supported by these results. For the model, it is necessary to find an average pulmonary ventilate rate that represents the activities agents undertake for the majority of the day. These activities are resting, light indoor activities and walking. A pulmonary ventilation rate of 8 L/min is chosen. This value lies somewhat above the resting or light activity values to account for the time agents walk around the ship.

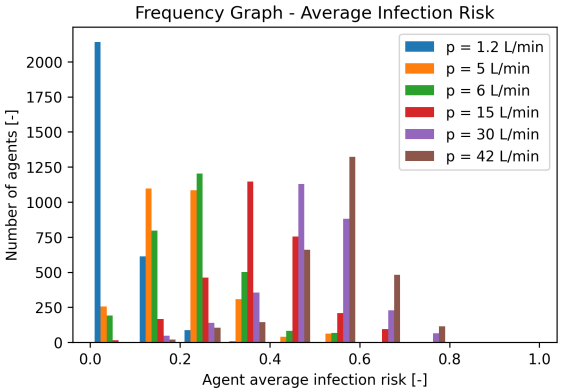

Figure 5.15: Average infection risk distribution - pulmonary ventilation rates

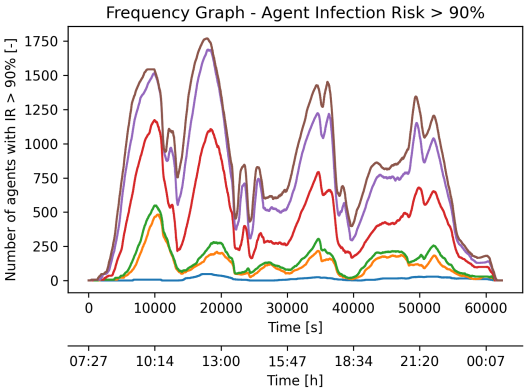

Figure 5.16: Infection risk above 90% - pulmonary ventilation rates

5.3.5. Quanta production rate

The last medical parameter investigated is the quanta production rate which quantifies the amount of airborne infection particles produced per infector. This value says thus says something about how contagious a disease is. This parameter is a highly debated parameter and the quanta production rate can vary with disease, disease variant, activity, type of space and the characteristics of the agents involved. The research by Sun and Zhai, developing the modified Wells-Riley model, uses a COVID-19 quanta production rate of 857 qph based on real-life infection scenarios. The quanta production rates mentioned in literature range from 10 qph to more than 2000 qph . [22] mentions quanta values of 10 qph and 25 qph for the delta variant used in enclosed space research and in [91], q was defined to be 14 qph when investigating COVID-19 infection risk during long-distance travel via train. Buonanno, Stabile, and Morawska specifically investigated the quanta emission rate of SARS-CoV-2 and define a quanta production rate of 142 qph for light activities [9]. A study focused on the different variants of SARS-CoV-2 settled on much higher values: 89-165 qph for the Alpha variant, 312-935 qph for the Delta variant, 725-2345 qph for the Omicron variant [16]. Taking these quanta production rates into account, the tested range was defined to be $q = [10, 100, 200, 400, 857, 1200, 2000]$ qph.

Figure 5.17 shows the average guest, crew and total infection risk for different quanta production rates. The average infection risk will increase for higher quanta production rates and for low quanta production rates, the crew and guest average values converge.

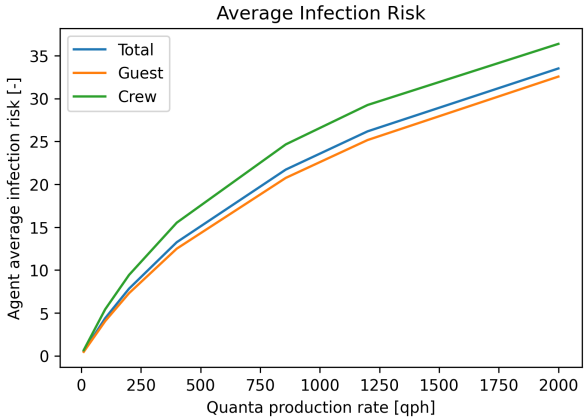

Figure 5.17: Average infection risk - quanta production rates

Figure 5.18 shows the average risk distribution for the different quanta production rates. The distribution lies centered below 10% for q-rates up to 200 qph and moves right for higher quanta production rates. For $q = 10qph$, all agents have an average infection risk below 10%. The results for the number of

agents with a risk above 90% can be seen in Figure 5.19. The risks for quanta production rates below 400 qph lie close together compared to the largest three quanta production rates. The trend of the extreme values in Figure 5.19 can be compared to the results for the social distance reduction and the pulmonary ventilation rate. The difference for the ventilation study in Figure 5.10 with respect to the extreme values and trend of the figure might thus be related to the impact of space dimensions which is only connected to the ACH parameter and not to the other parameters.

A change in quanta production rate does seem to have a significant impact on the infection results and the relative 'high' value used by Sun and Zhai is questionable compared to the other literature studies mentioned. It might also be related to the fact that the $q = 857qph$ value is derived from a single extreme outbreak event in a confined space compared to more general values presented in the other sources [84]. The choice is therefore made to use a smaller quanta production rate of $q = 100qph$. This value is a compromise taking different sources into account in an effort to avoid both under- and overestimating the infection risk.

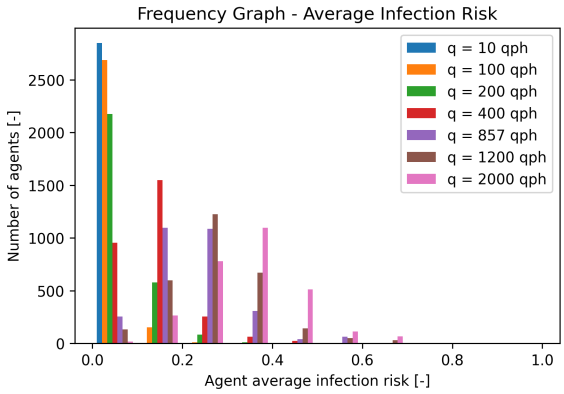

Figure 5.18: Average infection risk distribution - quanta production rates

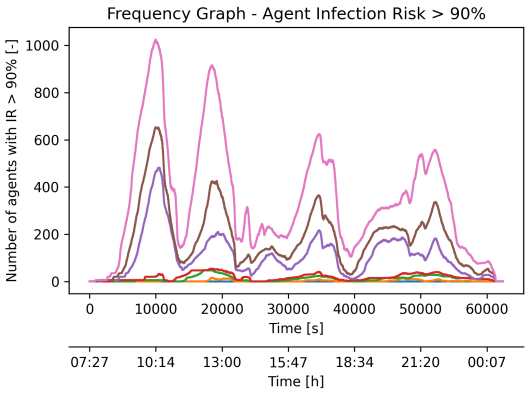

Figure 5.19: Infection risk above 90% - quanta production rates

5.4. Parameter choices

This section provides an overview of the chosen parameters based on the parameter sensitivity study in section 5.3. The choices are summarized in Table 5.7. These parameters will be implemented in section 5.5 where the five sample case runs are repeated with the chosen parameter values. This sample case will be the starting point for the simulations in chapter 6.

Parameter	Description	Assigned value	Unit
I	Number of infectors	1	[-]
ACH	Air changes per hour	15	[-]
d	Social distance	100	[%]
p	Pulmonary ventilation rate of susceptible individuals	8	$[L/min]$
q	Quanta production rate per infected individual	100	$[qph]$

Table 5.7: Chosen medical parameters for integrated model

5.5. Sample case with chosen parameters

The sample case is repeated for the parameters as defined in section 5.4. Table 5.8 gives the average values for these simulations. The average values are significantly lower than the results seen in Table 5.5. The average total infection risk with the previous parameters was 21.7% compared to the new value of 0.807%. One of the main changes is the implementation of a lower quanta production

rate which was expected to decrease the risk values significantly as demonstrated in subsection 5.3.5. The average crew infection risk remains somewhat higher than the guest average infection risk.

The node high-risk locations in Table 5.8, based on the highest frequency of agents that have their highest infection risk at that location, show similarities to the risk locations in Table 5.5. Node 33 is not among the top five locations anymore which can be attributed to the ATR change in the model. Agents no longer build up risk when they are not participating in the simulation yet or have finished the activity schedule. However, node 5, which was also a crew start location, can still be found in the top five risk locations. Even with the ATR implementation, agents seem to be building up high infection risks at this location.

In chapter 6, a more in-depth analysis will be presented specifically coupling ship locations and high infection risks. This analysis will form the basis for possible layout adjustments in order to reduce infection risk in section 6.1.

Result	Value
Average IR	0.807%
Average guest IR	0.730%
Average crew IR	1.04%
5 Risk locations	N330, N293, N388, N5, N299

Table 5.8: Results sample case simulations with parameters from section 5.4

Figure 5.20 presents the average infection risk over time for the guest, crew and total agent population onboard. The peaks for the crew average infection risk at 13:30, 17:00 and 20:40, reach higher values than the guest peaks. The crew average risk also deviates more from the total average risk compared to the guest average value. It is also relevant to compare the average infection risk to the agent activity schedules. This can be seen in Figure 5.21 and Figure 5.22.

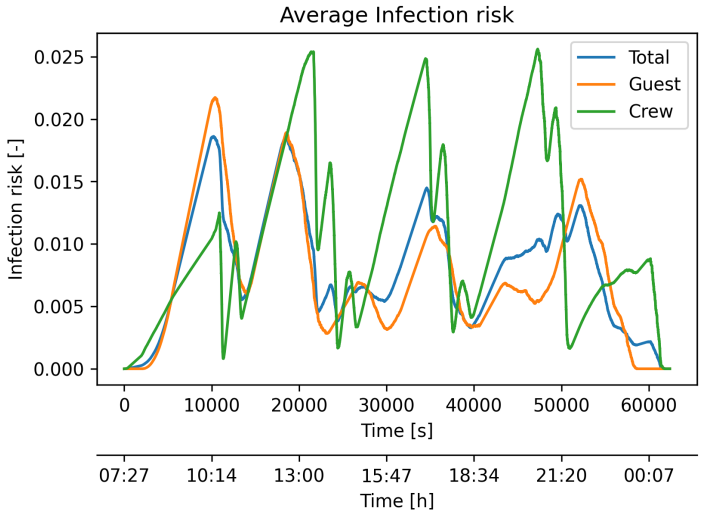

Figure 5.20: Average infection risk over time

Figure 5.21 gives the guest average infection risk against the activity schedule of an agent in the exact 'middle' of the schedule distributions. The guest will move to breakfast at 08:30 and every meal and activity will have a duration of 2 hours and 20 minutes. In Figure 5.21, a connection between the activity schedule and the average infection risk can be recognized: the average infection risk increases over the duration of a meal or activity and decreases just before the end of the meal or activity. The highest average infection risks are seen around the end of breakfast and the end of the first activity of the day. Another increase can be seen at the end of the last activity around 22:00.

Figure 5.22 presents the two crew shift schedules against the crew average infection risk over time. The green parts of the schedule represent the legs where the crew is at work and the yellow parts represent the breaks. The three minute late or early variation is not taken into account, so the schedule would be for a crew member who is always exactly on time. In general, the average risk increases over the 'at-work' part of the shift and decreases when the crew has a break. The average infection risk decreases when guests or crew change activities because they change locations and the exposure time in the risk calculation is reset. A returning trend can be seen just after the peaks at 13:30 and 17:00: decrease (1), small increase (2), decrease (3), small increase (4), small decrease (5) steady increase (6). The events correlating to this trend can be described as follows:

1. late shift break
2. risk build-up from late shift break and early shift 'at-work'
3. early shift break
4. risk build-up from early shift break and late shift again 'at-work'
5. early shift back 'at-work'
6. risk build-up from both early and late shift 'at-work'

The average crew risks at the start and end of the simulation are lower than the risks during the day. This can be explained by the fact that one shift is working and only half the crew population is involved.

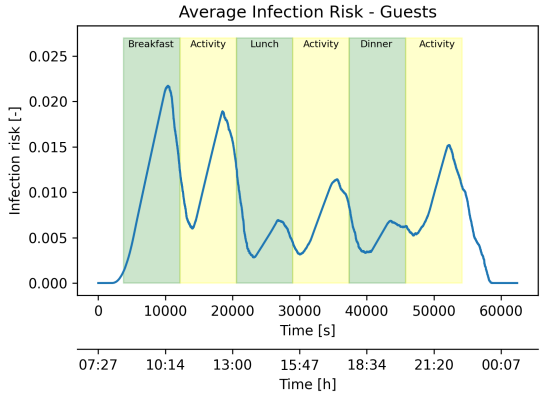

Figure 5.21: Average guest infection risk and activity schedule indication

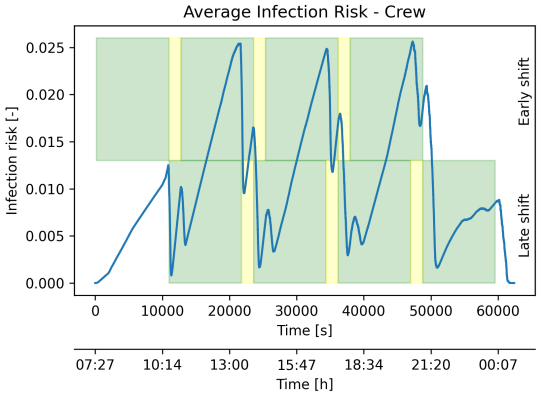

Figure 5.22: Average crew infection risk and crew shift indication

The average infection risk can also be plotted per agent which is visible in Figure 5.23. In general, the average guest values lie lower than the crew risks. There are outliers - agents who have a significantly higher average risk than the majority of the guests or crew population. Especially for the crew, there are agents with an average infection risk above 7%. More research into the agents with high average risks is conducted in the next chapter, looking into the activity schedules of these 'at-risk' agents and the infection risk at the locations where these agents spend their time.

Figure 5.24 shows the frequency distribution of the average infection risk. The distribution has moved left from Figure 5.4 and almost 80% of the agents now modeled has an average infection risk below 1%.

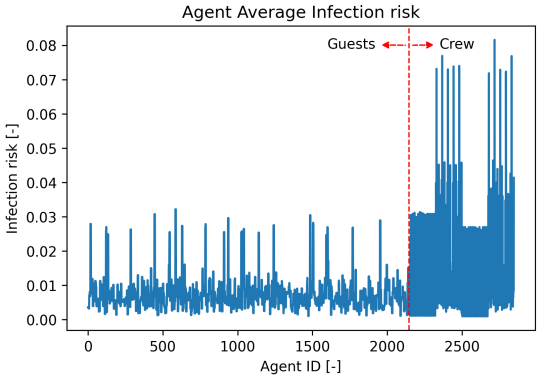

Figure 5.23: Agent average infection risk

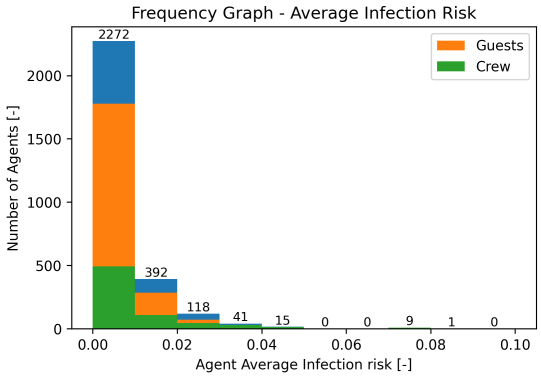

Figure 5.24: Average infection risk distribution

A frequency distribution for the number of agents with a certain infection risk over time is given in Figure 5.25. This figure is different from the frequency figures created during the parameter sensitivity study because the criteria has been brought down to 50%.

Peaks for the number of guests with a risk above 50% can be seen at 11:30, 15:50, 16:15 and 20:55 with respectively 18, 7, 7 and 14 guests. The five average infection risk peaks, as seen in Figure 5.20, can be recognized as the dashed red lines in Figure 5.25. The location of the red lines does not exactly correspond to the peaks for a high number of agents with a risk above 50%. Looking at for example 11:30, the average infection risk does not peak although there is a high number of guests with an infection risk above 50%. This highlights the need to investigate both the locations where high infection risks occur and the locations which present with high average infection risks.

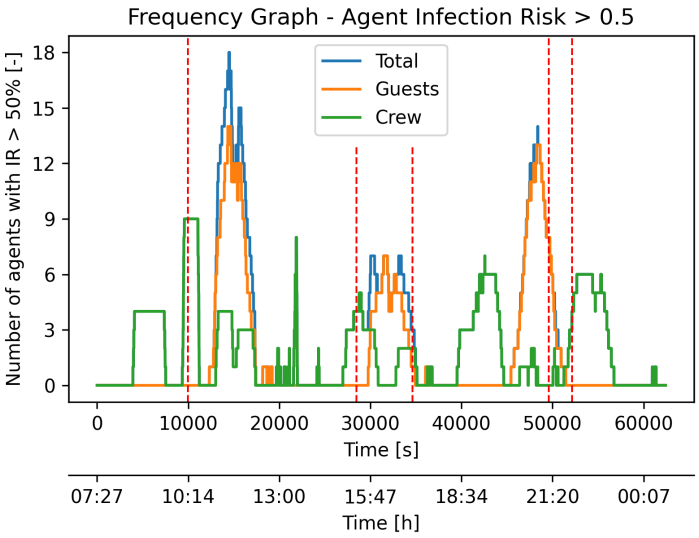

Figure 5.25: Infection risk above 50%

5.6. Sample case results validation

With the final sample case results calculated for the chosen parameters, it is important to reflect on the results in connection with the available literature. This section therefore aims to answer the following research question:

6. *How can the infection risk results from the integrated model be validated?*

Most COVID-19 studies onboard large passenger vessels present their results in terms of attack rates or reproduction numbers which are retrospectively calculated from real-life cases [75, 59, 53, 78]. A systematic review on the "Transmission of SARS-CoV-2 Associated with Cruise Ship Travel" found that these attack rates may range from 7% to over 60% depending on the ship and specific outbreak investigated [78]. For the outbreak onboard the Diamond Princess cruise vessel, the National Institute for Infectious Diseases in Japan reports that over 20 days, 22% of the ship's population was "detected to have been infected with SARS-CoV-2" [67]. The Diamond Princess cruise vessel had approximately 3700 guests and crew onboard at the time of the outbreak [67]. Comparing such an attack rate to results from the integrated infection and crowd behavior model is complicated because of various factors. First of all, the attack rate is based on actual infection cases while the integrated model only provides agent-based predictive risk. This risk is not processed further to determine agents who get infected or spread the disease. Also, the integrated model simulates a single day, while attack rates for COVID-19 ship outbreaks are calculated over multiple days or even weeks. The time frame between these types of research is thus quite different.

5.6.1. Attack rate

Keeping the described challenges in mind, it is possible to perform a rough calculation using the average infection rate of 0.807% from Table 5.8. The simulated agent population onboard is 2848 agents. At the end of a single day, theoretically, there would be $C = S * P_I = 2848 * 0.00807 \approx 23$ new cases. If these infected cases would directly isolate (removed from susceptible population) and the average infection rate would stay constant; there would be approximately 427 infections after 20 days. The attack rate over 20 days for the total population can then be calculated as: $AR = 427/2848 \approx 15\%$. This is slightly lower than the 22% attack rate for the Diamond Princess COVID-19 outbreak [67]. In reality, infected individuals might not isolate because they are asymptomatic or pre-symptomatic and it is also possible that symptomatic agents do not isolate at all. The result will be an increase of infected individuals in the agent population and the average infection risk is expected to rise over time instead of remaining constant. The actual number of cases and therefore attack rate could thus be higher.

5.6.2. Infection risk single office space

The next step would be to investigate literature which is related to COVID-19 infection risk indications for enclosed spaces. The first example is a paper that combines the Wells-Riley equation with a regression model for mean droplet nucleus concentration, in order to investigate the effect of portable air cleaners (PAC) in office spaces [18]. The Wells-Riley equation for infection risk can be recognized in Equation 5.1 and the C^+ therm represent a regression equation based on CFD analysis [18].

$$P = 1 - e^{-qtC^+} \tag{5.1}$$

The three investigated offices with 20, 40 and 73 m^2 floor areas can host two, six and eight people. Variations for these offices covered the mechanical ventilation rate, PAC characteristics and location of the infectious host [18]. The six-person office will be used for a comparison with the modified Wells-Riley equation used in the integrated model. An indicative office set-up can be found in Figure 5.26 and it should be noted that the presence of a PAC can not be taken into consideration for the integrated model. For a sample case, Dai and Zhao describe the infection risk to be 13.2% using Equation 5.1. This value could be compared to the results from Equation 3.1 and Equation 3.3 with the following input parameters: $d = 2\ m$, $I = 1$, $q = 14\ qph$, $t = 8\ h$, $Q = 0.15\ m^3/s$, $E_z = 1$ and the pulmonary ventilation rate is not specified and therefore assumed to be $p = 8\ L/min$ as chosen in Table 5.8 [84]. The infection risk P_I result for the modified Wells-Riley equation is 3.0%. If a quanta production rate of $q = 100\ qph$ from Table 5.8 is chosen, the infection risk becomes 19.6%.

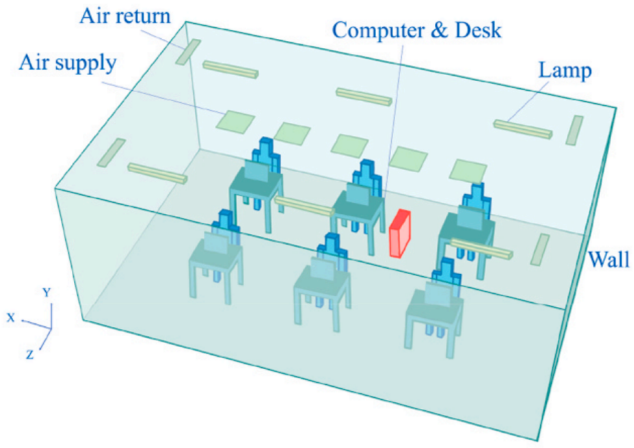

Figure 5.26: Six person office space geometry[18]

The first result using $q = 14\ qph$ is lower than the infection risk indication by Dai and Zhao and might indicate that the modified Wells-Riley equation underestimates infection risk. Equation 5.1 uses a regression formula derived from CFD analysis. This means that complex air/particle circulation and the position of the mechanical ventilation units is taken into account. This is not the case for the modified Wells-Riley equation. Additionally, the exposure time of eight hours is quite significant and much longer than the maximum exposure times (three hours) used in the integrated model. As mentioned in the literature section of this report, the modified Wells-Riley equation used in the integrated model is more suitable for short-term exposure situations as other factors than purely airborne transmission become important for long-term exposure [84].

When implementing a quanta production rate of 100 qph, the infection risk of 19.6% exceeds the result from the paper. The modified Wells-Riley equation with social distance index was calibrated by Sun and Zhai, who use a high quanta production rate over 800 qph. For the risk comparison using 14 qph; the social distance index decreases the infection risk for the integrated model compared to the work by Dai and Zhao. Using a higher quanta production rate produces the opposite effect and increases the infection risk. A conclusion from this validation is that the equation for the social distance index used in the integrated model is not independent from the quanta production rate implemented. This needs to be taken into account when comparing different types of modified Wells-Riley equations.

5.6.3. Infection risk multi-room office space

The research by Dai and Zhao is restricted to infection risk indications for a single office space with varying dimensions and characteristics [18]. However, in research by Srivastava, Zhao, Manay and Chen, agent-based infection risks for a 59-person office building with several rooms are calculated [83]. The geometry for the office building can be found in Figure 5.27. The goal of the investigation was to develop “an ultraviolet-C (UV-C) air disinfection device” but they also provide average infection risks for ‘case A’ and ‘case B’ without the disinfection device. ‘Case A’ has, however, a very small ventilation rate so ‘Case B’ with an equivalent ventilation rate of 4.55 air change per hour will be investigated further. The following parameters apply: $t_{exp} = 8\ h$, $q = 31\ qph$, $p = 5\ L/min$, $I = 4$, $Q \approx 4.8\ m^3/s$. The social distance is not directly available, so an assumption is made based on the geometry provided in the paper: $d = 1.5\ m$. Using Equation 3.1 and Equation 3.3 while assuming the office building to be a single open space, the infection risk can be calculated to be 0.62% for $q = 31\ qph$ and 1.97% for $q = 100\ qph$. The paper presents an average infection risk of 3.10% using a CFD tool to simulate airflow within the actual office geometry. Because of the geometry and variation on the Wells-Riley equation, it was not expected to achieve equal results but it shows that the infection calculations used in the integrated model present results relatively close to the sample case average infection risk of 0.807%.

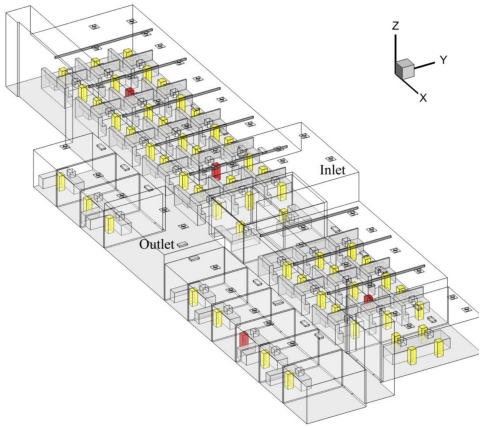

Figure 5.27: 59-person office space geometry [83]

5.6.4. Infection risk hospital waiting rooms

Moving towards even more complex geometries, [48] presents research into the infection risks in an out-patient hospital building in Shenzhen, China [48]. The study proposed “A modified Wells-Riley model combining the airborne route and close contact route” in order “to predict the infection risks of coronavirus disease 2019 (COVID-19) in main functional spaces” [48]. In 20 waiting rooms distributed over four floors, CO_2 was measured and used as an indication for the air change rate in the different spaces. The basic principle behind these measurements is, that a high occupancy in a space will lead to high CO_2 concentrations. In the spaces with high CO_2 concentrations, either occupancy should be controlled or a larger fresh air supply should be implemented [48]. The research concludes that in 20 waiting rooms in the hospital, the COVID-19 average infection risk ranges between 0.19% and 2.63% [48]. The average value over all 20 waiting rooms was 0.79% with a 2% infector proportion [48].

Looking at the sample case simulations done in section 5.5, it is possible to investigate the average infection risk at specific locations. The waiting rooms would relate best to the nodes in the ship model and the average infection risk per day can be found in Figure 5.28. The figure shows one specific outlier at node 107 with an average day infection risk of 16.2%. In Figure 5.28, the axes have been adjusted to better visualize infection risk for nodes other than node 107. This outlier will be further investigated in chapter 6. The day average infection risk for the nodes, excluding node 107, ranges between 3.58% and 0.75%. The average value for the 20 highest-risk nodes, excluding node 107, is 1.49% for a single infector per space. The infection results for the ship locations cover a bigger infection risk range, with more locations that present very little or no infection risk at all. This was expected since the focus in [48] was hospital waiting rooms, and perhaps less occupied spaces were not investigated. Taking the obvious geometry differences between a ship and a hospital into account, the results do seem to lie within a similar domain and this comparison supports the acceptability of integrated model ship results.

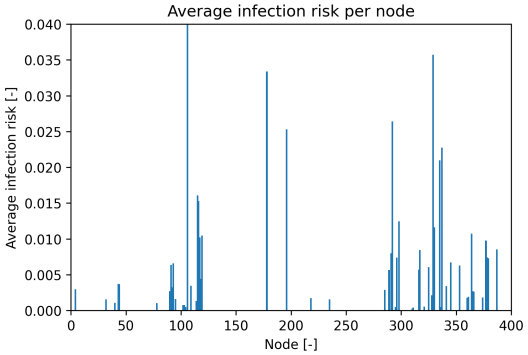

Figure 5.28: Day average infection risk per node for sample case

5.6.5. Infection risk at reception

The last research article considered in this section is specifically related to the calculation of COVID-19 infection risk in indoor environments [47]. The pertinent part of this research are the results of a reception event with a duration of three hours. Different from the research considered so far, this duration lies close to the exposure times considered in the cruise ship simulations. The reception in [47] has 100 subjects present at a location with a floor area of 100 m^2, $ACH = 2\ h^{-1}$, $p = 12\ L/min$ with a single index patient [47]. The individual risk at this reception is reported to be 1.6%.

This reception can be compared to the restaurant at node 45 in the ship simulation. This restaurant has a floor area of 120 m^2 and can accommodate up to 120 people. In the range $t = [20000, ..., 30800]\ s$, the average occupancy is 97 people. This range covers three hours and the average restaurant occupancy is almost the same as the reception occupancy. Figure 5.29 shows the average infection risk at node 45 for the selected time range. The reception infection risk from [47] can be seen as the horizontal line at 1.6%. Two separate infection risks were calculated. The blue line provides the average infection risk with the parameters from Table 5.8 and the orange line shows the average infection risk when three parameters are changed: $p = 12\ L/min$, $ACH = 2\ h^{-1}$ and the ceiling height is adapted to be 4 m [47]. The average infection risk for that three-hour range for the sample case is 0.49% and for the sample case with adapted parameters 3.18%. The sample case average lies below the value presented in [47] while the average value for the adjusted sample case lies higher than 1.6%. Some variation between the reception and the restaurant results was expected as the quanta production rate for the reception is not known. Instead, [47] uses an infective dose D50: “being the mean dose that causes an infection in 50% of susceptible subjects” while the restaurant assumes $q = 100\ qph$ [47]. For the adapted parameters, the average infection risk increases compared to the sample case. This can be explained by a decreasing pulmonary ventilation rate and a significantly reduced room ventilation rate. The decreased ACH will be slightly compensated by the larger ceiling height leading to an increase in the amount of cubic meters of ventilated air Q.

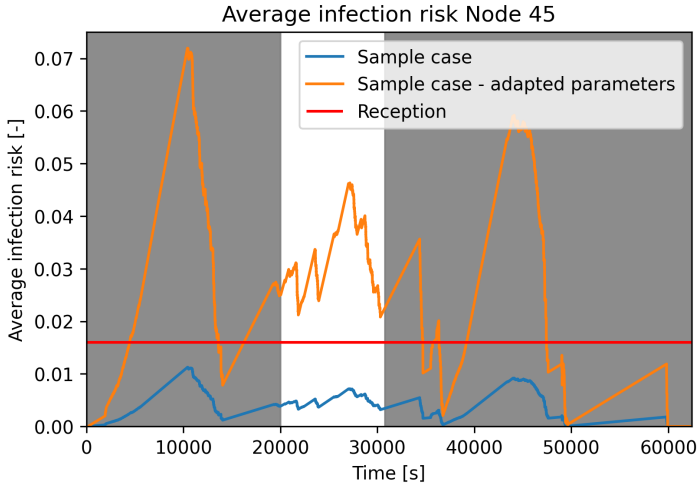

Figure 5.29: Average infection risk at node 45

5.6.6. Conclusion

In this validation section, the sample case results from section 5.5 were tested against five different research sources related to COVID-19 risk in enclosed spaces. These validation cases also highlighted the challenges for validating the results of the integrated infection and crowd behavior model applied to a large passenger ship. The situational factors like geometry, occupancy and location type matter to the infection risk outcome. It was therefore hard to find a ‘similar case’ to compare the final outcomes to. Additionally, the results from the ship simulations provide infection risk and this risk is not further processed to define infected cases. This makes validation with real-life COVID-19 outbreaks challenging as the number of cases is often the main focus. Other challenges include the time frame or exposure time used as seen for the office space research cases in subsection 5.6.2 and subsection 5.6.3. Lastly, it is meaningful to note that the research cases in subsection 5.6.2, subsection 5.6.3

and subsection 5.6.5 describe stationary behavior. This is fundamentally different from the integrated model which allows agents to move between spaces as they follow their activity schedule. The location-based approach in the research case for hospital waiting rooms perhaps best captures some form of movement as it measures occupancy and ventilation at different time steps.

On a population level, an attack rate comparison with a cruise ship population was made in subsection 5.6.1. The attack rate for the integrated model was lower than the COVID-19 attack rate onboard the Diamond Princess cruise vessel, which could be explained by the assumptions with respect to the daily infection risk. Focusing on a single space in subsection 5.6.2, the results from the social distance dependent Wells-Riley equation in the ship simulation and the regression based Wells-Riley equation for the single office space showed a high degree of variation. The difference can be directly related to the differences in the Wells-Riley equations used for the ship simulation and the office simulation. It was concluded that the implemented quanta production rate significantly influences the results and the input parameters of a specific situation might not be directly transferable between different modified Wells-Riley equations.

The modified Wells-Riley equation from the ship simulation is also used to calculate infection risk for a multi-room office space in subsection 5.6.3. This result is compared against the work from Dai and Zhao who implement a CFD tool to simulate airflow inside the multi-space geometry [18]. There are still differences between the infection risk results but the results lie much closer to the sample case average infection risk of 0.807%, compared to the results from the single office space.

In subsection 5.6.4 and subsection 5.6.5, a more location-based approach was used. Subsection 5.6.4 presents the infection risk range and average infection risk for 20 hospital waiting rooms compared to 20 high-risk ship locations. The risk ranges (0.19% - 2.63% versus 0% - 3.58%) and the average risk (0.79% versus 1.49%) seem sufficiently close to support the acceptability of the integrated model ship results. Finally, in subsection 5.6.5, a reception situation is compared to one of the onboard restaurants for a three-hour time frame. The restaurant average infection risk was calculated to be 0.49% or 3.18% depending on the input parameters. The reception risk was reported to be 1.6% which lies in between these results. The complication with this study was the use of a different viral load indication than a quanta production rate. This might have resulted in differences between the results because the calculation for the restaurant is based on a quanta production rate of 100 qph.

In conclusion, these five comparisons show both the challenges and strengths of the integrated infection and crowd behavior model when applied to a ship layout. The sample case infection results seem sufficiently validated as a baseline from which to investigate risk improvement. In the next chapter, the research will therefore focus on the implementation of layout adaptions, operational and behavioral measures in order to decrease COVID-19 infection risk.

6

Simulations

This chapter will investigate several options to improve the sample case infection risk results from chapter 5. This section therefore aims to answer the final research question:

7. *What are the infection risk results of selected prevention and/or control actions onboard a large passenger vessel when the integrated infection and crowd behavior model is applied?*

The first section focuses on the layout itself and proposes layout adjustments to achieve infection risk reduction. Several high-risk locations are identified and the proposed layout changes are tested against the sample case results. Section 6.2 describes two operational measures: one-way movement and a capacity reduction for both crew and guests. Additionally, section 6.3 presents the infection risk results when implementing mask wearing. Section 6.4 and section 6.5 show the conclusions related to the infection risk improvements achieved by implementing separate or combined layout adjustments, behavioral and operational measures.

6.1. Layout adjustments

In this section, the different layout adjustments have been investigated. The section first identifies the high-risk locations onboard the cruise vessel when the sample case from chapter 5 is simulated. Then, the high-risk locations and possible causes for the high infection risks at these locations are described. Three high-risk locations are chosen and layout adjustments for these locations are proposed. It is important to note the fact the the Radiance of the Seas cruise vessel has been retrofitted after the research from the SAFEGUARD project [8]. This means that there are significant differences between the SAFEGUARD layout and the current deck plans [14]. However, adjusting the current SAFEGUARD dataset lies beyond the scope of this research and the current dataset does provide a realistic representation of ‘a large passenger vessel’. This seems sufficient for the research done in this project.

6.1.1. Identification high risk locations

The integrated infection and crowd behavior model deals with nodes and links separately, depending on the agent state. Nodes are the locations where guests attend their activities and meals, and these locations also represent the ‘at-work’ or ‘break’ locations for the crew. Both the crew and guests spent the majority of their time on nodes. They travel via links when they are switching between nodes. Figure 6.1 and Figure 6.2 indicate the average infection risk per location onboard. The figures show that the nodes present with higher average infection risks than the links. The node average infection risk for all nodes lies at 0.145% against 0.0000184% for the link locations. Although the floor areas of links are often smaller than the node areas, the occupancy and longer exposure time lead to higher infection risks for node locations.

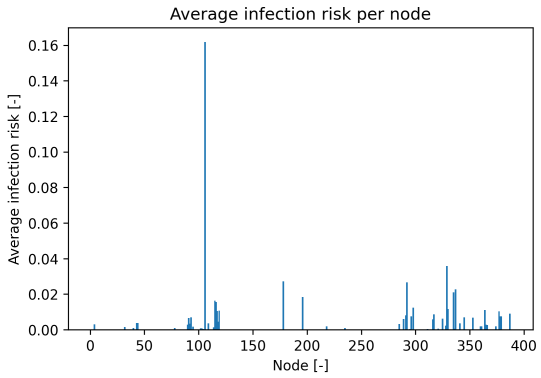

Figure 6.1: Average infection risk per node

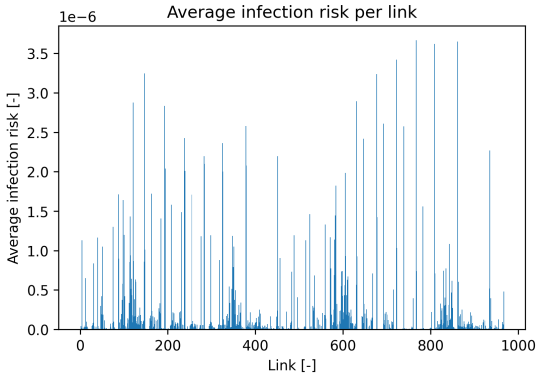

Figure 6.2: Average infection risk per link

Table 6.1 shows the five node locations with the highest average infection risks. Note that the deck numbering from the SAFEGUARD project is used. This deck numbering starts at deck 1 for the decks accessible to guests. Online deck plans for the Radiance of the Seas start counting at deck 2 for the guest-accessible decks. This is related to deck numbering for the crew quarters and machinery spaces. The SAFEGUARD deck numbers are used in order to avoid confusion related to the input data for the integrated model.

Node	Function	Location	Average IR
N107	Bar	SB - mid - deck 5	16.8%
N330	Restaurant	SB - aft - deck 11	3.59%
N179	Multi-functional lounge	CL - mid - deck 7	2.72%
N293	Restaurant	SB - aft - deck 10	2.67%
N338	Sundeck	SB - aft - deck 11	2.27%

Table 6.1: Node locations with highest average infection risk

As mentioned in section 5.5, a second analysis is needed to identify locations where a high number of agents reach their maximum infection risk over the day, even if these locations do not have high infection risks. The results for these five risk locations are given in Table 6.2.

Node	Function	Location	Average IR
N330	Restaurant	SB - aft - deck 11	3.59%
N293	Restaurant	SB - aft - deck 10	2.67%
N388	Lounge	CL - fwd - deck 12	0.897%
N5	Move through area	PS - mid - deck 1	0.294%
N299	Restaurant	SB - aft - deck 10	1.25%

Table 6.2: Node locations where ‘most’ agents reach their maximum infection risk

At this point, the analysis covers locations with a high average risk and locations where agents achieve high risk. The last perspective on high-risk locations can be found by investigating the infection risk over time from agents with the highest average infection risks as seen in Figure 5.23. The crew side of the figure clearly shows ten crew members with a day average infection risk around or above 7%. The infection risk over time for these ten crew members is plotted in Figure 6.3 and Figure 6.4. When these crew members were investigated, it turned out that they follow a similar activity schedule divided between an early and a late shift. For all ten crew members, the two highest infection risk peaks correlate to the same location: node 107. This procedure was repeated for all guests with a day average infection risk above 2%. The same situation appeared as they all visited the bar at node 107 during their day and built up infection risk above 25% for that location. Node 107 was already found

to be an outlier in Table 6.1 with a day average infection risk above 16% and should be investigated in more detail. Comparing Table 6.1 and Table 6.2, two node locations appear in both tables: N330 and N293 which are investigated further. Lastly, the occurrence of N5 in Table 6.2 demands further analysis as it is a move-through area that presents with a relatively low day average infection risk compared to the other high-risk nodes.

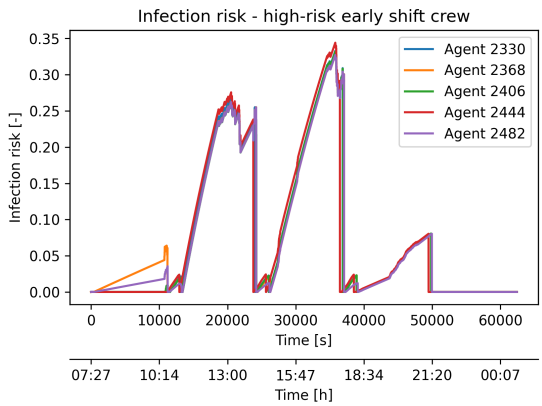

Figure 6.3: Infection risk for early shift high-risk crew

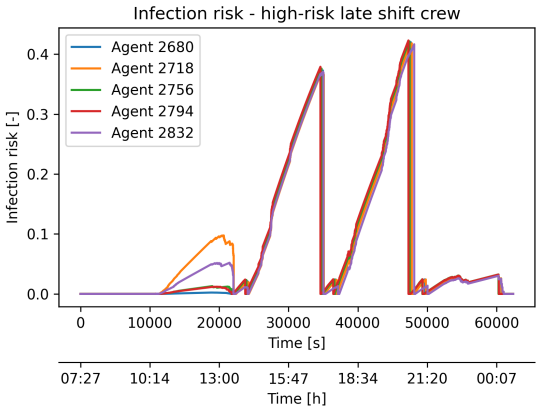

Figure 6.4: Infection risk for late shift high-risk crew

Node 5

The first high-risk node location discussed is N5. The node characteristics can be found in Table 6.3 and Figure 6.5. This specific location has come up already in subsection 5.2.2 as one of the two locations from which the crew starts their activity schedule, because the crew accommodations are not modeled. The choice was made to use an adjusted time range in the integrated model and avoid the unrealistic risk build-up which occurred at N5 and N33 at the start and end of the simulation. The crew occupancy in Figure 6.6 also shows this high occupancy at N5 for the late-shift crew at the start of the simulation and for the early-shift crew at the end of the simulation.

Function	Location	Node area	Maximum occupancy	Average IR
Move through area	PS - mid - deck 1	22 m^2	351	0.294%

Table 6.3: Characteristics node 5

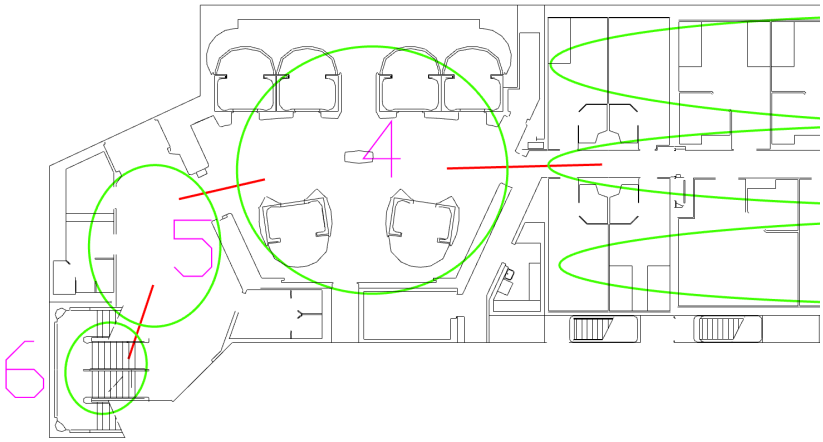

Figure 6.5: Deck 1 layout at node 5 [23]

For short periods of time in Figure 6.6, behavior similar to the situation before the crew shifts start and finish, can be seen. For these periods, the infection risk rises as the crew occupancy increases to 25% of the total crew population. The timings of these infection risk peaks coincide with the moment that the crew has their break. Looking at the activity schedules of the crew, it was discovered that the 'break' node location is set to be N5 or N33 for all crew, leading to high infection risks at N5. N33 has probably not occurred in subsection 6.1.1 because this node has a larger floor area of 34 m^2. The N5 average infection risk is not as high as the other nodes discussed in this section because the exposure duration is limited to 30-minute breaks. Further model improvements could be made by introducing and defining the crew accommodations for the ship layout. However, as discussed in chapter 5, this lies beyond the scope of this research project. Testing a layout change for N5 would not make sense because the problem lies with the use of this node as if it represents half the crew quarters, rather than the layout of this location itself. Therefore, no adjustments will be implemented for this location. In further work, it is recommended to model the crew accommodation more accurately to improve infection results during the crew breaks.

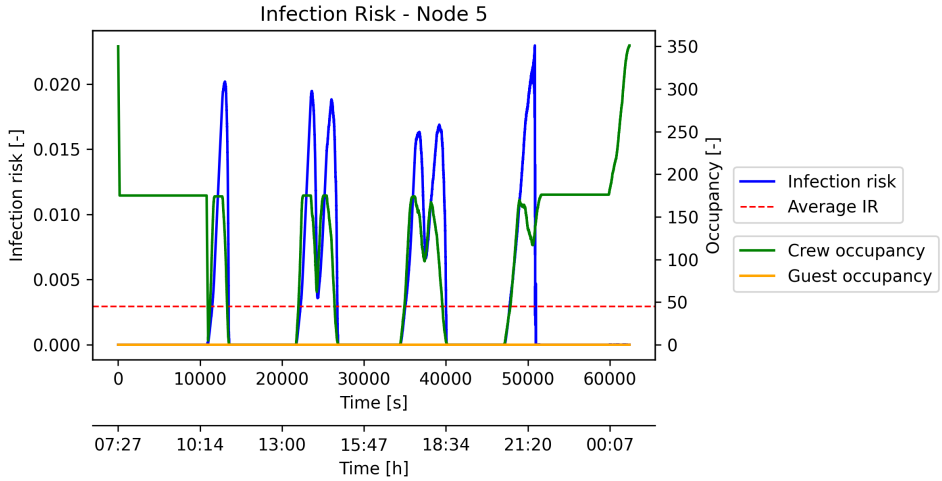

Figure 6.6: Infection risk and occupancy for node 5

Node 107

Node 107 presents as a significant outlier compared to the other high-risk nodes with an average infection risk of 16.8%. The high risk can be explained by the small node area of 6 m^2. The node characteristics are also presented in Table 6.4 and a partial layout of deck 5 can be seen in Figure 6.7. Node 107 equals node 4 in the drawing as the SAFEGUARD datasets restart their node numbering per deck [23]. Looking at the layout in Figure 6.7 it seems like there has been a node categorization error in the work by [26] and the activity schedule currently used. N107 has been designated as a bar and is used as an activity destination in the guest and crew activity schedules. However, it seems that N107(4) is a move-through area in front of the bar at N110(7).

Function	Location	Node area	Maximum occupancy	Average IR
Bar -> Move through area	SB - mid - deck 5	6 m^2	47	16.8%

Table 6.4: Characteristics node 107

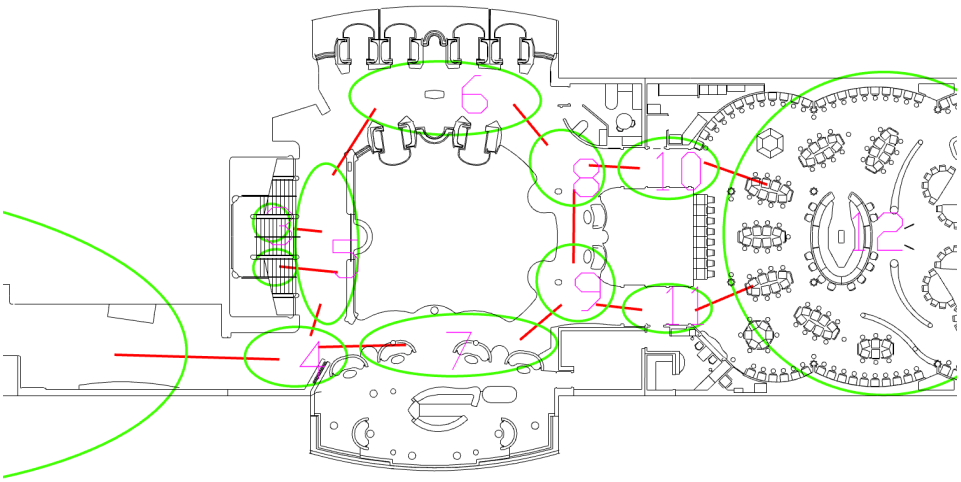

Figure 6.7: Deck 5 layout at node 107 (location 4 in drawing) [23]

Looking at Figure 6.8, the maximum infection risk at N107 reaches 30.2% which is much higher than the other high-risk locations N5, N293 and N330. Also, the infection risk stays high for longer periods of time which leads to the high average infection risk. The explanation for these results can be found in the combination of a 6 m^2 floor area and an average 20-person occupancy over the entire day. There are two options to deal with N107 and the extreme results. The first option would be to increase the floor area of N107 and decrease the floor area of N110 (which is the actual bar). The result would be a situation where there are two bars for this location. The second option merges the N107 'bar' with node 110. In this situation, the activity schedule is adjusted and the N107 activity entries for the crew and guests are replaced by N110. To stay closest to a realistic layout, the choice was made to substitute N107 for N110 in the activity schedule so that N107 becomes a move-through area. This adjustment thus presents an activity schedule correction rather than a direct layout change.

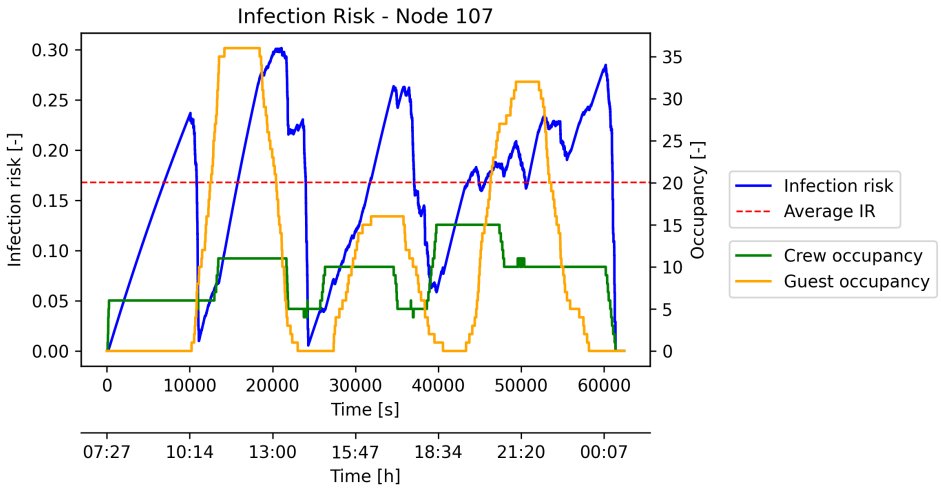

Figure 6.8: Infection risk and occupancy for node 107

Node 293

The third identified high-risk node is N293 which represents the location of a starboard side restaurant located on deck 10. Table 6.5 and Figure 6.9 show the local layout and characteristics of this node. N293 is given by location 10 in the layout drawing.

Function	Location	Node area	Maximum occupancy	Average IR
Restaurant	SB - aft - deck 10	32 m^2	166	2.67%

Table 6.5: Characteristics node 293

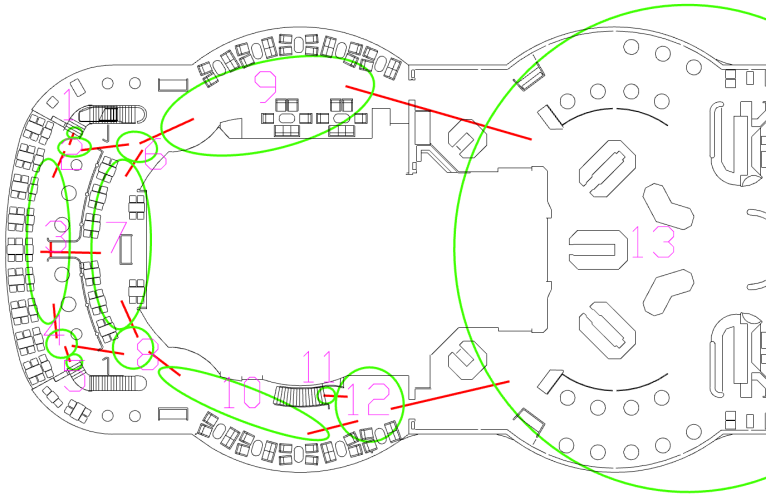

Figure 6.9: Deck 10 layout at node 293 (location 10 in drawing) [23]

Figure 6.10 gives the occupancy and infection risk specific to N293. The crew occupancy lies around fifteen crew members when one of the two crew shifts is working and around 30 agents when both shifts are at work. The highest guest occupancy can be found during breakfast with a maximum guest occupancy of 151 agents and a maximum infection risk of 5.82%. The guest occupancy increases during lunch to 84 agents and 116 agents for dinner. The crew and guest occupancy combined with extended exposure times, lead to high infection risks for the majority of the simulation.

In order to decrease the infection risk, the floor area of N293 should be increased. This area needs to be subtracted from surrounding nodes. The surrounding nodes are N291, N294 and N295 or respectively nodes 8, 11 and 12 in Figure 6.9. N291(8) has a floor area of 12m^2 and forms the connection between the N293(10) restaurant and the seating areas further aft. Placing tables and chairs at this location would be inconvenient as people move through this location and it does not have a large floor area. N294(11) is not an option either as this node represents the space close to the stairs with a small floor area of 5.58 m^2. Therefore, subtracting floor space from N295(12), with a floor area of 20 m^2, presents the most convenient choice. The N295 floor area will be reduced to 6 m^2 which is similar to other move-through locations and the N293 node area is increased to 46 m^2.

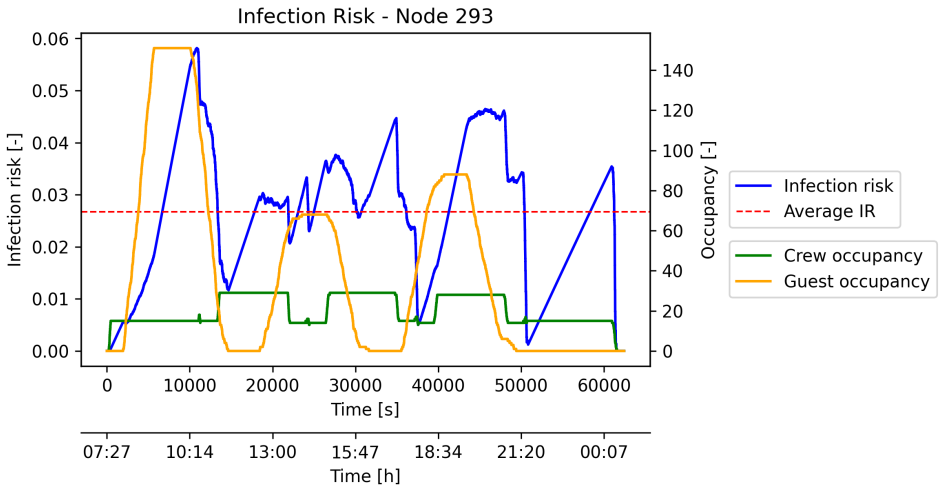

Figure 6.10: Infection risk and occupancy for node 293

Node 330

N330 is the last high-risk node analyzed in more detail. This node represents a restaurant on deck 11 as presented in Figure 6.11 with the characteristics mentioned in Table 6.6. The maximum occupancy is 160 agents, close to the maximum occupancy of node 293. However, the N330 area is only 25.2 m^2 against the 32 m^2 for N293. The average infection risk is 3.59% and this is the highest average risk (excluding outlier N107) compared to the other high-risk nodes discussed in this section.

Function	Location	Node area	Maximum occupancy	Average IR
Restaurant	SB - aft - deck 11	25.2 m^2	160	3.59%

Table 6.6: Characteristics node 330

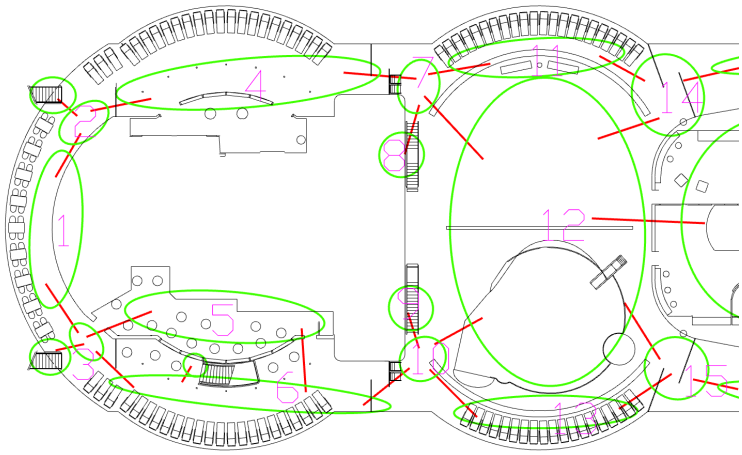

Figure 6.11: Deck 11 layout at node 330 (location 5 in drawing) [23]

The infection risk over time and node occupancy can be seen in Figure 6.12. The crew and guest occupancy trend for N330 shows similarities with the occupancy at N293. Just like the restaurant at N293, there is a guest occupancy peak around breakfast with 160 agents, and two additional smaller peaks corresponding to lunch and dinner with a total occupancy of 93 and 95 agents. The infection risk in Figure 6.10 follows the same trend as the infection risk in Figure 6.12 but the risk values for N330 are higher than the N293 risk values. This can be explained by the fact that N293 has a smaller area which leads to higher infection risk results.

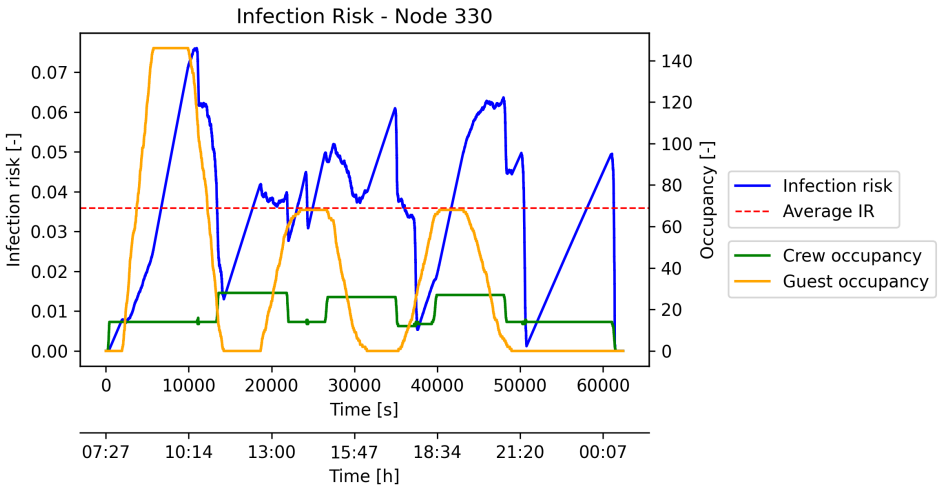

Figure 6.12: Infection risk and occupancy for node 330

To reduce the average infection risk of the restaurant at N330, the floor area should be increased. N330(5) lies close to the sundeck at N331(6) which has a floor area of 30 m^2. This sundeck could be adjusted in order to increase the area available for the restaurant. The neighboring N329(3) location shows less potential for area reduction as it is a move-through area in front of a staircase. The layout adjustment proposed for this node has more impact than the layout adjustment for N293. This can be supported by three considerations. Firstly, the average infection risk for N330 is higher than N293 which justifies a bigger layout adjustment to achieve a risk reduction. Secondly, the N331 sundeck has more space available to increase the restaurant area compared to N294. Lastly, for analysis purposes, it will be interesting to see the effect of a smaller layout change (N293) and a larger layout change (N330). The proposed changes around the N330 restaurant are as follows:

- The sundeck will be removed
- The node 331(6) becomes a move-through node of 6 m^2
- The N330 restaurant area increases to 49.2 m^2
- The link 328(3) - 331(6) and 331(6) - 328(3) will be removed
- The link 331(6) - 294(stairs) becomes 330(5) - 294(stairs)
- The link 294(stairs) - 331(6) becomes 294(stairs) - 330(5)
- The agents with the N331 sundeck in their activity schedule will be divided over the other three aft sundecks at N329(4), N336(11) and N338(13) in the following percentages: 60%, 20% and 20%. More agents will be assigned to N329(4) because it has three times the floor area of N336 and N338.

The layout adjustments for this situation also included the removal and adjustment of certain links in the route choice model. After careful consideration, this turned out to be more complex than anticipated. The RCM model in its current state does not allow for links to be removed or changed as it presents with errors after the first run. Also, it was noted that most agents do not reach their final scheduled destination, which gives problems for the second run. Instead of changing the layout itself, the choice was made to mimic a layout change by adjusting the activity schedule. The following schedule adjustments were made:

- The agents with the N331 sundeck in their activity schedule will be divided over the other three aft sundecks at N329(4), N336(11) and N338(13) in the following percentages: 60%, 20% and 20%.
- The agents with the N330 restaurant in their activity schedule will be divided 50/50 over N330 and N331 (which does not host sundeck guests anymore).
- The crew activity schedule, layout and node areas do not change.

6.1.2. Location-based evaluation for proposed layout adjustments

For the proposed layout adaptions, it is possible to run the integrated infection risk model and determine infection risk for every agent for every timestep. The evaluation of these results is divided into two subsections. In this subsection, the focus lies on the high-risk locations themselves to see if the layout adjustments impact local infection risk. In the second subsection, a more general evaluation is executed. In this evaluation, the overall infection risks for the whole ship and its population are analyzed for the proposed layout adjustments.

Node 107

Node 107 was identified as a high-risk location with an extreme average infection risk over 16%. This risk outlier can be seen in Figure 6.13, where the range for the y-axis has been restricted to match the axis range in Figure 6.14. Figure 6.14 shows the average node infection risks in the situation where N107 functions as a move-through area rather than a bar. The figure shows that N017 is no longer an outlier and has an average infection risk of almost 0%. This makes sense as the location has now become a move-through location where agents spend little time. Figure 6.14 also shows higher infection risks for N179, N197, N219 and N236. These nodes represent hallways on deck 7 and 8 next to the mid and forward staircases. The risk variations for these locations seems unrelated to the N107 layout change. They are perhaps more related to the agent route choices, including the controlled randomness, in the RCM model. This 'variance' in risk results is something to take into account when analyzing the general results and its significance in subsection 6.1.3.

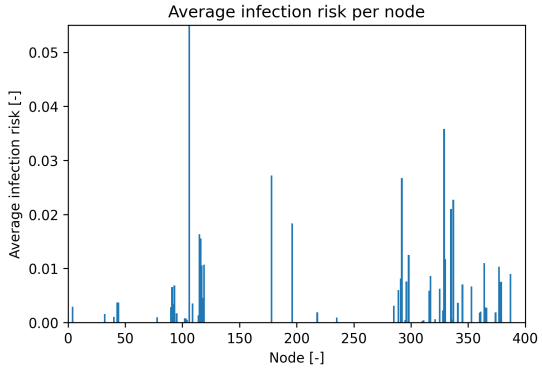

Figure 6.13: Average infection risk per node (y-axis range limited)

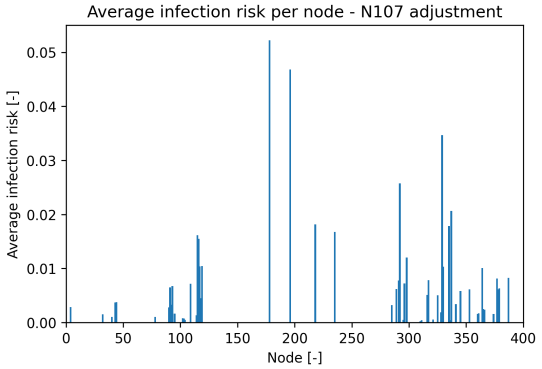

Figure 6.14: Average node infection risk for N107 layout adjustment

Node 293

The second layout adjustment was related to the restaurant at N293 which received a higher floor area at the expense of N295. Figure 6.15 presents the infection risk results at N293 for the sample case and adjusted layout. It can be seen that the adjusted layout leads to a lower infection risk over the day. In Figure 6.16, the restaurant and the average infection risk for node 293 and surrounding nodes are given. The average infection risk for the restaurant goes from 2.67% to 1.57%, a local risk reduction of more than 40%. Figure 6.16 also shows no risk increase for the surrounding nodes.

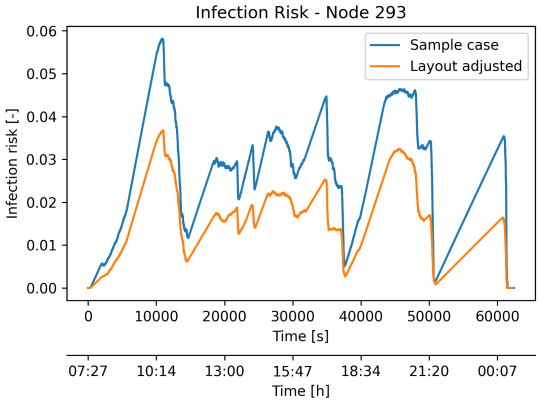

Figure 6.15: Infection risk for N293

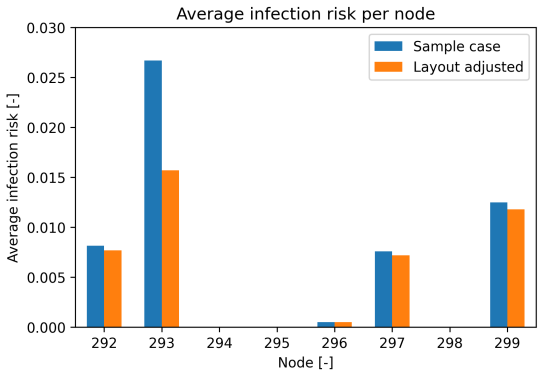

Figure 6.16: Average infection risk for N292 up to N299

Node 330

The final layout adjustment was proposed in an effort to decrease infection risk for the N330 restaurant. Figure 6.17 shows the infection risk over time for the sample case and adjusted layout. Different from the layout change for node 293, the N330 infection risk variations between the sample case and the adjusted layout are small. This is supported by the node average risk values presented in Figure 6.18. The average risk for N330 decreases from 3.59% to 3.30% while the average risk for N331 increases from 1.17% to 1.57%. The N330 risk decrease can be explained by the decreasing amount of guests eating at that location. The increasing risk for N331, which is now a restaurant space, might be related to the fact that the number of eating guests is higher than the amount of 'sundeck' guests in the sample case. Another consideration is the fact that the space is used at a different time because guests are spending their 'eating'-leg instead of an 'activity'-leg at N331. The rerouted guests using the other aft deck 11 sundecks do not significantly increase the infection risk for these locations (N329, N336 and N338). These sundecks remain at average infection risks of around 0.2% for both the sample case and layout adjustment.

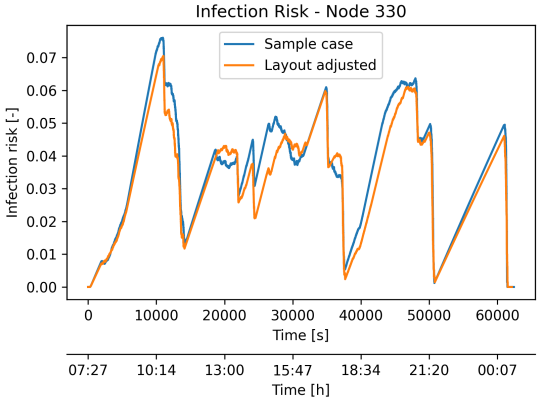

Figure 6.17: Infection risk for N330

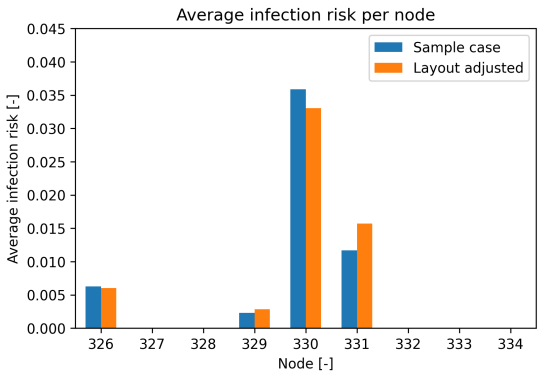

Figure 6.18: Average infection risk for N326 up to N334

6.1.3. General evaluation for proposed layout adjustments

In subsection 6.1.2, the infection risks for the sample case and three layout adjustments were investigated. The presented results in this section were location specific and no full ship results have been given yet. Therefore, in this section, a general evaluation of the proposed adjustments is given. Firstly, the average infection risk for the total population is calculated for the sample case and the layout adjustments. Secondly, the average infection risk over time is given for the different situations. Thirdly, two frequency figures are presented for the average agent infection risk and the number of agents with an infection risk above 50%.

Table 6.7 shows the average infection risk for the sample case (SC1) and the layout adjustments. The first observation is that risks for the adjustments and sample case lie relatively close together. The crew infection risks exceed the guest risks for both the layout adjustments and the sample case. Additionally, the layout adjustment results give slightly higher infection risks than the sample case. This would mean that the layout adjustments have a negative impact on the general risk, even if they do provide risk improvements on a local level. However, it is important to be careful formulating conclusions from these average risks because of two reasons. Firstly, the validation from section 5.6 should be taken into account when analyzing these results. This validation of the integrated model against similar cases showed variation in risk results. For the multi-room office space, the differences between the integrated model and the research by Dai and Zhao were in the order of 1 or 2%. One can question the significance of a 0.1 or 0.2% difference in the average infection risks between the tested cases.

The second reason to be careful when formulating conclusions based purely on Table 6.7, is the variation related to the RCM model outcomes. This variation comes from the controlled randomness embedded in the model to account for individual agent route choices. Therefore, a second sample case (SC2) is presented to showcase the infection risk for another RCM model outcome. This SC2 features higher infection risks than the original sample case (SC1). The average risk results for the layout adjustments lie between SC1 and SC2. Taking the discussed considerations into account, the layout adjustments do not have a significant effect on the general average infection risks for the crew, guests and total population. Also, comparing the different layout adjustments on a ship level is complicated because the risk variations can not be distinguished from risk variations related to the RCM model.

Result [%]	SC1	SC2	N107	N293	N330	All adjustments
Average IR	0.807	1.05	0.922	1.02	1.03	0.902
Average guest IR	0.730	0.935	0.839	0.914	0.913	0.829
Average crew IR	1.04	1.39	1.17	1.34	1.39	1.12

Table 6.7: Average infection risks sample cases and layout adjustment

The average infection risk over time can be seen in Figure 6.19. Both the sample cases and the layout adjustments follow the same trend over the day. However, SC1 does not show the infection risk increase between 13:30 and 16:00. This might explain the lower average infection risk results in Table 6.7. Additionally, the N330 and N293 layout adjustments present with higher peak risks around 13:00 which correlates with the end of the first activity. This seems again related to variation for the RCM model as the layout adjustments mainly cover restaurant spaces. For the N330 layout adjustment, the peak could be related to the distribution of sundeck agents to other locations. However, in subsection 6.1.2 it was already mentioned that these other sundeck locations do not present with an increased infection risk. It is therefore unlikely that the increased infection risk at 13:00 for the N330 adjustment correlates to the layout adjustment itself.

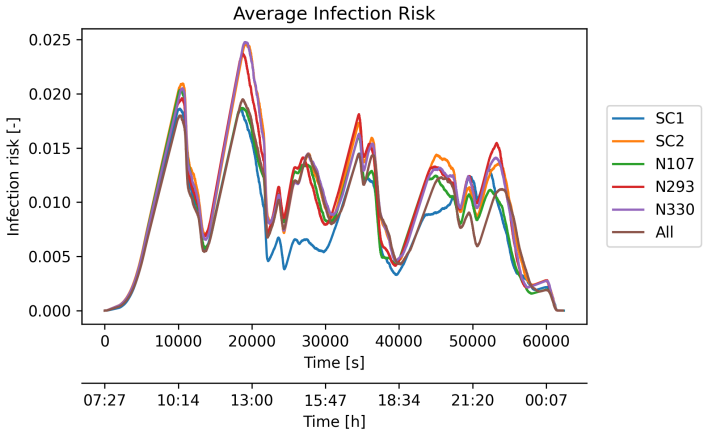

Figure 6.19: Average infection risk - layout adjustments

Figure 6.20 and Figure 6.21 visualize frequency figures for the average infection risk and number of agents with an infection risk above 50%. Just like Table 6.7 and Figure 6.19, the SC2 results and adjusted layout simulation results provide similar distributions. Most agents have an average infection risk below 1% which lies close to the average infection risk result. Both figures do not show significant risk improvements for the layout adjustments when focusing on the whole ship and the total population. Sample case 1 does give interesting results compared to sample case 2 and the layout adjustment. It has fewer agents with an infection risk over 50% and it shows a higher number of agents with an average infection risk below 1%. Comparing the layout adjustments and the second sample case results with SC1, it can be concluded that SC1 lies somewhat on the positive side of the range of results (related to the RCM outcome variation). The combination of SC1 and SC2 is very useful when the layout adjustments, operational and behavioral measures are tested. Sample case 1 is conservative in the sense that it already has 'low' infection risk values without any adjustments or measures. SC1 thus provides a conservative reference when investigating risk improvements. This helps to put the significance of achieved improvements into perspective while the second sample case provides a more mid-range reference.

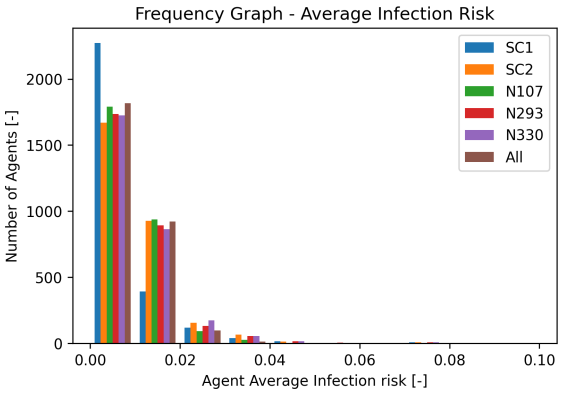

Figure 6.20: Average infection risk distribution - layout adjustments

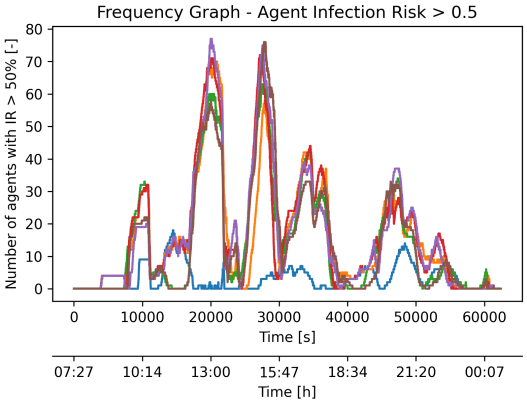

Figure 6.21: Infection risk above 50% - layout adjustments

Two additional frequency figures for agents at high-risk can be found in Figure 6.22 and Figure 6.23. In these figures, the number of agents with a risk above 90% is given over time for the two sample cases, N107 layout adjustment and the scenario combining all layout adjustments. For the N293 and N330, there are no significant improvements compared to the base cases and they are therefore not shown in the figures. For the N107 categorization correction and the combined scenario, a significant improvement can be recognized. For these two cases, there are respectively three moments and one moment in time where agents present with risks above 90%. For the rest of the day, there are no agents with infection risks above 90%. The improvement for the combined scenario is probably only related to the N107 adjustment because the other two adjustments do not significantly decrease the number of at-risk agents.

In conclusion, the full-ship average infection risk differences for the layout adjustments and the two sample case situations are difficult to distinguish from the RCM-induced variations. It does make sense that the layout adjustments do not result in large general risk changes as the layout adjustments are relatively small compared to the size of the total ship. Also, the agents affected by the layout change only cover a small part of the total population. There is a notable difference between the agents at high risk for the N107 adjustment and the case where all layout adjustments are implemented. The amount of agents at high risk is reduced to either 3 moments (N107) or 1 moment (all adjustments) where there are any agents with a risk above 90%.

It is advised to implement the N107 and N293 layout adjustments even if they provide mainly infection risk improvements on a local level. The N107 adjustment is important as it solves a categorization issue that resulted in very high local infection risks and a high number of agents with a risk above 90%. The N293 restaurant adjustment does provide local risk improvement and it does not negatively affect sur-

rounding nodes. The local positive risk improvement for the N330 adjustment is less straightforward as the improvement comes with a risk increase for N331. This adjustment is therefore not recommended and other measures or adjustments might be considered at this location. For example, limiting the number of people allowed, promoting other restaurants onboard or working with reservations to spread the local occupancy.

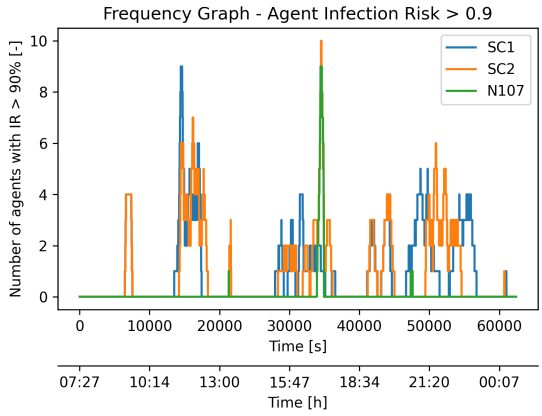

Figure 6.22: Infection risk above 90% - N107 adjustment

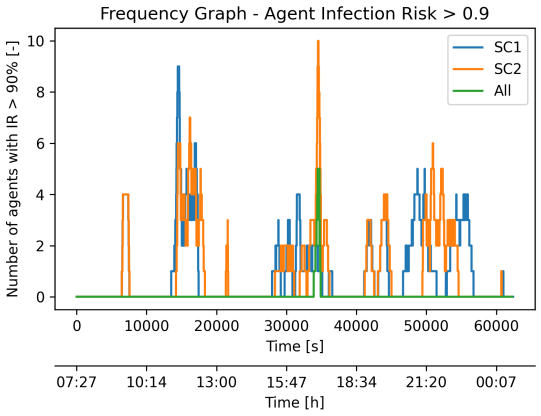

Figure 6.23: Infection risk above 90% - all layout adjustments

6.2. Operational measures

This section covers two types of operation measures described in chapter 2: one-way movement and a capacity reduction. For the one-way movement measure, two scenarios are explored from which one covers the mid and fwd staircases. The other scenario involves the walking route to and from the main restaurant (N296) on deck 10.

6.2.1. One-way movement

Forced one-way movement is an operational measure which was applied widely during the COVID-19 pandemic. The basic idea is that people all walk in the same direction which improves flow movement and thus decreases risk. It is important to realize that counter-flow in hallways and corridors is not simulated in the RCM model. The links are bi-directional themselves but they are split up in two direction paths which do not interact with each other. This assumption might affect the results for the forced one-way simulations. Additionally, in subsection 6.1.1 it was noted that the RCM in its current state does not function when links are removed. The logical way to mimic forced one-way movement is to remove the links from the input files. Alternatively, the choice was made to increase the length of the relevant links to 200m. The route via these links will have a lower utility and therefore be a less favorable route choice for the agent. However, this does mean that some agents might still choose a route via these links. If the agent does choose to move against a 'one-way' link, the travel time will increase significantly because of the link length.

The results of the one-way movement are described in Appendix F. The implementation of the tested one-way movement scenarios is currently not recommended. The nodes proved to have a significantly higher infection risk than the links and one-way movement specifically targets movement and thus link locations. In general, this operational measure was explored but further model development and research are required to justify the implementation of this measure.

6.2.2. Capacity reduction

The second investigated operational measure is a general capacity reduction for both the crew and guests. This measure was implemented through the adjustment of the activity schedule input. The investigated capacity reductions are $CR = [10, 20, 30, 40, 50, 60, 75]$% or [2562, 2280, 1994, 1708, 1422, 1140, 711] agents. For every case, the required number of agents has been randomly removed from the activity schedule while the guest-to-crew ratio is kept the same. The five RCM repetitions were executed for one random population draw in order to decrease the total simulation and post-processing time. It is important to note that a single random population draw might result in additional variation besides the route choice model variation. Both the reduction percentages and the number of remaining agents are given in all legends for the result figures.

Figure 6.24 presents the average infection risk for the reduced populations. The results are presented in a figure with the capacity reduction on the x-axis rather than a table. The risk increases from CR = 20% to CR = 30% and the crew risk increase between CR = 50% and CR = 60% are probably related to the randomness from the population draws and the RCM output. The sample case 1 and sample case 2 results can be seen as horizontal lines. The first observation is that the average infection risks decrease for higher capacity reduction. This was expected as fewer agents will result in higher social distances and thus lower infection risk. However, the average infection risk decrease remains small compared to the sample cases, even for higher capacity reductions. Take for example a 75% capacity reduction, which means that there are only 175 crew members and 536 guests onboard. The total average infection risk is 0.630%, only 22% lower than SC1 (conservative reference). The average infection risks become smaller than SC1 after a 50% capacity reduction. The total average infection risk for a 50% and 60% capacity reduction are 0.786%(-2.6%) and 0.755%(-6.5%) compared to SC1. All capacity reductions result in lower average infection risks than the less conservative sample case 2. Compared to SC2, a 50% capacity results in a 25% risk reduction, CR = 60% leads to a 28% risk reduction and CR = 75% gives a 40% risk reduction.

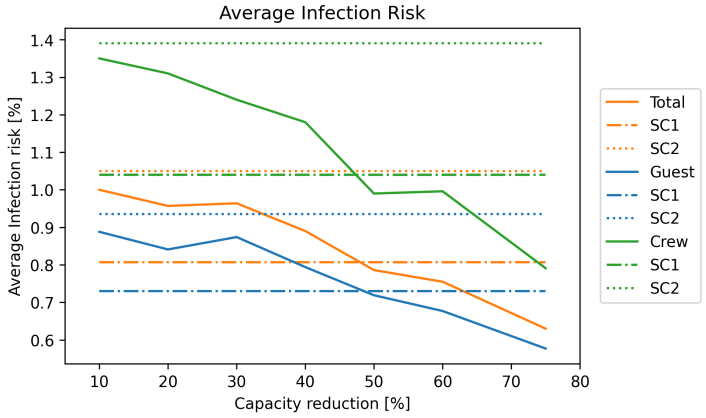

Figure 6.24: Average infection risk over capacity reduction

The average infection risk over time is given in Figure 6.25 and Figure 6.26. The results are presented over two figures to increase the readability as the results lie close together for the majority of the time. Figure 6.25 covers the capacity reductions from 10% up to 40%. The different cases present with similar average infection risks over time related to the sample cases. In Figure 6.26, the average infection risk for the higher capacity reductions is visualized. For a smaller amount of agents onboard, the risk peak values decrease which in turn will lead to a lower total average infection risk as seen in Figure 6.24.

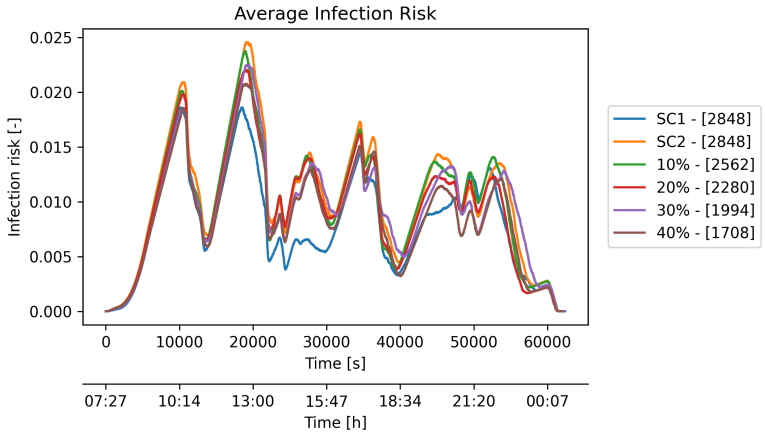

Figure 6.25: Average infection risk - capacity reduction 10%, 20%, 30% and 40%

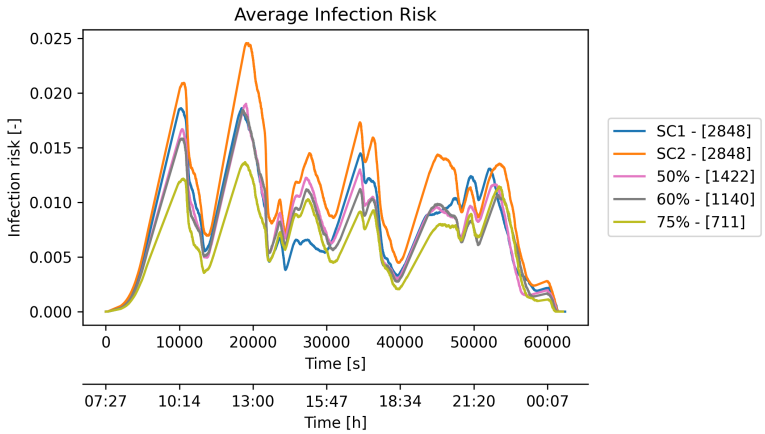

Figure 6.26: Average infection risk - capacity reduction 50%, 60% and 75%

Figure 6.27 shows the agent average infection risk for the different capacity reductions. The results are presented in percentages rather than absolute numbers because the cases all have different population sizes. The frequency distribution moves left for increasing population reductions. This means that a higher percentage of the population has a lower agent average infection risk. For capacity reductions over 50%, the distributions come close to sample case 1 and for 75%, the distribution lies more left than SC1. This observation matches the observations relating to the average infection risks over time.

In Figure 6.28, the agents with risks above 50% for 10% up to 40% capacity reductions are given. Just like the average risk over time, the results have been presented in two separate figures. Figure 6.29 shows the 50%, 60% and 75% capacity reduction scenarios. Different from Figure 6.25, the 'smaller' capacity reductions do seem to affect the number of agents at high risk in Figure 6.28. For example, the 20% and 40% capacity reductions decrease the peaks at 13:00. The 40% capacity reduction also has a smaller percentage of high-risk agents around 12:00. It is important to note the fact that the variation related to the RCM model input clearly influence the results in this figure. The 10% reduction, for example, does show a decrease for second peak but is also shows an increase for the third and fifth peak compared to the second sample case. And, when investigating the second 13:00 peak, a 20% reduction decreases the result while the 30% reduction result lies above the 20% result. This is contrary to the general idea the a smaller population using the same layout will have more space available and therefore smaller infection risks. This was seen for the average values in Figure 6.24 up to Figure 6.27. On a more local level, however, RCM model output variations might lead to less predictable results as seen in Figure 6.28.

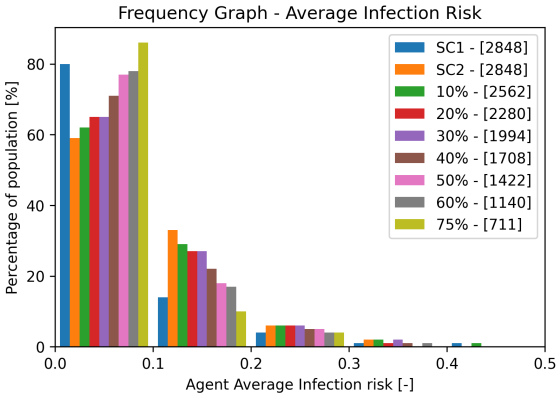

Figure 6.27: Average infection risk distribution - capacity reduction

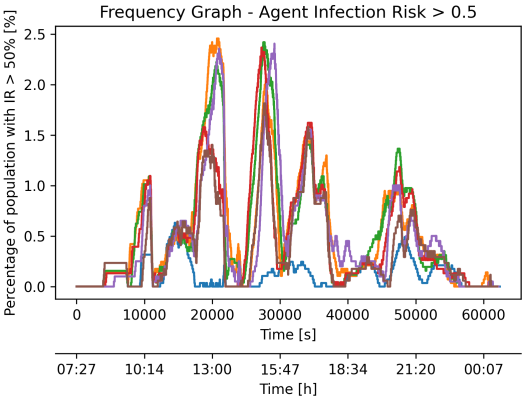

Figure 6.28: Infection risk above 50% - capacity reduction 10%, 20%, 30% and 40%

The final figure for the capacity reduction results is given in Figure 6.29 for 50%, 60% and 75% reduction scenarios. In general, for larger capacity reductions the percentage of agents with a risk above 50% reduces. This is specifically seen for the 10:15, 13:00 and 15:30 peaks when the reduction scenarios are compared to the SC2.

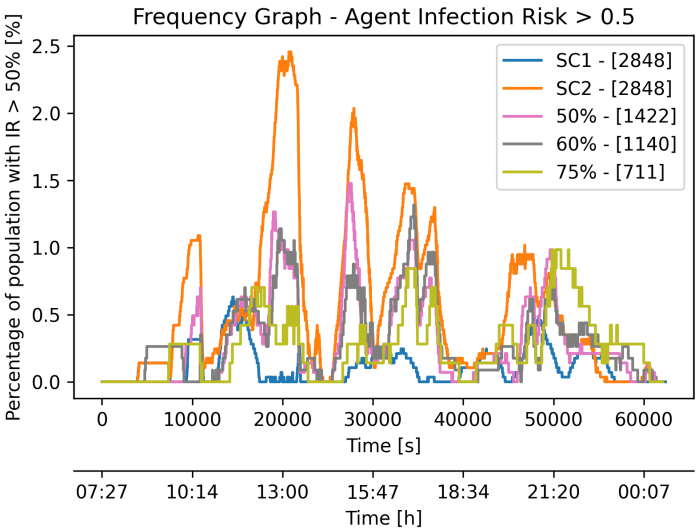

Figure 6.29: Infection risk above 50% - capacity reduction 50%, 60% and 75%

Combining all the presented results for the capacity reductions, the following conclusions can be drawn. First of all, a reduction in the amount of agents does decrease the average infection risk and the percentage of agents at high-risk. The size of the average risk reduction depends on the chosen reference. Compared to CS1, it takes a 50% capacity reduction to achieve lower average infection risks than the reference. However, compared to the less conservative sample case 2, a 50% reduction results in a 25% average infection risk reduction and all tested capacity scenarios have lower average infection risks. A possible reason for the the fact that high capacity reductions are required to achieve average risk improvements compared to SC1, might be found in the initial densely populated environment onboard.

Taking a high capacity reduction might be the best choice from an infection point of view but it is important to realize that this operational measure has major consequences. For example, a cruise ship is optimized to host a maximum number of guests and crew to increase and ensure profitability. Running a cruise ship at lower capacity means that cruises become more expensive and for a 75% capacity

reduction, the cruise ship might not be profitable at all. For a naval vessel, which is optimized in terms of crew complement and operability, a capacity reduction can have far-reaching effects as there is less personnel available to execute a certain mission or operate the systems onboard. Implementing a high capacity reduction thus might not be a workable option when operability and profitability are taken into account. It is therefore advised to consider a limited capacity reduction in combination with other measures. To further investigate this option, section 6.4 presents six combination scenarios for layout adjustments, behavioral and operational measures. The capacity reductions used for further testing are a 50% reduction as this was the first scenario which presented with lower average risk results than SC1. Also, a smaller 30% capacity reduction is tested in the combination scenarios. This capacity reduction functions as a compromise between infection risk, profitability and operability considerations.

6.3. Behavioral measures

This section focuses on behavioral measures in order to decrease infection risk. In chapter 2, different behavioral measures were described like social distancing, vaccinations, personal protective equipment and personal hygiene. The measure analyzed in more detail is personal protective equipment in the form of wearing a surgical mask. This behavioral measure was frequently implemented during the COVID-19 pandemic. Three variations of this behavioral measure are modeled and described in the subsections below.

6.3.1. Modeling mask wearing

Wearing is a mask can be conveniently covered by the implementation of an exhalation filtration efficiency η_E and a respiratory filtration efficiency η_R. The exhalation filtration efficiency affects the quanta production rate as presented in Equation 6.1. This efficiency covers the infector wearing a mask which reduces the amount of infectious particles spread. The respiratory filtration efficiency affects the pulmonary ventilation rate as given in Equation 6.2, representing the susceptible agent wearing a mask and therefore inhaling fewer infectious particles. The adjusted pulmonary ventilation and quanta production rates are implemented in the modified Wells-Riley Equation 3.3. Literature reports the filtration efficiencies of surgical masks between 50% and 60% [102, 17]. In this research, the mask filtration efficiency is chosen to be 50%. Listing G.1 shows the two filtration efficiencies and a third parameter used to impose specific actions for either the guests or the crew.

$$q_{adjusted} = q(1 - \eta_E) \tag{6.1}$$

$$p_{adjusted} = p(1 - \eta_R) \tag{6.2}$$

Masked agent movement

The first scenario is the situation where the guests wear a mask whenever they are moving. Movement means that the agent has a state of 0, 2 or 3. The crew is assumed to wear a mask continuously over the day. Listing G.2 shows the additional code to account for this masked movement scenario. This code is implemented after *Line 2* in Listing C.6.

Continuous mask wearing

In the second scenario, the guests are wearing a mask during movement and their activities. However, wearing a mask at breakfast, lunch and dinner does seem rather impractical. The agents are therefore not wearing a mask when they are eating in one of the restaurants. The node locations for these restaurants are as follows: N330, N299, N297, N296, N293, N292, N290, N286, N105, N104, N79, N45, N44 and N41. The crew is, again, assumed to continuously wear a mask. The code modifications can be found in Listing G.3 and Listing G.4. Listing G.3 is added after *Line 7* in Listing C.4 when the agent is located at a node. Listing G.4 is inserted after *Line 8* in Listing C.5 when the agent moves over a link.

Mask wearing based on social distance

The final variation tested is social distance based mask wearing. In this situation, the crew and guests are obliged to wear a mask when the social distance becomes smaller than a set safe distance. It is assumed that all crew and guests are compliant with this behavioral measure. In real life, there are probably agents who do not wear the mask even if the social distance becomes small. During the

COVID-19 pandemic, the CDC recommended a 6ft social distance and in Europe a distance of 1 to 2 meters was recommended [11, 20]. The safe distance used for the simulations is set to 1.5 meters. The guests will not wear a mask during breakfast, lunch and dinner, even if the social distance becomes smaller than $1.5m$. The model modifications are presented in Listing G.5 and Listing G.6. Listing G.5 is inserted after *Line 27* in Listing C.4 and Listing G.6 is implemented after *Line 24* in Listing C.5.

6.3.2. Evaluation mask scenarios

The average infection risks for the scenarios with mask wearing can be found in Table 6.8. For all scenarios involving face masks, the average total risk results are lower than both sample cases. When guests only wear masks when they are moving, the average risk reduction is 2.4% compared to SC1 and 25% compared to SC2. In the movement scenario, the crew is continuously wearing a mask which results in a significant decrease in the crew average infection risk. This crew risk reduction affects the total average result as the guest risk does not show improvement. The fact that the guests are wearing masks during movement in itself thus does not significantly improve infection risks.

The highest improvements are achieved for continuous and social distance(SD) based mask wearing with average infection risk of 0.451% and 0.487%. This represents a 44% and 40% risk reduction compared to SC1. The crew average risk in the SD based scenario is slightly higher compared to the situations where the crew is continuously wearing a mask.

The guest infection risk for the second and third scenario variations lie close together. In both situations, the guests are not wearing a mask when they are eating. For the rest of the day, there seems to be little difference in risk for either continuous or social distance based mask wearing. One possible reason could be that the social distance is smaller than the set safe distance for a majority of the time. This means that guests in the social distance scenario are almost continuously wearing a mask which would result in similar risk results.

Result [%]	**SC1**	**SC2**	**Movement**	**Continuous**	**SD based**
Average IR	0.807	1.05	0.787	0.451	0.487
Average guest IR	0.730	0.935	0.925	0.478	0.481
Average crew IR	1.04	1.39	0.362	0.369	0.506

Table 6.8: Average infection risks sample cases and mask wearing cases

Figure 6.30 gives the average infection risk over time. The masked movement scenario follows a similar trend to the conservative sample case 1 which is supported by similar total average infection risk values in Table 6.8. The average infection risk for the continuous and SD based scenarios is lower for the majority of the time. However, the 10:15 risk peak showcases interesting behavior as this peak does not decrease, even for continuous or SD based mask wearing. This peak correlates with the end of breakfast and can be explained by the fact that guests do not wear masks when they are eating. Continuing on this reasoning, the end of lunch peak around 15:30 and end of dinner peak around 20:00 are also expected to show little risk improvement for the masked scenarios. The figure indeed shows that for these timings there is little risk improvement for the tested cases compared to SC1. Contrary to the meals, more pronounced risk decreases are recognized for the activities in between the meals around 13:00, 17:00 and after 21:30 for the evening activity. This makes sense as the guests are wearing masks during these activities either continuously or based on social distance.

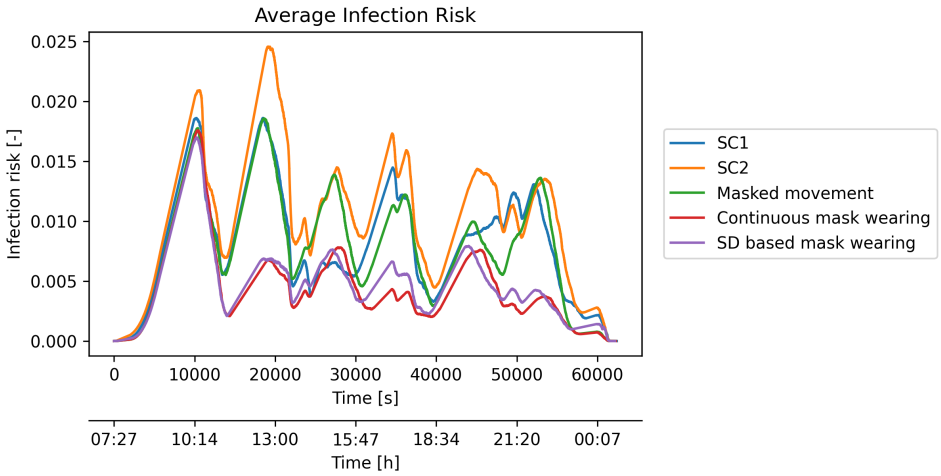

Figure 6.30: Average infection risk - mask wearing

The frequency figures for the mask wearing scenarios are presented in Figure 6.31 and Figure 6.32. For the second and third masked cases, the frequency distribution of the agent average infection risk moves left as expected. The masked movement shows a slight improvement compared to the second sample case. This improvement can be attributed to the crew, who are continuously wearing masks. Looking at the number of agents with infection risks over 50%, continuous and social distance based mask wearing result in significant improvement. The maximum number of agents with a risk above 50% is 6 agents for these two cases compared to 70 agents for SC2. The masked movement scenario even results in 80 agents at high risk around 15:30. With the differences in when guests and crew are wearing masks, it is useful to present two additional figures which show the amount of guests or crew with an infection risk above 50%.

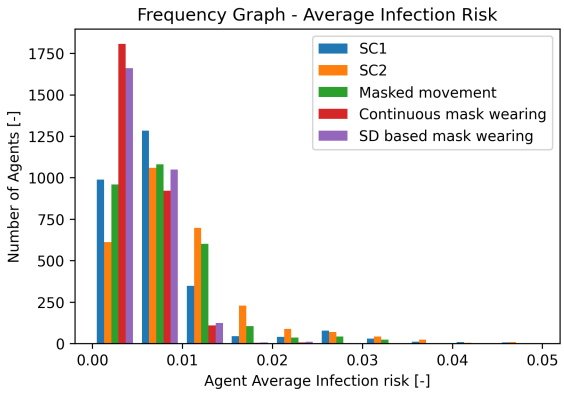

Figure 6.31: Average infection risk distribution - mask wearing

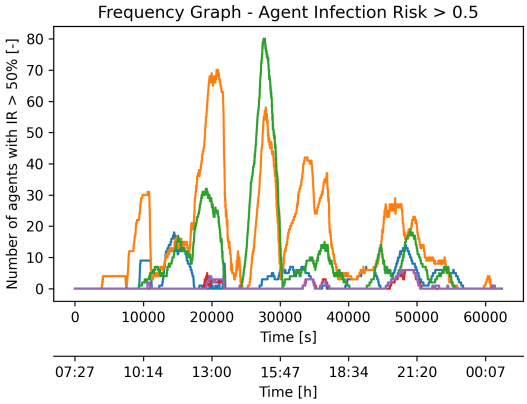

Figure 6.32: Infection risk above 50% - mask wearing

In Figure 6.33, the amount of guests at high risk is presented. For the masked movement scenario, the results follow the same trend as the second sample case. The peak increase around 15:30 can probably be assigned to variations in the RCM model input. In general, wearing a mask solely during movement does not significantly improve the infection risks experienced by the guests. This figure also shows that there are no guests with a risk above 50% for the two other scenarios involving masks, except around 13:00. This is a major improvement. For the crew, a similar improvement can be seen in Figure 6.34, especially with SC2 as a reference. The amount of at-risk crew members is significantly reduced for all three mask wearing scenarios. The maximum number of crew members at high risk is 6 compared to 9 and 38 crew members for SC1 and SC2.

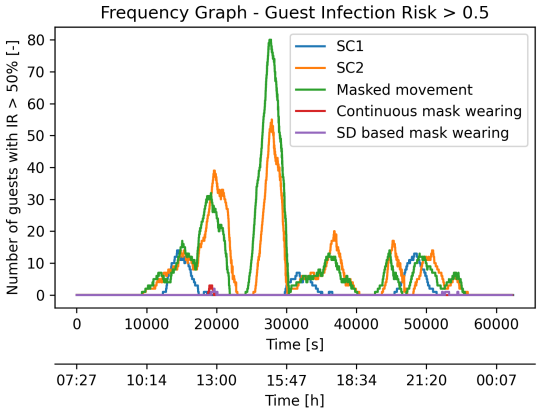

Figure 6.33: Guest infection risk above 50% - mask wearing

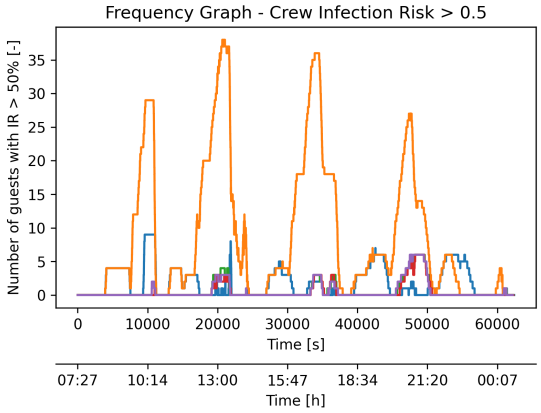

Figure 6.34: Crew infection risk above 50% - mask wearing

Taking the presented results into account for both the crew and guests, the continuous and social distance based mask wearing show the most potential. Choosing between these two behavioral measures, which show similar results in terms of infection risk, might instead be a question of preferred policy. Continuous mask wearing as a measure provides more clarity as both guests and crew know when to wear a mask. Also, it avoids the situation where agents are taking off and putting on the masks multiple times. This might be unhygienic and decrease the efficiency of the masks itself. Instead, a social distance based measure does help to create awareness around social distancing and crowded spaces. Guests can choose a different activity or route based on how busy it is so that they do not have to wear a mask.

Also, it would be interesting to investigate the effect of combined mask wearing measures, capacity reductions and layout adjustments. The continuous and social distance based mask wearing measures are combined with operational measures and layout adjustments in section 6.4 as they showed the most potential.

6.4. Combined measures

The layout, operational and behavioral measures evaluated in the previous sections can also be implemented in combinations. The N293 layout adjustment was proven to decrease local infection risk and the N107 adjustment solves a categorization issue. The 50% capacity reduction is tested because it presented the first CR with an average infection risk below the SC1. The 30% capacity reduction represents a compromise between infection risk, economic and operational feasibility. The layout and capacity interventions are combined with continuous and social distance based mask wearing. These combinations have to potential to further decrease average infection risks and decrease the number of agents at high risk. The combinations are presented in Table 6.9 and the average infection results are given in Table 6.10.

Combination	Layout adjustment	Capacity reduction	Mask wearing
C1	N107 & N293	CR = 30%	-
C2	N107 & N293	CR = 50%	-
C3	N107 & N293	CR = 30%	Continuous mask wearing
C4	N107 & N293	CR = 50%	Continuous mask wearing
C5	N107 & N293	CR = 30%	SD based mask wearing
C6	N107 & N293	CR = 50%	SD based mask wearing

Table 6.9: Specifications combined measures

Combination C1 and C2 do not feature mask wearing. Implementing the layout adjustments does result in slightly better average infection values: 0.787% and 0.667% compared to 0.964% and 0.786% as

presented in subsection 6.2.2. Combination C3 and C4 achieve the highest average risk improvements. These combinations feature capacity reductions combined with continuous mask wearing. The average infection risk decreases to 0.343% and 0.295%, with even lower crew infection risks. This presents a 57% and 64% risk reduction compared to SC1 while a 44% reduction was achieved for continuous mask wearing as a stand-alone measure. For C3 and C4, the crew infection risk is smaller than the guest infection risk because the crew is continuously wearing masks while the guests take off their masks during meals. The risk reductions for C5 and C6 are slightly smaller than the reductions for C3 and C4 which matches with the findings in section 6.3. Again, the crew and guest risks are similar because both groups are wearing masks whenever the social distance is smaller than $1.5m$. Evaluating the capacity reductions, a 50% capacity reduction does decrease the infection risk compared to 30%. However, these differences seem rather small compared to economic and operational impact which a 50% reduction might have compared to a 30% capacity reduction. The results in Table 6.10 are supported by Figure 6.35 which shows a significant decrease in average infection risk for C3 up to C6 after breakfast.

Result [%]	**SC1**	**SC2**	**C1**	**C2**	**C3**	**C4**	**C5**	**C6**
Average IR	0.807	1.05	0.787	0.667	0.343	0.295	0.427	0.396
Average guest IR	0.730	0.935	0.724	0.624	0.377	0.324	0.432	0.397
Average crew IR	1.04	1.39	0.978	0.800	0.240	0.207	0.412	0.392

Table 6.10: Average infection risks sample cases and combined measures

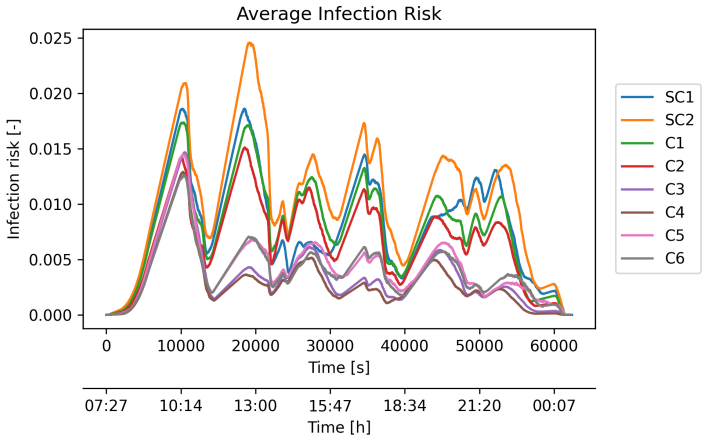

Figure 6.35: Average infection risk - combined measures

Figure 6.36 shows that for C3 up to C6, almost 100% of the agent average infection risks are below 0.1%. This is a higher percentage of the population compared to Figure F.3 for capacity reduction as a stand-alone measure. When the number of agents with a risk above 50% is calculated, it turns out that for C3 and C5, there are no agents with a risk above 50%. For C4 and C6, there is only a single moment in time, 10:30 (C4) and 14:15 (C6), where there are 2 agents with an infection risk above 50%. This shows a further improvement compared to Figure 6.33 and Figure 6.34 for mask wearing scenarios without capacity reduction.

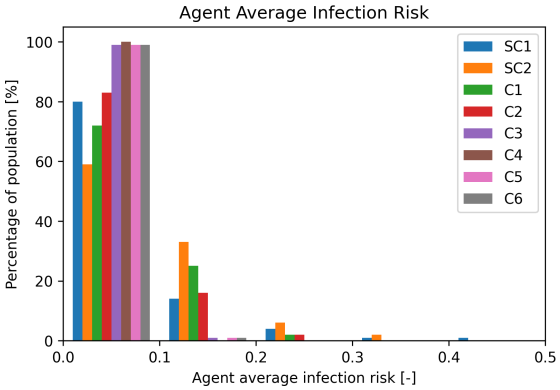

Figure 6.36: Average infection risk distribution - combined measures

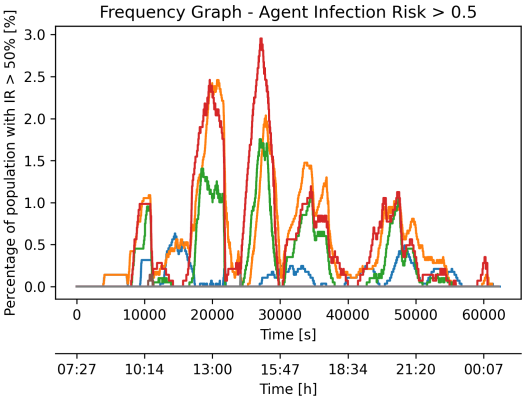

Figure 6.37: Infection risk above 50% - combined measures

6.5. Conclusion

Table 6.11 visualizes an overview of the average infection risks for the measures and combinations that showed the most potential. The N107 adjustment dealt with a categorization error, improving the number of agents at a risk above 50%. The average infection risk for the N293 adjustment lies, like the N107 adjustment, in between the sample cases which can be related to the randomness in the RCM model. The N293 layout adjustment did provide local risk improvement without compromising adjacent node locations and is therefore implemented in the combination cases.

Applied measure(s) and adjustment(s)	**Average IR compared to SC1 [%]**	**Average IR compared to SC2 [%]**	**Reduction number of agents IR > 50%**
Layout N107	+ 14	- 12	Yes
Layout N293	+ 26	- 3	No
CR = 30%	+ 19	- 8	No
CR = 50%	- 3	- 25	Yes
Continuous mask wearing	- 44	- 57	Yes
Social distance based mask wearing	- 40	- 54	Yes
C3	- 57	- 67	Yes
C4	- 63	- 72	Yes
C5	- 47	- 59	Yes
C6	- 51	- 62	Yes

Table 6.11: Applied measures and adjustments results overview

For higher capacity reductions, the average infection risk and number of agents at high risk decreases. However, implementing these high capacity reductions might introduce issues around economic and operational feasibility which should be further investigated. Therefore, implementing a 'lower' capacity reduction in combination with other measures could be preferable. Significant risk reductions were achieved when crew and guests start wearing masks. The most promising results were realized for continuous and social distance based mask wearing. With these mask wearing measures, four combinations were evaluated which showed large average risk reductions reducing the number of agents with a risk above 50%. The highest average risk reductions were found for C3 and C4 combining continuous mask wearing with a capacity reduction. It was noted that the additional risk decrease, when the capacity is reduced from 30% to 50%, is relatively small. This is relevant when a capacity reduction is considered against non-infection risk related requirements like a feasible manning.

7

Discussion

The integrated infection and crowd behavior model provides a proof of concept that implementing an infection and movement model is possible while incorporating crew and guest circulation through a ship layout. The integrated model was used to simulate COVID-19 infection risk for a selection of measures and layout adjustments onboard a cruise vessel. Certain assumptions were required during the model development and scenario evaluation in order to move forward. These general assumptions cover for example the agent activity schedule, the ship layout and the selected parameters.

Next to these assumptions, the evaluated sample cases revealed the variation related to the route choice model output. Sample case 1 presented relatively low infection risks without implementing any layout adjustments or measures. Thus, a second sample case was generated, providing an additional reference that showed higher infection risk results. SC1 is used as a conservative reference while the second sample case provides a more average situation. These sample cases show that for the same input parameters, there is RCM output variation even when the runs are repeated five times. For the capacity reduction scenarios, additional variation is introduced by the random population draws. The achieved variation is also a strength of the model because people movement is hard to predict and should thus have some degree of randomness. If the RCM model would always provide similar results, it would not realistically mimic crew and guest movement. In reality, implemented disease prevention and control measures might have more effect during day A than they have during day B. However, it is recommended to increase the number of route choice model repetitions and execute additional population draws for the capacity reduction scenarios. This will further improve the quality of the results even if it requires additional simulation time or increased computing power.

As mentioned in the scope of this research, ventilation and ventilation system design onboard large passenger vessels has not been considered. In the literature review, it became clear that there is a vast body of research focused on ventilation onboard large passenger vessels and its connections to contagious disease spread. The research presented in this report should be complemented by a ventilation study in order to provide a more complete perspective on contagious disease spread onboard large passenger vessels.

Concerning the integrated infection and crowd behavior model, there are ample opportunities for further model development. A selection of these opportunities is presented below. One should note that the current choice for the combination of a mesoscopic route choice model and the modified Wells-Riley infection calculation is based on the proposed set of requirements. If these requirements were to change, the model combination choices should also be revised. For example, if the disease angle is to be investigated further, a microscopic movement model might be a better fit in order to simulate disease progression, multiple transmission modes and the number of infected cases. The disease state could then be linked to the exact spatial location of the agents and it would be possible to model movement through the ship layout in more detail.

Parameter selection
The integrated model is based on a set of selected parameters which include both spacial and medical parameters. The model will become even more realistic if these parameters are based on specific circumstances. For example, the air change per hour is taken constant over the entire ship while the air change rate could be space or time-dependent. The pulmonary ventilation rate is also assumed to be constant for every agent. One could argue that this ventilation rate is agent-specific or even space-related. A higher pulmonary ventilation rate can be justified for the crew members as they are working and continuously moving around. The p-rate could also be related to a specific space like the gym or stairs where the pulmonary ventilation rate increases.

When the various measures were tested, the compliance to these measures was assumed to be 100%. An additional parameter covering measure compliance could be introduced to deal with this assumption. Lastly, the number of infected agents per space is assumed to be one. For large restaurants and activity spaces, a situation with multiple infectors might actually be more accurate. For further model development, an occupancy-dependent number of infectors could be a possible parameter improvement without moving to more complex infection models.

Activity schedule
The integrated model results are very much activity schedule dependent. It is relevant to note that the implemented activity schedule is connected to the investigated ship type as a cruise ship activity schedule differs from a schedule for a naval vessel. It would be beneficial if the agent activity schedule was investigated in more detail and if possible improved. In an ideal case, field testing onboard the investigated vessel should inform an activity schedule matching the actual movement of crew and guests. It is noted, however, that such research is time-intensive and comes at a significant cost.

Transmission modes
The modified Wells-Riley infection model integrated in this research only assesses airborne infection risk for COVID-19. Other modes of transmission like contract transmission might also play a role in disease transmission onboard a ship. The transmission modes not included in the current model can further increase the infection risk. Also, implemented control and prevention measures might prove more or less useful when multiple transmission modes are taken into consideration. Next to the modes of transmission, two additional considerations can be described which fall under the medical aspect of this research. Firstly, the exposure time in the integrated model is reset every time an agent changes spaces. The exposure time is thus purely based on the space an agent is in. If an agent happens to move to another space together with the infector, the reset of this exposure time makes less sense. Also, the current model does not account for the infectious particles, or 'shadow', that an infector leaves behind after leaving a space. This 'shadow' decays over time. If further research means to take considerations like these into account and model disease progression (agents getting infected), it might be advised to transfer to an agent-based infection model. With these microscopic models, the location of every agent can be linked to the disease state and disease progression can be visualized. In this situation, the route choice movement model might require adjustments in order to provide spatial agent locations.

One-way movement
When the one-way movement scenarios were evaluated, complications arose for the route choice model. These one-way movement scenarios are specifically connected to the link locations. This research, using the current integrated model, showed the main infection risks to be located at the nodes. It was therefore decided not to investigate this measure in more detail. However, if there is a specific interest in one-way movement modeling, the following considerations should be taken into account.

The initial idea was to remove the links between certain nodes, creating a forced one-way route for the agents to follow. However, removing the links resulted in issues with the RCM outputs. The choice was then made to change the length of the links, discouraging agents from using them. In this situation, the agents who still use the 'removed' links experience unrealistic travel times because of the increased link length. The issues for the one-way movement scenarios are also connected to crew accommodations modeling which leads to unfeasible crew movement behavior when the one-way routes are implemented. For further research, the RCM should be adjusted so that links can be easily removed and compliance with a one-way movement measure is taken into account.

It is also important to note that the RCM does not simulate cross-flow in the corridors. The RCM in its current state splits every corridor into two walking lanes: one link from location A to location B and one from location B to location A. Cross-flow is the situation where the agents in these links (A-B) and (B-A) interact with each other. This phenomenon is not modeled although it could be relevant when investigating an operational measure like one-way movement. In general, the movement model and ship layout should be further developed if one-way movement is to be investigated.

Social distance
The social distance calculation is an integral part of the infection risk calculation. The social distance is based on the assumption that agents evenly distribute themselves over the available space and do not group together. This way, the agents have the largest possible social distance in a space. Onboard a real cruise vessel, however, agents might avoid certain areas in a space and group together, using the available space less efficiently. This can result in smaller social distances and higher infection risks. A more comprehensive social distance estimation would improve the infection risk results.

Ship layout
Finally, the ship layout used for the integrated infection and crowd behavior model features areas for improvement. The SAFEGUARD cruise vessel layout used in this research was created for evacuation model validation. During evacuations, the elevators are not in use and the elevators are therefore not provided in the layout. These elevators are small spaces where agents stand close together, potentially resulting in high infection risks. Also, the outside spaces like sundecks are currently modeled as if they are inside spaces, overestimating the infection risk. A subsequent layout iteration could take both elevators and outside spaces into account.

Additionally, the current layout does not model the crew accommodation. This can also be related to the initial function of the SAFEGUARD layout as the crew is assumed to be trained during an evacuation and the evacuation modeling is focused on the guests. The guest cabins in the layout are modeled in large groups. This results in unexpected movement and infection risk before the agents start moving and after they have finished their schedule. Additionally, all crew members spent their break time at node 5 or 33, which are not appropriate locations to accommodate large groups of people. Adding appropriate guest and crew accommodations to the layout would solve these issues. Also, it would be interesting to implement a cabin infection risk indication covering the time crew and guests are in their cabins. It is possible that the modified Wells-Riley infection model currently used, is not suitable for a cabin risk calculation. This might require a different infection model and additional modification in the implemented ship layout.

8

Conclusions

This report aimed to develop an integrated infection and crowd behavior model which could be used to investigate contagious disease spread onboard large passenger vessels. The integrated model could then be applied to a cruise vessel evaluating COVID-19 infection risk for layout adjustments, operational and behavioral measures. The research and integrated model development was structured around seven research questions leading to the main research goal. This section therefore formulates the conclusions based on the same seven research questions.

1. *What is the state-of-the-art of contagious disease spread, contagious disease prevention and contagious disease control in confined spaces such as a large passenger vessel?*

Contagious disease spread can be described using four transmission modes: contact transmission, airborne transmission, common vehicle transmission and vector-borne transmission. Onboard a large passenger vessel, the densely populated environment, shared and confined spaces contribute to contact transmission. Airborne transmission can be related to shared HVAC systems while common food and water sources could cause common vehicle transmission. The transmission of a contagious disease can be prevented or controlled by various measures. These measures include operational measures like: restricted movement, embarkation requirements, improved onboard routines and disease management covering monitoring and surveillance. Also, there are options for behavioral measures related to social distancing, vaccinations, PPE and personal hygiene. Lastly, the ship layout design itself could support disease spread prevention and promote disease control if prevention fails. For example, high-risk spaces could benefit from relocation and a re-configurable design might provide additional medical facilities and isolation zones during a disease outbreak.

2. *What are the requirements for an integrated infection and crowd behavior model, if this model is used to investigate the effect of ship layout design, operational and behavioral measures on contagious disease spread?*

The formulated model requirements are directly linked to the scope and boundaries of the research. Medical complexity and convergence requirements make sure that the infection risk results convergence within a time frame acceptable for *initial stage retrofit design*. The investigated ship type is a *large passenger vessel* with a population size requirement of 3000 up to 4000 individually modeled agents. The preferred result of the model simulation is the *limitation of contagious disease spread* covered by a disease performance requirement. Also, the model should provide options to implement disease-specific parameters and thus take differences between contagious diseases into account. The evaluation of *Layout adjustments* is supported by requirements linked to space occupancy and exposure time. Space occupancy and exposure time are equally important when *operational and behavioral measures* are investigated. Two key model specifications are the *incorporation of crew and guest circulation* and the *incorporation of movement through a ship layout*. Five additional requirements form the foundation for these key specifications connected to: individual movement, random movement, multi-leg movement and layout incorporation with defined space capacity and flow limits.

3. *Which infection model and which crowd behavior model can be combined to fulfill the requirements of research question 2?*

Various types of infection and agent movement models were investigated as a first step in finding suitable models for integration. The options for the movement models feature different levels of detail like the macroscopic pipe flow model frequently used in ship evacuation modeling. Also, a mesoscopic route-choice model and microscopic agent-based models were considered. The medical infection model options include: compartment models, risk-based models and agent-based models. Twelve infection and movement model combinations were constructed and tested against the requirements from the second research question. A combined mesoscopic route choice model and modified Wells-Riley infection model best matched the requirements. This combination is layout-dependent and provides agent-based infection risk without being overly complex and time-intensive.

4. *What is the architecture of the integrated infection and crowd behavior model?*

The route choice model simulates the movement of all crew and guests based on a one-day activity schedule. The output of the RCM is used as input for the infection risk calculation combined with a set of start parameters. These start parameters include medical parameters, ventilation assumptions and spatial parameters like node area and link length. The start parameters and RCM output are used to calculate node occupancy and location specific ventilation rate. At this point, all information is available for the agent infection risk calculation executed at every time step.

5. *What are the infection risk results of a sample case scenario when the integrated infection and crowd behavior model is applied?*

The sample case scenario was defined by a cruise ship layout from the SAFEGUARD project, an activity schedule for the crew and a schedule for the guests. Additionally, a sensitivity study was conducted to investigate the effect of parameter variations on infection risk results and inform the final selection of these parameters. The average infection risk for the sample case is 0.807%, variating between 0% and 2.5% over the day. The average crew infection risk of 1.04% exceeds the 0.730% average guest infection risk. Besides the average infection risk, the number of agents with an infection risk above 50% was calculated. For the sample case, three peaks were found around 11:30, 16:00 and 21:00 with respectively 18, 7 and 14 agents at high risk.

6. *How can the infection risk results from the integrated model be validated?*

The sample case infection risk results were validated against similar cases from literature. Using the day average infection risk for the sample case, a 15% attack rate was calculated for a 20-day COVID-19 outbreak. This value can be compared against the 22% attack rate reported for a 20-day outbreak onboard the Diamond Princess cruise vessel. The slight difference is explained by the constant infection rate and 'perfect' isolation of infected cases in the sample case. In real life, the infection rate increases over an outbreak resulting in higher attack rates. The sample case was also validated for a single office space, a multi-office space, an out-patient hospital building and a reception scenario. Focusing on location specific infection risk, 20 waiting rooms in an out-patient hospital building were compared to the 20 highest risk locations in the sample case. A day average infection risk of 0.79% and an infection risk range between 0.19% and 2.63% was reported for the hospital waiting rooms. For the 20 locations in the sample case, a 1.49% average infection risk and a range between 0.75% and 3.58% was calculated. Finally, a reception scenario was compared to one of the onboard restaurants in the sample case with similar occupancy, space dimensions and three-hour exposure time. The restaurant presented a 3.18% average infection risk versus a 1.6% average infection risk for the reception. These validations prove the sample case to be sufficiently validated for application as a baseline when evaluating prevention and control actions.

7. *What are the infection risk results of selected prevention and/or control actions onboard a large passenger vessel when the integrated infection and crowd behavior model is applied?*

The integrated model was used to evaluate three small-scale layout adjustments, capacity reductions and mask wearing scenarios. Investigating the high-risk locations in the layout, the node locations were found to have significantly higher infection risks than the link locations. This can be explained by the occupancy and extended exposure time when agents are located at a node. The layout adjustments for the bar at N107 solved a categorization error, which resulted in a realistic local infection risk and

decreased the number of agents with risks above 50%. The layout adjustment at the N293 restaurant resulted in a local risk improvement from 2.67% to 1.57% without increasing risk for surrounding nodes. The local infection risk improvements are too small to be detectable in the average infection risks for the complete ship.

The evaluated operational measure is a general capacity reduction with fewer guests and crew onboard the vessel. The average infection risk decreases with increasing capacity reductions. Risk improvements compared to sample case 1 were seen for higher capacity reductions with an average infection risk of 0.755% for CR = 60% and 0.630% for CR = 75%. The initial densely populated environment might be a possible reason for the fact that large capacity reductions are required to achieve any average infection risk improvements. It should be noted that these large capacity reductions might result in operational and economic feasibility issues.

Compared to the layout adjustments and the operational measures, the highest risk improvements were achieved when the crew and guests started wearing masks. The average infection risk for continuous and social distance based mask wearing is 0.451% and 0.487%, a risk reduction over 40% compared to the sample cases. Additionally, significant improvements became visible for the number of agents with infection risks above 50%.

Based on the results from the separately implemented measures, six combinations covering multiple adjustments and measures were evaluated. Combining continuous mask wearing with a 30% or 50% capacity reduction, the average infection risk was reduced with 57% and 63% compared to SC1. The limited risk improvement between a 30% and 50% capacity reduction should be evaluated against non-infection related considerations like sufficient manning. When continuous mask wearing is combined with a 50% reduction there is a single moment when 2 agents have an infection risk above 50%. This shows significant improvement compared to the sample cases.

Considering the infection risk results for the evaluated scenarios, the developed model has proven to be a valuable tool when investigating contagious disease spread onboard a large passenger vessel. It can be concluded that the research goal to: *Investigate the effect of ship layout design, operational and behavioral measures on contagious disease spread onboard large passenger vessels, by combining an infection model with a crowd behavior model* was accomplished.

Future research

In this report, the integrated model was applied to a cruise ship layout testing specific layout adjustments and measures for COVID-19 infection risk. The measures tested were limited to: capacity reduction, mask wearing and small-scale layout adjustments. It would be relevant to also evaluate other scenarios like significant activity schedule changes, implementing different zones or large-scale layout adjustments. Additionally, further research might evaluate a feedback loop related to agents who make different choices when certain measures are applied. For example, if agents know how crowded spaces are beforehand, they could choose a different activity or time to move. Another example can be found for mask wearing. In the current research, agents wear their masks in certain situations and the activity schedule is kept unchanged. In reality, the behavioral measure (mask wearing) might lead agents to change their activity schedule, thus introducing secondary effects.

Furthermore, the model could be used for other ship layouts like a ferry or a large naval vessel, investigating infection risk under different circumstances and for other contagious diseases. A final research suggestion moves beyond retrofit ship design, where the integrated model might be used during the initial design stage. In this design stage, the integrated model could determine infection risk performance for a set of initial deck plans. This would provide infection risk insight before design decisions are made and the ship design is finalized.

References

[1] *A breath of fresh air: Science leads the way for Royal Caribbean Group's HVAC system - Royal Caribbean Group*. Feb. 2021. URL: https://www.royalcaribbeangroup.com/a-breath-of-fresh-air-science-leads-the-way-for-royal-caribbean-groups-hvac-system/.

[2] Dionne M. Aleman, Theodorus G. Wibisono, and Brian Schwartz. "Accounting for individual behaviors in a pandemic disease spread model". In: *Proceedings - Winter Simulation Conference*. 2009, pp. 1977–1985. ISBN: 9781424457700. DOI: 10.1109/WSC.2009.5429727.

[3] Benjamin M Althouse et al. "Stochasticity and heterogeneity in the transmission dynamics of SARS-CoV-2". In: *arXiv: Populations and Evoluation* (May 2020).

[4] Tzivakou Andriana. "The Covid-19 Pandemic Outbreak and the Impact on the Seafarers Lives". PhD thesis. Piraeus: University of Piraeus, Oct. 2020.

[5] Parham Azimi et al. "Mechanistic transmission modeling of COVID-19 on the Diamond Princess cruise ship demonstrates the importance of aerosol transmission". In: *PNAS* 118 (Jan. 2021). DOI: 10.1073/pnas.2015482118/-/DCSupplemental.

[6] Gentry Berry et al. "A review of methods to reduce the probability of the airborne spread of COVID-19 in ventilation systems and enclosed spaces". In: *Environmental Research* 203 (Jan. 2022). ISSN: 10960953. DOI: 10.1016/j.envres.2021.111765.

[7] Rebecca K Brewster, Alexander Sundermann, and Corey Boles. "Lessons learned for COVID-19 in the cruise ship industry". In: *Toxicology and Industrial Health* 36.9 (2020), pp. 728–735. DOI: 10.1177/0748233720964631.

[8] R Brown et al. "Passenger Response Time Data-sets for Large Passenger Ferries and Cruise Ships derived from sea trails". In: *International Journal of Maritime Engineering* 155.A1 (Dec. 2021). ISSN: 1479-8751. DOI: 10.5750/IJME.V155IA1.894. URL: https://www.researchgate.net/publication/268212815_Passenger_Response_Time_Data-Sets_for_Large_Passenger_Ferries_and_Cruise_Ships_Derived_from_Sea_Trials.

[9] G. Buonanno, L. Stabile, and L. Morawska. "Estimation of airborne viral emission: Quanta emission rate of SARS-CoV-2 for infection risk assessment". In: *Environment international* 141 (Aug. 2020). ISSN: 1873-6750. DOI: 10.1016/J.ENVINT.2020.105794. URL: https://pubmed.ncbi.nlm.nih.gov/32416374/.

[10] Jing Cai et al. "Indirect Virus Transmission in Cluster of COVID-19 Cases, Wenzhou, China, 2020". In: *Emerging Infectious Diseases* 26 (June 2020), pp. 1343–1346. DOI: 10.3201/eid2606.200412.

[11] CDC. *Social distancing : keep a safe distance to slow the spread*. July 2020. URL: https://stacks.cdc.gov/view/cdc/90522.

[12] Miao Chen et al. "A ship evacuation model considering the interaction between pedestrians based on cellular automata". In: *Ocean Engineering* 281 (Aug. 2023), p. 114644. ISSN: 0029-8018. DOI: 10.1016/J.OCEANENG.2023.114644.

[13] E Chrysikou, E Hernandez Garcia, and E Savvopoulou. *International Research Project on Emergency Response to Infectious Disease Outbreak on Cruise ships. Report submitted to The International Academic Forum*. Tech. rep. The International Academic Forum (IAFOR), 2021. URL: https://discovery.ucl.ac.uk/id/eprint/10128854/3/Chrysikou_Report%20UCL.pdf.

[14] CruiseMapper. *Radiance Of The Seas deck plan*. 2024. URL: https://www.cruisemapper.com/deckplans/Radiance-Of-The-Seas-563.

[15] Eilif Dahl. "Cruise tap versus handshake: using common sense to reduce hand contamination and germ transmission on cruise ships". In: *International Maritime Health* 67.4 (2016), pp. 181–184. ISSN: 2081-3252. DOI: 10.5603/IMH.2016.0034. URL: https://journals.viamedica.pl/international_maritime_health/article/view/IMH.2016.0034.

[16] Hui Dai and Bin Zhao. “Association between the infection probability of COVID-19 and ventilation rates: An update for SARS-CoV-2 variants”. In: *Building Simulation* 16.1 (Jan. 2023), pp. 3–12. ISSN: 19968744. DOI: 10.1007/s12273-022-0952-6.

[17] Hui Dai and Bin Zhao. “Association of the infection probability of COVID-19 with ventilation rates in confined spaces”. In: *Building Simulation* 13.6 (Dec. 2020), pp. 1321–1327. ISSN: 19968744. DOI: 10.1007/S12273-020-0703-5/METRICS. URL: https://link.springer.com/article/10.1007/s12273-020-0703-5.

[18] Hui Dai and Bin Zhao. “Reducing airborne infection risk of COVID-19 by locating air cleaners at proper positions indoor: Analysis with a simple model”. In: *Building and Environment* 213 (2022), p. 108864. DOI: 10.1016/j.buildenv.2022.108864. URL: https://doi.org/10.1016/j.buildenv.2022.108864.

[19] EU SHIPSAN. *EU SHIPSAN ACT Joint Action*. 2016. URL: https://www.shipsan.eu/.

[20] European Centre for Disease Prevention and Control. *Questions and answers on COVID-19: Travelling*. June 2023. URL: https://www.ecdc.europa.eu/en/covid-19/questions-answers/questions-answers-travel.

[21] Ewout Fanoy et al. “Outbreak of COVID-19 on an industrial ship”. In: *International Maritime Health* 72.2 (2021), pp. 87–92. ISSN: 2081-3252. DOI: 10.5603/IMH.2021.0016. URL: https://journals.viamedica.pl/international_maritime_health/article/view/IMH.2021.0016.

[22] Matthew David Gaddis and Valipuram S Manoranjan. “Modeling the Spread of COVID-19 in Enclosed Spaces”. In: *Mathematical and Computational Applications* 26.79 (2021). DOI: 10.3390/mca26040079. URL: https://doi.org/10.3390/mca26040079.

[23] Ed Galea, Steven Deere, and Lazaros Filippidis. *THE SAFEGUARD VALIDATION DATA SET – SGVDS2 A GUIDE TO THE DATA AND VALDIATION PROCEDURES*. Tech. rep. University of Greenwich, Oct. 2012.

[24] Edwin R. Galea et al. “A validation data-set and suggested validation protocol for ship evacuation models”. In: *Fire Safety Science*. Vol. 11. International Association for Fire Safety Science, 2014, pp. 1115–1128. DOI: 10.3801/IAFSS.FSS.11-1115.

[25] Caroline X. Gao et al. “Multi-route respiratory infection: When a transmission route may dominate”. In: *Science of the Total Environment* 752 (Jan. 2021). ISSN: 18791026. DOI: 10.1016/j.scitotenv.2020.141856.

[26] Daan van Gisbergen. *Development of a crowd behavioral model for large-scale simulation on large vessels*. Tech. rep. Delft: Delft University of Technology, Dec. 2022.

[27] Lara Goscé, David A.W. Barton, and Anders Johansson. “Analytical modelling of the spread of disease in confined and crowded spaces”. In: *Scientific Reports* 4 (May 2014). ISSN: 20452322. DOI: 10.1038/srep04856.

[28] Sarah Anne J. Guagliardo et al. “Cruise Ship Travel in the Era of Coronavirus Disease 2019 (COVID-19): A Summary of Outbreaks and a Model of Public Health Interventions”. In: *Clinical Infectious Diseases* 74.3 (Feb. 2022), pp. 490–497. ISSN: 1058-4838. DOI: 10.1093/CID/CIAB433. URL: https://dx.doi.org/10.1093/cid/ciab433.

[29] Arun Gupta et al. “A comparative analysis of control measures on-board ship against COVID-19 and similar novel viral respiratory disease outbreak: Quarantine ship or disembark suspects?” In: *Medical Journal Armed Forces India* 77 (July 2021), S430–S436. ISSN: 0377-1237. DOI: 10.1016/J.MJAFI.2020.06.003.

[30] Christos Hadjichristodoulou et al. “Surveillance and control of communicable diseases related to passenger ships in Europe”. In: *International Maritime Health* 62.2 (2011), pp. 138–147. ISSN: 2081-3252. URL: https://journals.viamedica.pl/international_maritime_health/article/view/26190.

[31] Thomas Harweg, Mathias Wagner, and Frank Weichert. “Agent-Based Simulation for Infectious Disease Modelling over a Period of Multiple Days, with Application to an Airport Scenario”. In: *International Journal of Environmental Research and Public Health* 20.1 (Jan. 2023). ISSN: 16604601. DOI: 10.3390/ijerph20010545.

[32] Healthy Sailing. *Prevention, mitigation, management of infectious diseases on cruise ships and passenger ferries*. 2024. URL: https://healthysailing.eu/.

[33] Chaitra Hegde et al. “Modeling Social Distancing and Quantifying Epidemic Disease Exposure in a Built Environment”. In: *IEEE Journal on Selected Topics in Signal Processing* 16.2 (Feb. 2022), pp. 289–299. ISSN: 19410484. DOI: 10.1109/JSTSP.2022.3145622.

[34] National Center for Immunization and Division of Viral Diseases Respiratory Diseases. *Norovirus | CDC*. May 2023. URL: https://www.cdc.gov/norovirus/index.html.

[35] International Maritime Organization. *REVISED GUIDELINES ON EVACUATION ANALYSIS FOR NEW AND EXISTING PASSENGER SHIPS*. London, June 2016.

[36] Elmira T Isakbaeva et al. *Norovirus Transmission on Cruise Ship*. Tech. rep. Jan. 2005, pp. 154–157. URL: www.cdc.gov/eid.

[37] R S Joustra. “Analysis of evacuation performance of early stage ship designs using a Markov Decision Process model”. PhD thesis. Delft: TU Delft, Sept. 2018. URL: http://repository.tudelft.nl/..

[38] Vivek Kak. *Infections in Confined Spaces: Cruise Ships, Military Barracks, and College Dormitories*. Sept. 2007. DOI: 10.1016/j.idc.2007.06.004.

[39] Matthew R. Kasper et al. “An Outbreak of Covid-19 on an Aircraft Carrier”. In: *New England Journal of Medicine* 383.25 (Dec. 2020), pp. 2417–2426. ISSN: 0028-4793. DOI: 10.1056/nejmoa2019375.

[40] Tuba Keçeci. “Importance and applicability analysis of the health and safety measures taken against the coronavirus disease on merchant vessels Tuba KEÇECİ”. In: *Aquatic Research* 5.3 (2022), pp. 171–185. ISSN: 2618-6365. DOI: 10.3153/AR22017. URL: http://aquatres.scientificwebjournals.com.

[41] Hongtae Kim et al. “Establishing the methodologies for human evacuation simulation in marine accidents”. In: *Computers & Industrial Engineering* 46.4 (July 2004), pp. 725–740. ISSN: 0360-8352. DOI: 10.1016/J.CIE.2004.05.017.

[42] Ann Christin Kordsmeyer et al. “Systematic review on outbreaks of sars-cov-2 on cruise, navy and cargo ships”. In: *International Journal of Environmental Research and Public Health* 18.10 (May 2021), p. 5195. ISSN: 16604601. DOI: 10.3390/IJERPH18105195/S1. URL: https://www.mdpi.com/1660-4601/18/10/5195/htm%20https://www.mdpi.com/1660-4601/18/10/5195.

[43] Anna Kormanová. “Combining Social Forces and Cellular Automata Models In Pedestrians’ Movement Simulation”. In: *Journal of Information, Control and Management Systems* 10.1 (2012), p. 61.

[44] Tahaniyat Lalani et al. “SARS-CoV-2 Infections and Serologic Responses Among Military Personnel Deployed on the USNS COMFORT to New York City During the COVID-19 Pandemic”. In: *Open Forum Infectious Diseases* (2021). DOI: 10.1093/ofid/ofaa654.

[45] Dale N Lawrence. “Outbreaks of Gastrointestinal Diseases on Cruise Ships: Lessons from Three Decades of Progress”. In: *Current Infectious Disease Reports* 6 (2004), pp. 115–123. ISSN: 1523-3847.

[46] Dongkon Lee et al. “The current status and future issues in human evacuation from ships”. In: *Safety Science* 41.10 (Dec. 2003), pp. 861–876. ISSN: 0925-7535. DOI: 10.1016/S0925-7535(02)00046-2.

[47] Jos Lelieveld et al. “Model Calculations of Aerosol Transmission and Infection Risk of COVID-19 in Indoor Environments”. In: *International Journal of Environmental Research and Public Health* 17.8114 (2020). DOI: 10.3390/ijerph17218114. URL: https://www.mpic.de/4747065/risk-calculation..

[48] Chunying Li and Haida Tang. “Study on ventilation rates and assessment of infection risks of COVID-19 in an outpatient building”. In: *Journal of Building Engineering* 42 (2021), p. 103090. DOI: 10.1016/j.jobe.2021.103090. URL: https://doi.org/10.1016/j.jobe.2021.103090.

[49] Hua Li, Shuhan Meng, and Helong Tong. “How to control cruise ship disease risk? Inspiration from the research literature”. In: *Marine Policy* 132 (Oct. 2021), p. 104652. ISSN: 0308597X. DOI: 10.1016/J.MARPOL.2021.104652. URL: /pmc/articles/PMC8463129/%20/pmc/articles/PMC8463129/?report=abstract%20https://www.ncbi.nlm.nih.gov/pmc/articles/PMC8463129/.

[50] Y. Li et al. “Modelling Route Choice in Crowd Evacuation on Passenger Ships”. In: *International Journal of Maritime Engineering* 163.A2 (July 2021), A33–A48. ISSN: 1479-8751. DOI: 10.5750/IJME.V163IA2.754. URL: https://www.intmaritimeengineering.org/index.php/ijme/article/view/754.

[51] Yapeng Li, Wei Cai, and Austin A. Kana. “Design of level of service on facilities for crowd evacuation using genetic algorithm optimization”. In: *Safety Science* 120 (Dec. 2019), pp. 237–247. ISSN: 18791042. DOI: 10.1016/j.ssci.2019.06.044.

[52] Marc Lipsitch et al. “The contribution of asymptomatic SARS-CoV-2 infections to transmission on the Diamond Princess cruise ship”. In: *eLife* (2020). DOI: 10.7554/eLife.58699. URL: https://doi.org/10.7554/eLife.58699.

[53] Feng Liu, Xin Li, and Gaofeng Zhu. “Using the contact network model and Metropolis-Hastings sampling to reconstruct the COVID-19 spread on the “Diamond Princess””. In: *Science Bulletin* 65.15 (Aug. 2020), pp. 1297–1305. ISSN: 2095-9273. DOI: 10.1016/J.SCIB.2020.04.043.

[54] Alexandra Mangili and Mark A. Gendreau. “Transmission of infectious deceases during commercial air travel”. In: *Lancet* 365 (Mar. 2005), pp. 989–996.

[55] Bradley Dean Martin and Trupti Brahmbhatt. *Readiness Implications of Coronavirus Infections on U.S. Navy Ships*. Tech. rep. Rand Corporation, 2021.

[56] G. D. Mathur. “Influence of vehicle age on build-up of carbon dioxide in cabin to monitor indoor air quality (IAQ)”. In: *Institution of Mechanical Engineers - VTMS 10, Vehicle Thermal Management Systems Conference and Exhibition* (2011), pp. 623–634. DOI: 10.1533/9780857095053.8.623. URL: https://www.researchgate.net/publication/301089884_Influence_of_vehicle_age_on_build-up_of_carbon_dioxide_in_cabin_to_monitor_indoor_air_quality_IAQ.

[57] Yvette S. McCarter. “Infectious Disease Outbreaks on Cruise Ships”. In: *Clinical Microbiology Newsletter* 31.21 (Nov. 2009), pp. 161–168. ISSN: 0196-4399. DOI: 10.1016/J.CLINMICNEWS.2009.10.001.

[58] Arézou Minooee and Leland S Rickman. *Infectious Diseases on Cruise Ships*. Tech. rep. San Diego, California: University of California, June 1999, pp. 737–743. URL: https://academic.oup.com/cid/article/29/4/737/451491.

[59] Kenji Mizumoto and Gerardo Chowell. “Transmission potential of the novel coronavirus (COVID-19) onboard the diamond Princess Cruises Ship, 2020”. In: *Infectious Disease Modelling* 5 (Jan. 2020), pp. 264–270. ISSN: 24680427. DOI: 10.1016/j.idm.2020.02.003.

[60] Jinyoung Moon and Byung Han Ryu. “Transmission risks of respiratory infectious diseases in various confined spaces: A meta-analysis for future pandemics”. In: *Environmental Research* 202 (Nov. 2021). ISSN: 10960953. DOI: 10.1016/j.envres.2021.111679.

[61] David M. Morens and Anthony S. Fauci. “Emerging Infectious Diseases: Threats to Human Health and Global Stability”. In: *PLoS Pathogens* 9.7 (July 2013). ISSN: 15537366. DOI: 10.1371/journal.ppat.1003467.

[62] Varvara A Mouchtouri et al. “State of the art: public health and passenger ships”. In: *International maritime health* 61.2 (2010), pp. 53–98. ISSN: 1641–9251. URL: https://journals.viamedica.pl/international_maritime_health/article/view/26229.

[63] Rosanda Mulića et al. “Infectious Risks on Different Types of Ships with Reference to the COVID-19 Pandemic Infectious Risks on Different Types of Ships with Reference to the COVID-19 Pandemic”. In: *Transactions on maritime science* 01 (2022), pp. 286–293. DOI: 10.7225/toms.v11.n01.w04.

[64] Jishnu Narayan et al. “Activity and Agent Based Simulation Model with Path-Size Logit Mixture for Passenger Flow to Evaluate Ship Layout”. Unpublished. Apr. 2021.

[65] National Center for Environmental Health. *Vessel Sanitation Program | VSP*. 2023. URL: https://www.cdc.gov/nceh/vsp/default.htm.

[66] National Center for State Tribal Local and Territorial Public Health Infrastructure and Workforce - Division of Workforce Development. *Principles of Epidemiology | Lesson 3 - Section 2*. 2012. URL: https://www.cdc.gov/csels/dsepd/ss1978/lesson3/section2.html.

[67] National Institute for Infectious Diseases Japan. "Epidemiology of COVID-19 Outbreak on Cruise Ship Quarantined at Yokohama, Japan, February 2020". In: *Emerging Infectious Diseases* 26.11 (Nov. 2020), p. 2591. ISSN: 10806059. DOI: 10.3201/EID2611.201165. URL: /pmc/articles/PMC7588545/%20/pmc/articles/PMC7588545/?report=abstract%20https://www.ncbi.nlm.nih.gov/pmc/articles/PMC7588545/.

[68] Daniel B Neill et al. *Tracking Infectious Disease Spread for Global Pandemic Containment*. Tech. rep. 2013, pp. 60–64. URL: www.computer.org/intelligent.

[69] Christos Nicolaides et al. "Hand-Hygiene Mitigation Strategies Against Global Disease Spreading through the Air Transportation Network". In: *Risk Analysis* 40.4 (Apr. 2020), pp. 723–740. ISSN: 15396924. DOI: 10.1111/risa.13438.

[70] C. J. Noakes et al. "Modelling the transmission of airborne infections in enclosed spaces". In: *Epidemiology and Infection* 134.5 (Oct. 2006), pp. 1082–1091. ISSN: 09502688. DOI: 10.1017/S0950268806005875.

[71] Zahra Noorimotlagh et al. "A systematic review of possible airborne transmission of the COVID-19 virus (SARS-CoV-2) in the indoor air environment". In: *Environmental Research* 193 (Feb. 2021). ISSN: 10960953. DOI: 10.1016/j.envres.2020.110612.

[72] Mateusz M. Plucinski et al. "Coronavirus Disease 2019 (COVID-19) in Americans Aboard the Diamond Princess Cruise Ship". In: *Clinical Infectious Diseases* 72.10 (May 2021), E448–E457. ISSN: 15376591. DOI: 10.1093/cid/ciaa1180.

[73] Princess. *Diamond Princess® Cruise Ship*. URL: https://www.princess.com/ships-and-experience/ships/di-diamond-princess/.

[74] Konstantinos Ritos, Dimitris Drikakis, and Ioannis W. Kokkinakis. "Virus spreading in cruiser cabin". In: *Physics of Fluids* 35.10 (Oct. 2023). ISSN: 10897666. DOI: 10.1063/5.0169992/2919102. URL: /aip/pof/article/35/10/103329/2919102/Virus-spreading-in-cruiser-cabin.

[75] J. Rocklöv, H. Sjödin, and A. Wilder-Smith. "COVID-19 outbreak on the diamond princess cruise ship: Estimating the epidemic potential and effectiveness of public health countermeasures". In: *Journal of Travel Medicine* 27.3 (2021), pp. 1–7. ISSN: 17088305. DOI: 10.1093/JTM/TAAA030.

[76] Enrico Ronchi and Ruggiero Lovreglio. "EXPOSED: An occupant exposure model for confined spaces to retrofit crowd models during a pandemic". In: *Safety Science* 130 (Oct. 2020). ISSN: 18791042. DOI: 10.1016/J.SSCI.2020.104834.

[77] Roisin M Rooney et al. "A Review of Outbreaks of Foodborne Disease Associated with Passenger Ships: Evidence for Risk Management". In: *Research Articles Public Health Reports* 119 (2004), p. 427.

[78] Elena Cecilia Rosca et al. "Transmission of SARS-CoV-2 Associated with Cruise Ship Travel: A Systematic Review". In: *Tropical Medicine and Infectious Disease* 7.10 (Oct. 2022). ISSN: 24146366. DOI: 10.3390/TROPICALMED7100290.

[79] Royal Caribbean Press Center. *Radiance of the Seas Fact Sheet*. 2024. URL: https://www.royalcaribbeanpresscenter.com/fact-sheet/15/radiance-of-the-seas/.

[80] Valerio Ruggiero, Eugenio Guglielmino, and Cucinotta Filippo. "An interactive approach for the design of an Italian fast medical support ship as consequence of world emergency due to Sars2-Covid 19". In: *International Journal on Interactive Design and Manufacturing* 16 (2008), pp. 409–417. DOI: 10.1007/s12008-022-00845-w. URL: https://doi.org/10.1007/s12008-022-00845-w.

[81] Erica Silverstein. *What's the Best Cruise Ship Size for You?* 2022. URL: https://www.cruisecritic.co.uk/articles/whats-the-best-cruise-ship-size-for-you.

[82] Ahmed Sodiq et al. *Addressing COVID-19 contagion through the HVAC systems by reviewing indoor airborne nature of infectious microbes: Will an innovative air recirculation concept provide a practical solution?* Aug. 2021. DOI: 10.1016/j.envres.2021.111329.

[83] Shubham Srivastava et al. “Effective ventilation and air disinfection system for reducing coronavirus disease 2019 (COVID-19) infection risk in office buildings”. In: *Sustainable Cities and Society* 75 (2021). DOI: 10.1016/j.scs.2021.103408. URL: https://doi.org/10.1016/j.scs.2021.103408.

[84] Chanjuan Sun and Zhiqiang Zhai. “The efficacy of social distance and ventilation effectiveness in preventing COVID-19 transmission”. In: *Sustainable Cities and Society* 62 (Nov. 2020), p. 102390. ISSN: 2210-6707. DOI: 10.1016/J.SCS.2020.102390.

[85] Sijian Tan et al. “Beyond well-mixed: A simple probabilistic model of airborne disease transmission in indoor spaces”. In: *Indoor Air* 32.3 (Mar. 2022). ISSN: 16000668. DOI: 10.1111/ina.13015.

[86] Kangkang Tang and Bing Chen. “Resilient Hospital Design: From Crimea War to COVID-19”. In: *Health Environments Research and Design Journal* (May 2023). ISSN: 21675112. DOI: 10.1177/19375867231174238/ASSET/IMAGES/LARGE/10.1177{_}19375867231174238-FIG16.JPEG. URL: https://journals.sagepub.com/doi/full/10.1177/19375867231174238.

[87] The Associated Press. *Sailors on sidelined USS Theodore Roosevelt get virus for second time*. May 2020. URL: https://www.nbcnews.com/politics/politics-news/sailors-sidelined-uss-theodore-roosevelt-get-virus-second-time-n1208076.

[88] Eugenia Tognotti. “Lessons from the History of Quarantine, from Plague to Influenza A”. In: *Emerging Infectious Diseases* 19.2 (2013), p. 254. ISSN: 10806059. DOI: 10.3201/EID1902.120312. URL: /pmc/articles/PMC3559034/%20/pmc/articles/PMC3559034/?report=abstract%20https://www.ncbi.nlm.nih.gov/pmc/articles/PMC3559034/.

[89] Wade Turvold and Jim Mcmullin. “Ships Become Dangerous Places During a Pandemic”. In: *Asia-Pacific Center for Security Studies* (May 2020).

[90] Diego Vicente et al. “U.S. Navy’s Response to a Shipboard Coronavirus Outbreak: Considerations for a Medical Management Plan at Sea”. In: *Military Medicine* 186.1-2 (Jan. 2021), pp. 23–26. ISSN: 1930613X. DOI: 10.1093/milmed/usaa455.

[91] Zhaozhi Wang et al. “A coupled Computational Fluid Dynamics and Wells-Riley model to predict COVID-19 infection probability for passengers on long-distance trains”. In: *Safety Science* 147 (Mar. 2022), p. 105572. ISSN: 0925-7535. DOI: 10.1016/J.SSCI.2021.105572.

[92] Conghua Wen et al. “Heterogeneous epidemic modelling within an enclosed space and corresponding Bayesian estimation”. In: *Infectious Disease Modelling* 7.2 (June 2022), pp. 1–24. ISSN: 24680427. DOI: 10.1016/J.IDM.2022.02.001.

[93] N W A N Y Wijesekara et al. “COVID-19 Case Prediction and Outbreak Control of Navy Cluster in Sri Lanka: Effectiveness of SIR Model”. In: 2020. DOI: 10.21203/rs.3.rs-70722/v2. URL: https://doi.org/10.21203/rs.3.rs-70722/v2.

[94] Mary E. Wikswo et al. “Disease transmission and passenger behaviors during a high morbidity norovirus outbreak on a cruise ship, January 2009”. In: *Clinical Infectious Diseases* 52.9 (May 2011), pp. 1116–1122. ISSN: 10584838. DOI: 10.1093/cid/cir144.

[95] Kathryn S Willebrand et al. “A review of COVID-19 transmission dynamics and clinical outcomes on cruise ships worldwide”. In: *Euro Surveillance* 27.1 (2022). DOI: 10.2807/1560-7917.ES.2022.27.1.2002113. URL: www.eurosurveillance.org.

[96] World Health Organization. *Guide to ship sanitation, 3rd edition*. 2011. URL: https://www.who.int/publications/i/item/9789241546690.

[97] Pengcheng Xu et al. “Transmission routes of Covid-19 virus in the Diamond Princess Cruise ship”. Hong Kong SAR, Apr. 2020. DOI: 10.1101/2020.04.09.20059113. URL: https://doi.org/10.1101/2020.04.09.20059113.

[98] Devran Yazir et al. “Effects of COVID-19 on maritime industry: a review”. In: *International Maritime Health* 71.4 (Dec. 2020), pp. 253–264. ISSN: 2081-3252. DOI: 10.5603/IMH.2020.0044. URL: https://journals.viamedica.pl/international_maritime_health/article/view/72044.

[99] Nan Zhang et al. “Contact infection of infectious disease onboard a cruise ship”. In: *Scientific Reports* 6.38790 (2016). DOI: 10.1038/srep38790. URL: www.nature.com/scientificreports.

[100] Wangzheqi Zhang et al. “COVID-19 outbreaks on ships: Analysis of three representative cases”. In: *Public Health in Practice* 4 (Dec. 2022). ISSN: 26665352. DOI: 10.1016/J.PUHIP.2022.100320.

[101] Xingwang Zhao et al. “Airborne transmission of COVID-19 virus in enclosed spaces: An overview of research methods”. In: *Indoor Air* 32.6 (June 2022), e13056. ISSN: 1600-0668. DOI: 10.1111/INA.13056. URL: https://onlinelibrary.wiley.com/doi/full/10.1111/ina.13056%20https://onlinelibrary.wiley.com/doi/abs/10.1111/ina.13056%20https://onlinelibrary.wiley.com/doi/10.1111/ina.13056.

[102] Lijie Zheng et al. “Evaluation of intervention measures for respiratory disease transmission on cruise ships”. In: *Indoor and Built Environment* 25.8 (Dec. 2016), pp. 1267–1278. ISSN: 1420-326X. DOI: 10.1177/1420326X15600041. URL: http://journals.sagepub.com/doi/10.1177/1420326X15600041.

A

Disease Prevention and Control

This appendix provides background information relating to disease prevention and control.

A.1. Ship layout design

A.1.1. HVAC

Preventing and controlling a disease outbreak can be achieved by limiting disease spread throughout the ship. The first intervention which is frequently mentioned is the redesign of HVAC systems. For example, negative pressure in certain isolation areas might prevent leakage of contaminated air [80]. Also, the total capacity of the ventilation system could be increased so that air in spaces is replaced more often. An in-depth HVAC analysis and redesign lies beyond the scope of this research but it remains an important design aspect to mention as it shows significant potential [49].

A.1.2. Layout

With respect to the accommodation and general shared spaces, the literature suggests certain layout and design adjustments to limit disease spread. Rosca et al. conclude in their systematic literature review that lower guest-to-space ratios lead to lower attack rates [78]. This attack rate is defined in epidemiology as: “the risk of getting the disease during a specified period” and calculated by dividing the number of new cases by the total population [66]. Rosca et al. also suggest that the cabins should be spread out over multiple decks and more cabins should be available. This suggestion is supported by a consistent dose-response relationship for cabins, where more guests per cabin lead to higher attack rates [78]. Increasing the number of cabins will decrease the number of guests sharing a cabin and therefore also decrease attack rates. An alternative could be to design a large passenger vessel to accommodate fewer people [7]. In that situation, there can be larger cabins and guests will have more personal space when they use shared areas like the restaurants or shops [7].

A.1.3. Movement

Design adaptions can also be related to how guests and crew move through the ship layout. The elevator hall is for example a commonly mentioned risk place where people meet in a small confined space and wait close together [78]. Waiting lines because of (dis)embarkation processes, arranged travel from/to the ship and tours onboard all present situations with a high risk of exposure [78]. Perhaps design changes in the embarkation, disembarkation and reception areas are needed to decrease waiting lines, improve movement flow and increase the space available for these processes. It could also be possible to set up part of these processes on the dock instead. In general, it might be helpful to create more alternative routes in the layout combined with additional staircases or elevators. This way, guests and crew can take different routes to reach the same destination.

A.1.4. Medical facilities

Large passenger vessels are often designed with limited medical and health facilities [58]. Li et al. found that for the Diamond Princess cruise vessel COVID-19 outbreak, “non-traditional quarantine measures such as classified isolation and batch transfer were not taken in time” because of insufficient medical facilities [49]. Instead, the entire ship went into quarantine which might not always match the severity of the situation and potentially put other people on the ship at risk [49]. Suppose there are only one or two infected individuals, then it would be preferred to isolate or disembark these individuals and execute contact tracing instead of quarantining the entire ship. These actions are only possible if the medical and health facilities onboard meet the requirements for these situations. Referring to hospital design resilience, it is suggested to have a partly re-configurable design “enabling it to adapt effectively to changing future demands” [86]. In the design, some multi-functional spaces could be accounted for [86]. These spaces can be used in case of an outbreak to set up basic medical or quarantine facilities. It might also be possible to design part of the accommodation in a way that facilitates quarantine and isolation when needed.

A.1.5. Zones

The WHO has, for cargo and navy ships, suggested a system based on four zones during the COVID-19 epidemic. The zones were defined as follows: “potentially contaminated zones (1) where suspected cases can be isolated, zones for interaction of crew members (such as mess rooms, the bridge, control rooms, or shared cabins) (2), zones for encountering with shore personnel (3) and such where no interaction takes place (like single cabins) (4)” [42]. The behavioral measures taken like mask wearing or social distance are linked to the different zones. The use of (vertical) spatial zones is something very familiar to the shipping industry as it is used in damage control in terms of fire zones and watertight compartments. Zones could also be applied during an outbreak. For example, all accommodation in vertical zone 1 on deck 4 is reserved for isolated individuals. They will stay within this zone and have only limited contact with crew delivering basic necessities and medical care. The accommodation in vertical zone 1 on deck 3 might hold suspected cases in quarantine and awaiting test results. The layout design should take a potential zone plan for an outbreak into account so that sanitary facilities are sufficient and isolated access routes are available.

A.2. Operational measures

A.2.1. Embarkation requirements

Embarkation requirements can be instituted to prevent infectious individuals from boarding the vessel. For example, a cruise company could dissuade guests with known symptoms from boarding by arranging flexible cancellation or re-booking policies [36]. Also, the crew could do a screening at the gate, with a checklist to avoid possible infectious individuals from boarding. There are suggestions in literature concerning COVID-19 to require guests and crew to be vaccinated or tested before embarkation [62, 69, 38]. This requirement does raise questions regarding equal treatment and privacy which remain the subject of public debate.

Another interesting concept applied onboard navy vessels, is the institution of a ‘preventive bubble’. This means that, for example, the entire crew will form a 14-day bubble with none or very limited interaction with individuals outside the bubble [44]. In combination with testing and symptom surveillance, this measure minimizes the risk of exposure [44]. The bubble could be maintained during the entire mission [44]. A bubble could also be applied on a cargo ship but has limited applicability for a cruise vessel because guests stay onboard much shorter than the crew of a naval vessel or cargo ship. Additionally, cruise ship guests might not want to isolate in a bubble before a cruise.

A.2.2. Onboard routines

Next to embarkation requirements, disease spread can be prevented and controlled by adjusting or implementing certain operational routines onboard the vessel. For example, more frequent and thorough cleaning and disinfecting can be implemented [69, 90]. Cleaning and disinfecting of touch surfaces might hinder the disease transmission mode related to the contaminated intermediate host [54, 82]. Cleaning, sanitizing and executing checklists can help prevent disease transmission via the common vehicle transmission route which is connected to food and water sources [54, 77, 36]. A report on

Norovirus transmission onboard cruise ships suggests implementing paid sick leave for ill crew may also help to avoid contaminated food sources and person-to-person disease transmission [36]. Frequently mentioned in literature are operational routines regarding increased ventilation and the application of HEPA filters [6, 5]. Increased ventilation rates and filters can often be applied within the boundaries of the current system so that no ship design adjustments are needed.

In section A.1 on ship layout design, it was proposed to alter the ship layout in an effort to limit exposure during the (dis)embarkation processes, tours and travel from/to the ship [78]. There are also operational measures that could limit exposure in these situations. For example, guests might receive scattered boarding and disembarkation times which avoids waiting lines and crowded situations [78]. Taking this idea of spreading the movement of people over time a step further; the crew could be given scattered work schedules. Also, guests could be assigned a shift that corresponds to a certain time frame for activities or meals. It might be possible to let guests sign up for certain time spots based on a maximum occupancy and spread the movement of people in that way.

A.2.3. Management, monitoring and surveillance

In order to be prepared for infections onboard any ship, it is important to discuss and document procedures and plans beforehand [42]. A disease management plan could prevent early infections leading to an outbreak and it can help to control the situation if an outbreak does occur [42]. The plan can also involve shore-based facilities and medical teams to assist the crew onboard when needed [90]. Several institutions provide guidelines and inspections concerning public health on ships [62]. For example, the EU Joint Action SHIPSAN “deals with the impact on maritime transport of health threats due to biological, chemical and radiological agents, including communicable diseases” [19]. The project includes, among others: a literature and legislation review, ship inspections according to EU standards, manuals, an upgraded information system to monitor and record outbreak information and training [19]. The World Health Organisation issued the International Health Regulations and for ships, they published the WHO guide to ship sanitation [62]. This guide aims “to present the public health significance of ships in terms of disease and to highlight the importance of applying appropriate control measures” [96]. In the US, there is the CDC Vessel Sanitation Program which “helps the cruise ship industry prevent and control the introduction, transmission, and spread of GI illnesses on cruise ships” [65]. Integral parts of these programs are inspections to ensure compliance, certificates, outbreak reporting and outbreak investigations [62]. Outbreak investigations are necessary in order to find infection sources, monitor the effectiveness of interventions and revise or expand regulations and guidelines when needed [62, 30].

Surveillance and monitoring are not only important after, but also before and during an outbreak [7, 88]. In order to identify cases, guests and crew might be asked to do a daily temperature check and actively monitor if they notice symptoms [60, 7]. Surveillance onboard might also include regular preventive testing and testing procedures for suspected cases [28, 78, 7]. When there is an infectious case onboard, the medical crew needs to trace the contacts and manage the suspected cases that arise from this investigation [62, 88]. The suspected or infected cases might need to isolate, disembark or require medical care, which means management of the infected cases. Additionally, there should be a guideline specifying when these individuals are no longer considered infected and can return to join the rest of the population onboard.

A.2.4. Restricted movement

The last type of operational measures covers a (partial) restriction of guest and crew movement. The most drastic type of restricted movement measures would be a total lockdown of the ship [60]. All guests and crew stay onboard for a certain period and might be asked to isolate in their cabins. Essential crew needs to maintain essential ship functions and provide basic necessities for the isolated guests and crew like food and medical care. Other options include the evacuation of all crew and guests, the evacuation of non-essential crew for ships without guests or a complete crew change-over [75, 100, 21].

Restricted movement measures also concern isolation and quarantine measures which are frequently mentioned in literature [36, 5, 62, 28, 49]. Infectious individuals or individuals who might be infected are isolated from the rest of the population to contain the situation and delay disease spread [88]. As

the disease spread slows down, there is a possibility that these measures prolong the overall length of the outbreak [59]. However, a longer outbreak might be preferred to a shorter outbreak with a high number of infections at its peak [59]. Isolation and quarantine measures are only possible when monitoring and surveillance measures are also implemented. Testing helps, for example, to determine who needs to isolate, if suspected cases are infected and it might inform the decision when someone can exit isolation [29]. The choice can also be made to evacuate infected cases as shore-based medical facilities are better equipped or when isolation proves to be impossible to achieve onboard the ship [21]. It is important to consider the impact on the mental health of the individuals in isolation. Spending days or even more than a week in a small space without social interaction can be challenging for anyone [42]. 'Fresh air' time, physical activity and digital contact can help to make this isolation period more tolerable.

The activities onboard and onshore could also lead to higher infection risk [78]. Therefore, management might decide to restrict congregate events onboard and limit shore-based interactions [28, 4]. A "Research Report on Restart of Chinese Cruise Industry" even suggested a 'cruise safety bubble' where the population onboard a cruise vessel forms a small and secure environment detached from the general situation [49]. This general situation could be a country or region that has not controlled the disease outbreak yet [49]. Limiting or even completely eliminating interaction with the general situation outside the 'cruise safety bubble' could help to limit the infection risk for those onboard. It should be considered that cruise guests might not be interested in this type of cruise as their movement is restricted to the ship. Management could also restrict the maximum capacity of general areas and close certain general areas [21]. During the Diamond Princess outbreak, for example, "public dining was replaced by room service" to reduce the risk of infection [7]. A further implementation of reducing capacity beyond specific spaces can be a total reduction of crew and guests allowed onboard. A paper on COVID-19 modeling public health interventions onboard a cruise ship concluded that for both a 7-day and 14-day cruise voyage; a 40% guest and 20% service crew (high level of contact) reduction together with social distancing (80% reduction in daily contact rate) showed significant potential [28]. Their model suggests that more than 40% of the infection cases are averted compared to a non-intervention scenario [28]. They also conclude this set of measures to be more effective than testing and daily symptom screening [28].

A.3. Behavioral measures

A.3.1. Personal protective equipment

In general, personal protective equipment (PPE), covers a range of different behavioral measures that one can implement to protect oneself and aid the limitation of disease spread between individuals [70, 21, 4]. The most frequently mentioned measure is mask wearing [60, 82, 5, 21, 4]. Wearing a mask prevents infectious particles from spreading when you sneeze or cough and medical-grade masks/respirators can also prevent inhalation of infectious particles by the one wearing the mask. The quality of the mask or respirator (FFP2/FFP3) and the way it is used might influence the effectiveness of this behavioral measure. Other personal protective equipment include: gloves, protective glasses, a face shield or a gown.

A.3.2. Personal hygiene

Next to PPE, personal hygiene measures can help limit disease spread. Personal hygiene includes hand washing, disinfecting and sneeze or cough etiquette [69, 82, 71, 36, 38, 40, 49, 29]. Additionally, a paper written in 2016 on handshakes onboard cruise ships suggests using a 'cruise tap' to avoid germ transmission and hand contamination because of handshakes [15]. This 'cruise tap' is a fist bump where only the knuckles are touching. The paper suggests this alternative greeting because they concluded that hand washing compliance was insufficient [15]. During the COVID-19 pandemic, it was indeed common not to shake hands but to greet each other in some alternative way like a fist bump or using your elbow.

A.3.3. Social distancing

Another well-documented behavioral measure is social distancing, as close contact is directly related to a high risk of disease transmission [60, 82, 71, 40, 93, 21, 84, 4, 29, 28]. Keeping a social distance

means that the number and length of close contacts is limited as much as possible. This results in a lower risk for disease transmission. The actual distance considered safe is always debated [84]. For COVID-19, for example, the WHO defined a close contact as anyone who “had physical contact (face to face contact within 1 meter for more than 15 min) or were in a closed environment with a suspected or confirmed COVID-19 case” [4]. Social distancing onboard a ship can be a challenging measure. For example, corridors might not be wide enough to accommodate social distancing when people move past each other and sleeping accommodations or working spaces can be too cramped to keep a safe distance.

A.3.4. Vaccinations

A final behavioral measure is vaccinations [69, 38, 62]. Vaccinations have already been discussed as an operational option where crew and guests are required to vaccinate before boarding the vessel. Vaccination is also mentioned as a behavioral measure when people decide to vaccinate not because of an obligation per se but as a measure to protect themselves and the population they are part of.

B

Movement and Infection Models

This appendix investigates three different types of movement models and three different types of medical infection models. The search terms for the literature on movement models included: *people movement model, ship, evacuation model, agent-based model* and *circulation*. With respect to the various infection models, the following search terms were used: *infection model, infection probability, transmission, disease model, COVID-19, pandemic, outbreak* and *compartment model*.

B.1. Crowd behavior movement models

B.1.1. Macroscopic models

Pipe flow models are used to inform early-stage layout design while incorporating evacuation regulations [41]. These types of flow models are classified as macroscopic models [46]. IMO specifies a simplified pipe flow model in Annex 2 of MSC.1/Circ.1533 where the layout of a vessel is represented by a hydraulic network [37]. Figure B.1 shows an example of a schematic hydraulic network for staircase A during day operation. In this hydraulic network, corridors and staircases are modeled as pipes and doors are modeled as valves [37]. The basic principle of this method is that gas or liquid flow behaves similarly to pedestrian flow [46]. This model is useful in early-stage design because of its simplicity. However, the model does not account for the behavior of individual agents and it is not possible to add variations in the characteristics of the agents itself [12]. Also, the IMO pipe flow model makes several assumptions. For example, counter flow is not modeled and all guests start evacuating at the same time [37].

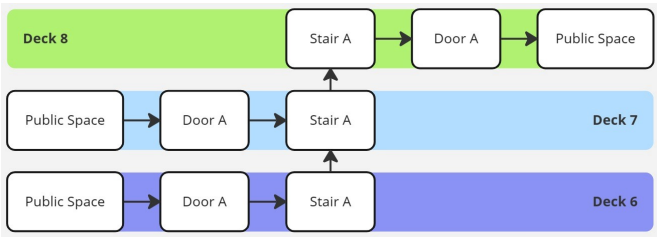

Figure B.1: Hydraulic network schematisation stairs A in day operation [35]

B.1.2. Mesoscopic models

This model is presented in subsection 3.2.1.

B.1.3. Microscopic models

The last category of movement models are microscopic agent-based movement models. Examples of microscopic movement models are: social force models and cellular automata models. [12]. A social force model is a continuous model where the movement of the agent is influenced by received infor-

mation about its surroundings. This surrounding information is presented as a vector quantity which affects the agent [43]. Basic forces are for example: separation (which avoids agent collision), obstacle avoidance and gradient following (which allows agents to find an alternative route avoiding an obstacle) [43]. All vector forces are summed and the agent will be impacted by the vector at its location [43]. Figure B.2 shows a possible vector map with summed vector forces, an obstacle and two agents.

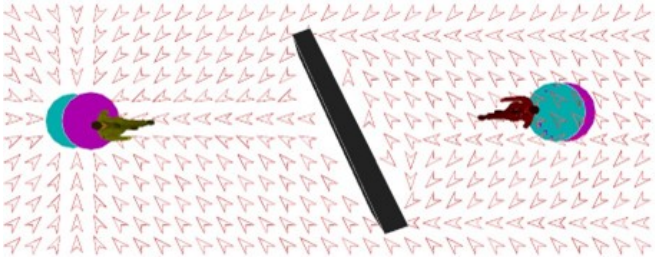

Figure B.2: Social force model vector map [43]

The dynamic cellular automata model is a second example of a microscopic agent-based movement model [12]. This model features discrete spaces, times and states [12]. Cellular automata "is named after the principle of automata (entities) occupying cells according to localized neighborhood rules of occupancy" [43]. The total available space is divided into square cells and each cell can be occupied by one entity [43]. The agent chooses the adjacent cell to move to according to a specified function. This function represents pedestrian goals like avoiding collisions or minimizing the distance traveled [43]. Both social force and cellular automata models can simulate the behavior of individual agents in great detail [41]. In these models, it is also possible to simulate heterogeneity in the population and give each agent their own set of parameters like age, gender and behavior characteristics [12]. For example, Li et al. used an agent-based route choice model to investigate passenger behavior during a ship evacuation [50]. In their model, the spatial location of all agents is known, contrary to the route choice models discussed in subsection 3.2.1. The focus of the research was to investigate: "passengers who are not familiar with the ship layout and passengers who have family members or friends with them" [50]. This example showcases the value of agent-based modeling as guest characteristics can be modeled and investigated. The simulation of individual behavior produces detailed results but also requires more computing power than a macroscopic model [41].

B.2. Medical infection models

B.2.1. Compartment models

Compartment models are deterministic models where every agent in the population has a certain state. The transfer of individuals from one state to another is based on probability. The probabilistic nature of disease spread is addressed by the transmission rates between states [70, 2]. Well-known deterministic models are "SIS and SIR models, and consist of systems of first-order differential equations describing the progression from susceptible (S) to infectious (I) individual" [70]. The third (R) state is either susceptible or recovered. The recovered compartment also includes infected cases resulting in death. Compartment models are known for their simplicity and thus require a short computational time and low computational capacities [27]. However, this simplicity comes at a cost as significant assumptions are required. For example, the population modeled is assumed to be homogeneous, which means that there are no differences in age, sex and behavior. Additionally, these compartment models assume a confined space and constant population size [101, 70]. Mobility patterns are not taken into account because the population is assumed to be well-mixed [76]. Every individual in the population has an equal chance to have contact with any other individual in the population. Because of these assumptions, compartment models might be less useful at the start of an epidemic as stochastic effects (contact patterns) are more important [33]. The transmission rates in compartment models are generally complex and are therefore often fitted using epidemiological data from real-life cases [92].

Most compartment models are based on the research from Wells and Riley et al [70]. The basic SIR model is presented in Equation B.1 to B.4 with S: susceptible individuals, I: infected individuals, R:

recovered individuals, *N*: total population, β: contact rate susceptible-infected, γ: recovery/removal rate and *t*: time [70].

$$\frac{dS}{dt} = -\beta SI \tag{B.1}$$

$$\frac{dI}{dt} = \beta SI - \gamma I \tag{B.2}$$

$$\frac{dR}{dt} = \gamma I \tag{B.3}$$

$$S + I + R = N \tag{B.4}$$

Wells developed the 'quantum' theory related to the dose of infectious particles needed to cause a person to transfer to the infected state [22]. A quantum is "the number of infectious airborne particles required to infect 63% of individuals in an enclosed space" [6]. This 63% comes directly from the assumption that infection chance follows a Poisson distribution ($1 - (1/e) \approx 63.2\%$) [22, 70]. Riley et al. published what became known as the Wells-Riley equation for steady-state quanta levels as seen in Equation B.5 [70]. The parameters are defined as follows; *C*: new cases, *I*: number of infectors, *p*: pulmonary ventilation rate of susceptible individuals [m^3/s], *q*: quanta production rate per infected individual [$quanta/s$], *A*: ventilation rate and *V*: space volume [m^3]. The Wells-Riley equation indicates more new cases and therefore a higher transmission probability when susceptible individuals are in "contact with infectious individuals for a cumulative period" [2].

$$C = S(1 - e^{-\frac{Ipqt}{AV}}) \tag{B.5}$$

There are several variations on the basic SIR model integrating more or new states like: vaccinated, dead, symptomatic and asymptomatic [31, 33]. An important adjustment has been the addition of an 'exposed' state which accounts for an incubation period before an individual moves to the infected state [70]. This model is called the SEIR model. The SEIR model is presented in Equation B.6 to B.10 with *E*: exposed individuals and α: progression rate exposed-infected. This presented SEIR model also includes the work from Gammaitoni and Nucci who linked the infection rate to room ventilation for unsteady exposure in an indoor environment [70]. This unsteady exposure is related to an increased total quanta level in a space when the ventilation stays constant and the quanta production increases with new cases. The original SIR model only accounted for steady-state quanta levels in the space. Comparing Equation B.1 and B.2 to Equation B.6 and B.7 one can recognize the definition of β as presented in Equation B.11.

$$\frac{dS}{dt} = -\frac{pq}{VA}SI \tag{B.6}$$

$$\frac{dE}{dt} = \frac{pq}{VA}SI - \alpha E \tag{B.7}$$

$$\frac{dI}{dt} = \alpha E - \gamma I \tag{B.8}$$

$$\frac{dR}{dt} = \gamma I \tag{B.9}$$

$$S + E + I + R = N \tag{B.10}$$

$$\beta = \frac{pq}{VA} \tag{B.11}$$

B.2.2. Risk based models

The second type of infection models are risk-based models. These models do not provide results like the number of infections or who is infected but instead give results in terms of infection risk. Specifically, two models found in the literature will be discussed: the EXPOSURE model and a modified Wells-Riley model [76, 84]. This modified Wells-Riley model gives COVID-19 infection risk based on the original Wells-Riley model while introducing a social distance index and a ventilation index [84].

EXPOSED model

Ronchi and Lovreglio noticed that policies adopted during pandemics such as COVID-19 are often based on macroscopic models which do not account for mobility patterns [76]. They argue that "It is therefore crucial to develop a general occupant exposure model which could be used to retrofit any type of microscopic crowd model and that is able to produce quantitative outputs for risk assessment" [76]. This general occupant exposure model is called EXPOSED and this model quantifies every exposure in a confined environment; when combined with a microscopic movement model. An exposure is defined as one agent that is within a set radius from another agent [76]. For every agent *i* in the simulation, a matrix E_t is created as presented in Equation B.12. Every column is a time step with $t = [t_0, t_1, \cdots, t_q, \cdots, t_f]$ and every row represents an agent $[1, \cdots, i, \cdots, n]$ [76]. From this matrix, relevant information for each agent can found: exposure times, maximum number of agents exposed at each time step and the distribution of exposure time over the different agents [76].

$$E_t^i = \begin{bmatrix} e_{t0}^1 & \dots & e_{tq}^1 & \dots & e_{tf}^1 \\ \vdots & \ddots & \vdots & \ddots & \vdots \\ e_{t0}^i & \dots & e_{tq}^i & \dots & e_{tf}^i \\ \vdots & \ddots & \vdots & \ddots & \vdots \\ e_{t0}^n & \dots & e_{tq}^n & \dots & e_{tf}^n \end{bmatrix} \tag{B.12}$$

To provide more insight into this method; an example has been provided in Equation B.13 with $[1-3]$ agents in a simulation for $t = [0-3]$. Equation B.13 is the exposure matrix for agent 1. This matrix shows that the first row only holds zeros as the agent itself will not be exposed to 'itself'. For the entire simulation, agent 1 is exposed to agent 2 and there is only exposure to agent 3 for $t = 2$. By summing the rows, one can see that the longest exposure time is 4 time steps to agent 2. By summing the columns, the maximum number of agents that agent 1 is exposed to is 2 agents at $t = 2$.

$$E_{0-3}^1 = \begin{bmatrix} 0 & 0 & 0 & 0 \\ 1 & 1 & 1 & 1 \\ 0 & 0 & 1 & 0 \end{bmatrix} \tag{B.13}$$

Modified Wells-Riley model

This model is presented in subsection 3.2.2.

B.2.3. Agent-based models

The final category of medical infection models covers the agent-based models. This category is rather broad as several different and complex models exist [68]. The agent-based models do have two main characteristics: the spatial location of each agent is known and infection or infection risk is individually calculated based on individual characteristics and movement [68]. The agent-based infection models go further than the risk-based models as it is possible to track which agents become infected and how they infect other agents using probabilities. In contrast, the risk-based models stop at the risk or probability indication and do not show individuals becoming infected, infecting others or even recovering. In a paper on tracking infectious disease spread, Tsui et al. mention a model that estimates the infection probability for each individual separately [68]. This probability is based on the contacts an individual has each day. The individual approach means that time, intensity and proximity of these contacts can be taken into account [68]. Additionally, it becomes possible to assign specific groups, like seniors, higher infection probabilities than younger groups [68]. Agent-based models can also feature simulations where agents are assigned states (like susceptible, infected and recovered). These states can

be used to calculate infection probabilities based on contacts with agents in a certain state [68]. For example, being within a certain proximity of an infected agent for a certain time causes that agent to change states from susceptible to infected. Then, it becomes possible to visually show the progression of the disease spread on an individual level.

Another agent-based modeling example can be found in research from Harweg et al [31]. They “introduce an agent-based social force model for tracking the spread of infectious diseases by modeling aerosol traces and concentration of virus load in the air” [31]. This model is used in a multi-day simulation for an airport building [31]. Their approach to infection risk is not based on close contacts but the authors model the localized viral load in the entire airport [31]. Each infected individual will leave an aerosol trail as they move around. When a susceptible individual moves to a certain location, the virus concentration can be calculated taking into account the respiratory rate, local viral load and the time spent at that location. The moving agent will accumulate viral load exposure over time and this total viral load can be compared with a threshold. The agent becomes infected when the total viral load exceeds the threshold and the agent itself starts spreading viral load on its trajectory. The threshold is related to the contagiousness of the virus; a low threshold for a very contagious disease means that a small amount of viral load already causes infection [31].

C

Listings Integrated Model Architecture

Listing C.1: Delayed agent simulation start

```
#Retrieve first non-zero value From-Nodes
m = Fnode_data_DF.ne(0).idxmax()

#Convert DataFrame 'm' to Numpy array
m = m.to_numpy(dtype=int)

#Create empty vector
No = np.empty(Number_of_agents,dtype=int)

#For all agents, store first none-zero From-Node in vector 'No'
for a in range(0,Number_of_agents):
    No[a] = Fnode_data[m[a],a]
```

Listing C.2: Node occupancy

```
#Create empty node occupancy matrix
Node_occupancy = np.empty((run_time,Number_of_nodes),dtype=int)

#Run nested loop for time and number of agents
for i in range(0,run_time):
    for j in range(0,Number_of_agents):

        #Calculate node occupancy for state = 1 (activity) and for state = 4 (end schedule)
        if State_data[i,j] == 1 or State_data[i,j] == 4:
            #Implement delayed agent simulation start location
            if Fnode_data[i,j] == 0:
                #Define location
                Local_fnode = No[j]
                #Add to occupancy at location
                Node_occupancy[i,Local_fnode] = Node_occupancy[i,Local_fnode] + 1

            else:
                #Define location
                Local_tnode = Tnode_data[i,j]
                #Add to occupancy at location
                Node_occupancy[i,Local_tnode] = Node_occupancy[i,Local_tnode] + 1
```

Listing C.3: Exposure time

```
#Create empty infection risk matrix
Infection_risk = np.empty((run_time,Number_of_agents))

#Run nested loop for number of agents and time
for j in range(0,Number_of_agents):
    #Reset exposure time
    t_exp = 1

    for i in range(0, run_time):
        #Reset exposure time when changing spaces
        if Tnode_data[i,j] != Tnode_data[(i-1),j]:
            t_exp = 1
        #Reset timer when agent starts activity (location data itself does not change)
        if State_data[i,j] == 1 and State_data[(i-1),j] == 0:
            t_exp = 1
```

Listing C.4: Social distance index - using node occupancy

```
        #Using node occupancy (state = activity or end activity schedule)
        if State_data[i,j] == 1 or State_data[i,j] == 4:
            #Implement delayed agent simulation start location
            if Fnode_data[i,j] == 0:
                Local_tnode = No[j]
            else:
                Local_tnode = Tnode_data[i,j]

            #Set social distance index to zero for occupancy = 0 or 1 (no infectors)
            if Node_occupancy[i,Local_tnode] <= 1:
                P_d = 0

            #Calculate social distance index
            else:
                #Account for node area index zero; while there is no node 0
                Local_tnode_A = Local_tnode - 1
                #Average node social distance
                d = Node_area[Local_tnode_A] /  Node_occupancy[i,Local_tnode]
                #Social distance index
                P_d = ((-18.19*np.log(d))+ 43.276)/100

            #Compensate for social distance > 10.8m is outside scope modified Wells-Riley
                model
            if P_d <= 0:
                P_d = 0

            #Define location node area
            Local_area = Node_area[Local_tnode_A]
```

Listing C.5: Social distance index - using link occupancy

```
        #Using link occupancy (state = wayfinding, walk, wait)
        else:
            Local_fnode = Fnode_data[i,j]
            Local_tnode = Tnode_data[i,j]

            #Determine link ID number
            Local_link = np.where(np.logical_and(Link_id_FN == Local_fnode,
            Link_id_TN == Local_tnode))[0]

            #Set social distance index to zero for occupancy = 0 or 1 (no infectors)
            if Link_occupancy[i,Local_link] <= 1:
                P_d = 0

            #Calculate social distance index
            else:
                d = Link_length[Local_link] / Link_occupancy[i,Local_link]
                P_d = ((-18.19*np.log(d))+ 43.276)/100

            #Compensate for social distance >10.8m - outside scope modified Wells-Riley model
            if P_d <= 0:
```

```
                P_d = 0

            #Define location link area
            Local_area = Link_area[Local_link]
```

Listing C.6: Infection risk

```
        #Calculate location-specific ventilation rate per second
        Q = (ACH*Local_area*H_c)/3600

        #Calculate infection risk
        Infection_risk[i,j] = 1-np.exp((-1*P_d*I*q*p*t_exp/(Q*E_z)))

        #Update exposure time
        t_exp  = t_exp + 1
```

Listing C.7: Find relevant indices

```
    #Find first index where state = 0
    m = State_data_DF.eq(0).idxmax()
    m = m.to_numpy(dtype=int)
    #Find first index where state = 4
    mm = State_data_DF.idxmax()
    mm = mm.to_numpy(dtype=int)
```

Listing C.8: Assume zero infection risk

```
            # ATR - put IR to zero first run, simulation not started for agent
            if Fnode_data[i,j] == 0:
                P_d = 0
            # ATR - Put IR to zero, agent not moving yet or simulated ended for that agent
            if i < m[j] or i > mm[j]:
                P_d = 0
```

D

Ship Layout

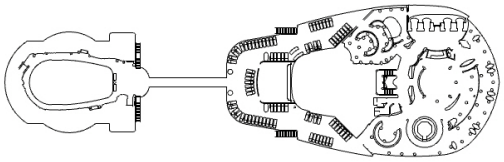

Figure D.1: SAFEGUARD data-set 2 cruise ship layout - deck 12 [23]

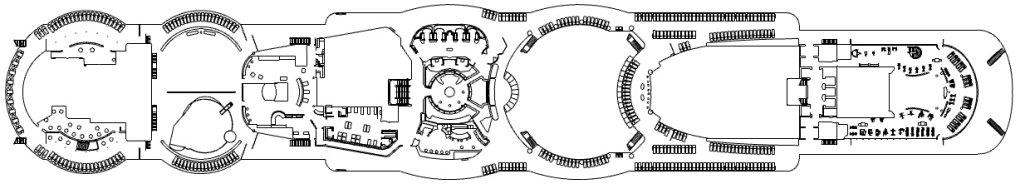

Figure D.2: SAFEGUARD data-set 2 cruise ship layout - deck 11 [23]

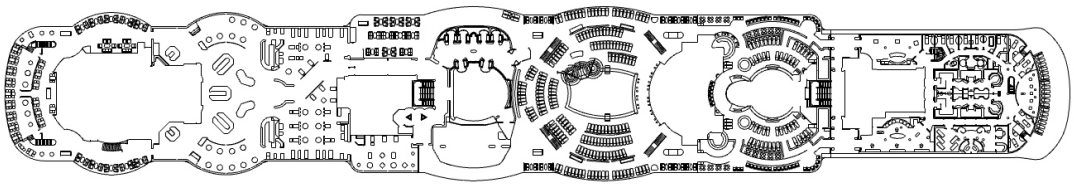

Figure D.3: SAFEGUARD data-set 2 cruise ship layout - deck 10 [23]

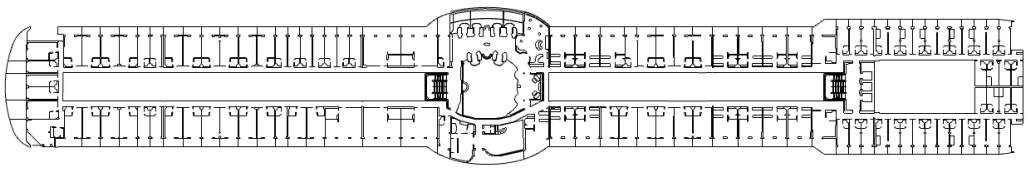

Figure D.4: SAFEGUARD data-set 2 cruise ship layout - deck 9 [23]

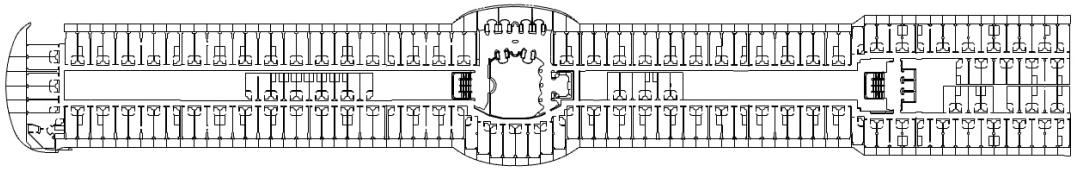

Figure D.5: SAFEGUARD data-set 2 cruise ship layout - deck 8 [23]

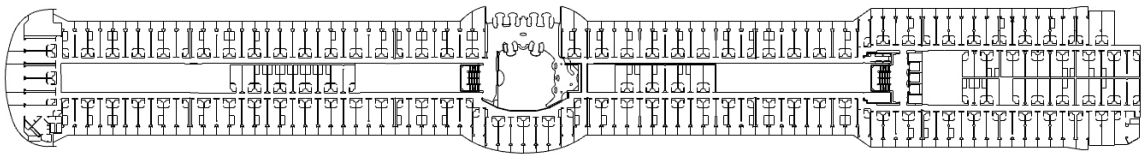

Figure D.6: SAFEGUARD data-set 2 cruise ship layout - deck 7 [23]

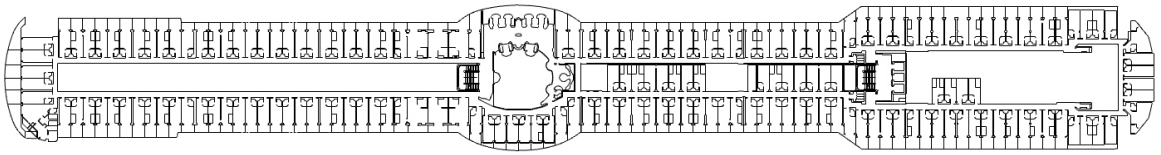

Figure D.7: SAFEGUARD data-set 2 cruise ship layout - deck 6 [23]

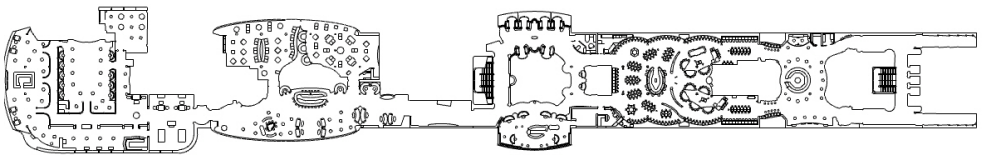

Figure D.8: SAFEGUARD data-set 2 cruise ship layout - deck 5 [23]

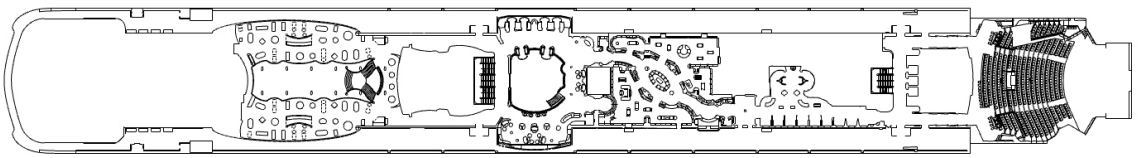

Figure D.9: SAFEGUARD data-set 2 cruise ship layout - deck 4 [23]

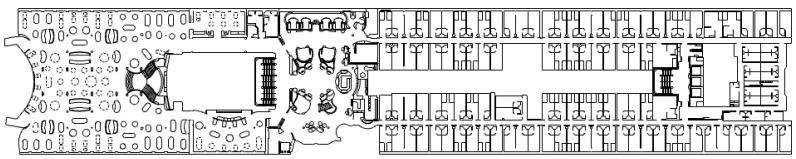

Figure D.10: SAFEGUARD data-set 2 cruise ship layout - deck 3 [23]

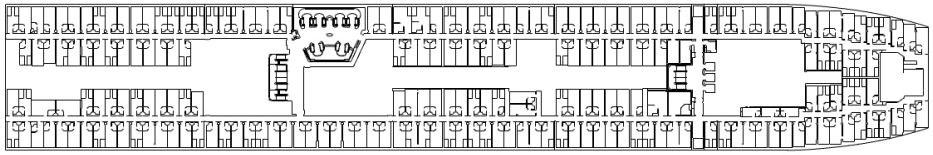

Figure D.11: SAFEGUARD data-set 2 cruise ship layout - deck 2 [23]

Figure D.12: SAFEGUARD data-set 2 cruise ship layout - deck 1 [23]

E

Sample Case Parameters

Agents & layout	Time & repetition	Chosen route choice model	Path separation
agent_data = [2850]	simulation_time = 100000	R_C_M = mixed logit	path1 = 0
network_data = [390][390]	time_step = 1	turn_penalty = 2	path2 = 0
number_of_agents = 2848	number_of_runs = 5	angular_penalty = 5	path3 = 0
number_of_nodes = 389		double gamma = 1	
number_of_links = 484		draws = 200	
		direction_angular_threshold = 5	

Table E.1: Start parameters route choice model

Parameter	Description	Assigned value	Unit
Number of links	Amount of connections between locations in the layout	968	[-]
Number of nodes	Amount of locations in the ship layout	389	[-]
Number of agents	Amount of agents in the simulation	2848	[-]
Partial time simulation	Decision to run a full or limited calculation	1 (full) or 0 (limited)	[-]
Simulated time	Define time steps for partial simulation	0 - 86400	[s]
I	Number of infectors	1	[-]
p	Pulmonary ventilation rate of susceptible individuals	$8.333 * 10e-5$	$[m^3/s]$
q	Quanta production rate per infected individual	0.238	$[quanta/s]$
ACH	Air changes per hour	15	[-]
H_c	Average ceiling height	2.35	[m]
Q_z	Ventilation index	1	[-]

Table E.2: Start parameters for integrated model

F

One-Way Movement

F.1. Mid and fwd staircases

The first scenario is constructed around the forward and mid main staircases. The staircase midships for decks 9,10,11 and 12 only allows for movement to a higher deck. The staircase forward for decks 9,10 and 11 only allows for movement to a lower deck. With this one-way movement, agents will theoretically use the midships staircase to move up and they can use the forward or any of the other staircases to move down. The smaller staircases, which often only cover one or two decks, are kept unchanged. Table F.1 provides the links which cover opposite movement and are thus set to 200m. The midships and forward staircases can also be recognized in Appendix D.

From-node	To-node	Description	From deck	To deck
256	258	Mid stairs	10	9
302	256	Mid stairs	10	9
301	302	Mid stairs	11	10
349	301	Mid stairs	11	10
348	349	Mid stairs	12	11
383	348	Mid stairs	12	11
276	275	Fwd stairs	9	10
275	315	Fwd stairs	9	10
315	313	Fwd stairs	10	11
313	369	Fwd stairs	10	11

Table F.1: Link list set to 200m

F.2. N296 restaurant

The second scenario relates to the main restaurant at deck 10 with a floor area of 510m^2 and this restaurant can host up to almost 700 people [26]. The deck 10 layout at the main restaurant can be seen in Figure F.1. From the midships staircase there are three main routes to the main restaurant: two routes over PS and one over SB. For this scenario, the PS corridor becomes the entry route to the restaurant. Agents can leave or move forward over deck 10 via the PS and SB seating areas but they are discouraged, by the link length, to use these routes to move aft. Table F.2 provides the links for which the length is set to 200m.

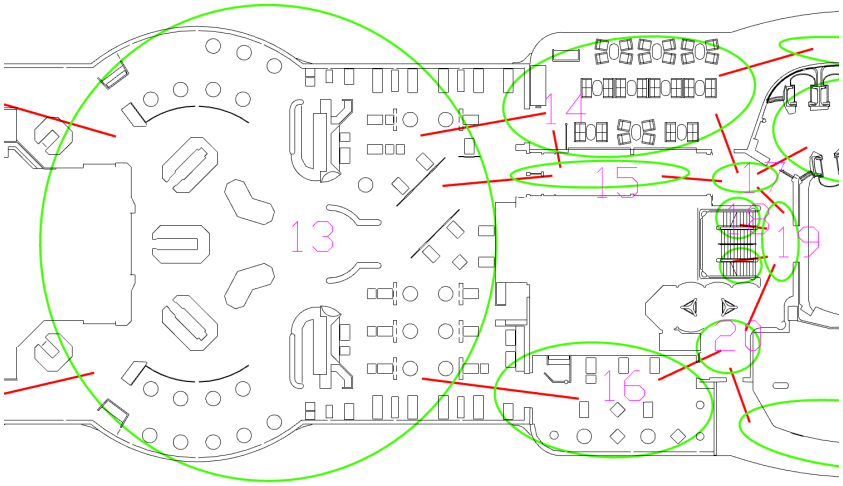

Figure F.1: Deck 10 layout at node 296 (location 13 in drawing) [23]

From-node	To-node	From	To
296 (13)	298 (15)	Main restaurant	Corridor PS
297 (14)	298 (15)	Seating area PS	Corridor PS
297 (14)	296 (13)	Seating area PS	Main restaurant
297 (14)	300 (17)	Seating area PS	Corridor PS of stairs
298 (15)	297 (14)	Corridor PS	Seating area PS
298 (15)	300 (17)	Corridor PS	Corridor PS of stairs
299 (16)	296 (13)	Seating area SB	Main restaurant
303 (20)	299 (16)	Corridor SB of stairs	Seating area SB

Table F.2: Link list set to $200m$

The average infection risk results for the one-way movement simulations are given in Table F.3. The N296 restaurant scenario shows average infection risks which lie between SC1 and SC2. The one-way stairs simulation presents a lower average guest infection risk of 0.636% and a higher 2.09% crew average infection risk compared to the sample cases. This guest and crew risk compensate each other which leads to a total average infection risk similar to the sample cases. The high crew average infection risk could be related to the assumptions around the crew accommodations. For example, the crew is assumed to have their break at node 33 or node 5. Node 5 is located close to the midships staircase at deck 1. With the one-way staircase scenario, the crew is discouraged from using the midships staircase to move down between decks 9 and 12. Something similar happens for N33, located in front of the fwd staircase on deck 2, as agents are discouraged from traveling upwards after their break via the fwd staircase between decks 9 and 11. This might lead the crew to choose inconvenient routes and increase the waiting times as a significant part of the crew has the same destination at the same time.

Result [%]	SC1	SC2	Mid and fwd stairs	N296 restaurant
Average IR	0.807	1.05	0.996	1.01
Average guest IR	0.730	0.935	0.636	0.897
Average crew IR	1.04	1.39	2.09	1.36

Table F.3: Average infection risks sample cases and one-way movement

Figure F.2 visualizes the average infection risk over time for the sample cases and one-way movement scenarios. The N296 restaurant scenario gives a similar results to SC2. However, the one-way stairs scenario has a higher risk peak around 13:00 with an average infection risk above 3%. The average

IR also stays high for a longer period after 13:00 compared to the sample cases. This could be caused by congestion when agents have finished their first activity and are moving to lunch. Agents need to take different routes to reach their lunch destination because they can not move down via the midships staircase. Certain links might reach their maximum flow and this means that agents have to wait before they can move. If agents therefore remain at their activity location where they have already built up risk for a longer time, the average risk increases. Additionally, the new movement patterns could lead to high occupancies at nodes with a limited area as agents are waiting before they can move. Later in the simulation, the average infection risk peaks seem flattened for the one-way stairs simulation. The average risk values are lower than the sample cases and there are wide humps instead of sharp peaks. The stairs simulation is also significantly longer than the other simulations as it takes more time for all the agents to reach their final destination. As mentioned before, the unfeasible crew quarter modeling might result in congestion at the end of the crew shifts around 21:00 and 00:00 when the crew tries to reach N5 or N33. This could be a potential reason for the prolonged high average infection risk after 22:00 which is not visible for the other cases.

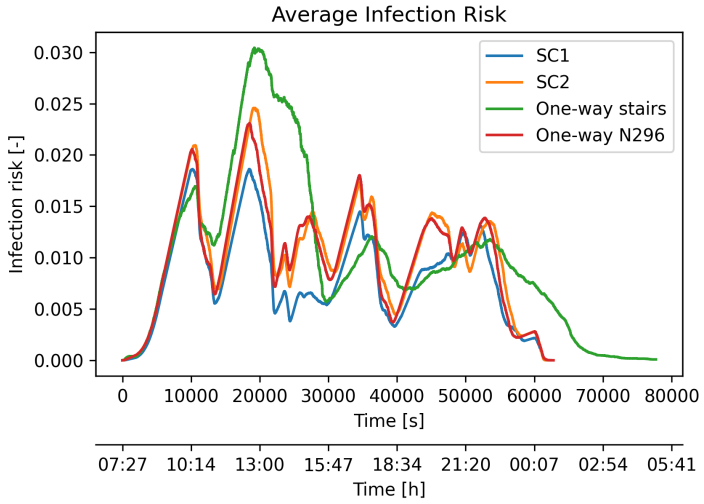

Figure F.2: Average infection risk - one-way movement

The frequency distribution for the agent average infection risk is given in Figure F.3. The one-way stairs scenario has results close to sample case 1 and the N296 restaurant scenario lies close to SC2. Figure F.4 shows the number of agents with an infection risk above 50%. The one-way N296 case has similar results as the second sample case. There is one moment in time where there is a difference in the number of at-risk agents. This moment is 13:00 where the second sample case reached 70 agents with a risk above 50% against 51 agents for the one-way N296 scenario. The question remains if this is an improvement because of one-way movement or if it is related to the variation in the RCM outcomes.

The one-way stairs scenario presents with very different results in Figure F.4, compared to the sample cases and the other one-way movement scenario. There is a peak at 13:00 with 127 agents who have an infection risk above 50%. This peak coincides with the peak in Figure F.2. Besides this peak, the number of agents with a risk above 50% is lower than SC2 and the N296 simulation. Again, looking at SC1, it remains hard to conclude that these lower values are the result of the one-way movement or within the range of RCM outcomes.

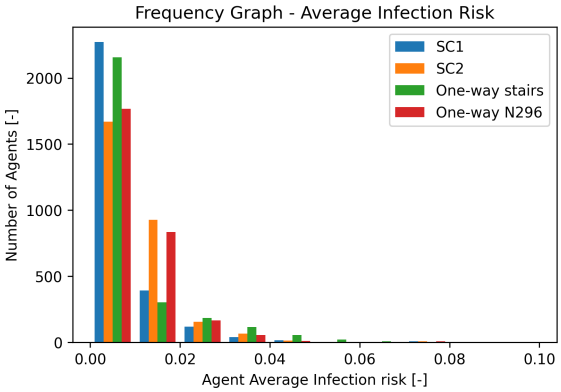

Figure F.3: Average infection risk distribution - one-way movement

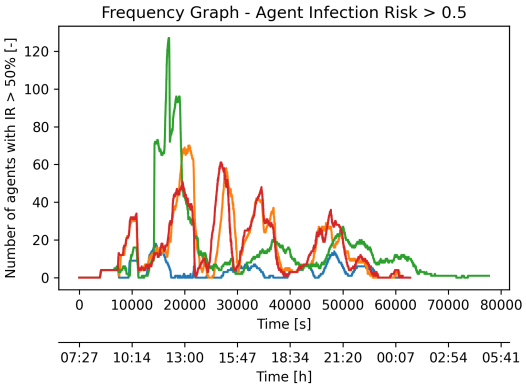

Figure F.4: Infection risk above 50% - one-way movement

Taking both the average infection risks and the frequency figures into account, the application of one-way movement requires more research. The N926 restaurant scenario might show a reduction in the number of agents with a risk above 50% around 13:00, but it does not show significant improvements for the total average infection risks. The one-way stairs scenario results in an average risk reduction for the guests but an average risk increase for the crew. Additionally, there is an increase in the number of at-risk individuals at 13:00.

The integrated model is relevant when measures like one-way movement are analyzed because it provides results based on the actual movement of agents. This is different from a general one-space population infection risk calculation where specific movement is not accounted for. However, in order to conclude that the tested one-way scenarios do or do not work; the RCM model should be developed further. For example, it would be beneficial for the results if the crew quarters were modeled realistically and if the RCM model allows links to be removed. If the links can be removed, the behavior of agents who do not follow the one-way movement is no longer an issue. One could argue that some agents will not adhere to the one-way movement directions, and removing the links does not allow for this situation. Another option could be to alter the RCM model to include some additional utility terms specific to one-way movement. This term could be changed to account for one-way movement without changing the length.

At this time, it is not recommended to implement the tested one-way movement measures as model development and additional research is required. Also, in section 6.1 the node locations presented with significantly higher infection risks than the links. The one-way movement measures target the reduction of infection risks at link locations and in this research, it is therefore not pertinent to adjust the integrated model and further investigate this operational measure.

G

Listings Behavioral Measures

Listing G.1: Additional start parameters

```
agentID_firstcrew = 2148    # agent ID for the first crewmember in the simulation
eta_E = 0.5                 # exhalation filtration efficiency surgical mask
eta_R = 0.5                 # respiratory filtration efficiency surgical mask
```

Listing G.2: Model adjustment mask wearing during movement

```
if j < agentID_firstcrew:                                   # Guests
    if State_data[i,j] == 1 or State_data[i,j] == 4:           # Activity state
        q_adjusted = q                                         # No mask
        p_adjusted = p                                         # No mask
    else:                                                      # Wayfinding, walk, stay state
        q_adjusted = q*(1-eta_E)                               # Wearing a surgical mask
        p_adjusted = p*(1-eta_R)                               # Wearing a surgical mask

else:                                                       # Crew
    q_adjusted = q*(1-eta_E)                                   # Wearing a surgical mask
    p_adjusted = p*(1-eta_R)                                   # Wearing a surgical mask
```

Listing G.3: Model adjustment continuous mask wearing - node

```
if j < agentID_firstcrew:                                   # Guests
    if Local_tnode == 330 or Local_tnode == 299 or Local_tnode == 297 or Local_tnode == 296
        or Local_tnode == 293 or Local_tnode == 292 or Local_tnode == 290 or Local_tnode ==
        286 or Local_tnode == 105 or Local_tnode == 104 or Local_tnode == 79 or Local_tnode
        == 45 or Local_tnode == 44 or Local_tnode == 41:
        q_adjusted = q                                         # No mask
        p_adjusted = p                                         # No mask
    else:
        q_adjusted = q*(1-eta_E)                               # Wearing a surgical mask
        p_adjusted = p*(1-eta_R)                               # Wearing a surgical mask
else:                                                       # Crew
    q_adjusted = q*(1-eta_E)                                   # Wearing a surgical mask
    p_adjusted = p*(1-eta_R)                                   # Wearing a surgical mask
```

Listing G.4: Model adjustment continuous mask wearing - link

```
    q_adjusted = q*(1-eta_E)                                   # Wearing a surgical mask
    p_adjusted = p*(1-eta_R)                                   # Wearing a surgical mask
```

Listing G.5: Model adjustment social distance based mask wearing - node

```
if j < agentID_firstcrew:                                   # Guests
    if Local_tnode == 330 or Local_tnode == 299 or Local_tnode == 297 or Local_tnode == 296
        or Local_tnode == 293 or Local_tnode == 292 or Local_tnode == 290 or Local_tnode ==
        286 or Local_tnode == 105 or Local_tnode == 104 or Local_tnode == 79 or Local_tnode
        == 45 or Local_tnode == 44 or Local_tnode == 41:
        q_adjusted = q                                      # No mask
        p_adjusted = p                                      # No mask
    else:
        if d < safe_distance:                               # check if social distance
            q_adjusted = q*(1-eta_E)                        # Wearing a surgical mask
            p_adjusted = p*(1-eta_R)                        # Wearing a surgical mask
        else:
            q_adjusted = q                                  # No mask
            p_adjusted = p                                  # No mask
else:                                                      # Crew
    if d < safe_distance:                                   # check if social distance
        q_adjusted = q*(1-eta_E)                            # Wearing a surgical mask
        p_adjusted = p*(1-eta_R)                            # Wearing a surgical mask
    else:
        q_adjusted = q                                      # No mask
        p_adjusted = p                                      # No mask
```

Listing G.6: Model adjustment social distance based mask wearing - link

```
if d < safe_distance:                                       # check if social distance
    q_adjusted = q*(1-eta_E)                                # Wearing a surgical mask
    p_adjusted = p*(1-eta_R)                                # Wearing a surgical mask
else:
    q_adjusted = q                                          # No mask
    p_adjusted = p                                          # No mask
```